8-2017

Soil-Structure Interaction Effects on the Seismic Response of Low-Rise Eccentrically Braced Frames

Luis Gerardo Buitrago Goyez
University of Arkansas, Fayetteville

Soil-Structure Interaction Effects on the Seismic Response of Low-Rise Eccentrically Braced Frames

A thesis submitted in partial fulfillment
of the requirements for the degree of
Master of Science in Civil Engineering

by

Luis Gerardo Buitrago Goyez
Technological University of Panama
Bachelor of Science in Civil Engineering, 2006

August 2017
University of Arkansas

This thesis is approved for recommendation to the Graduate Council.

_____
Dr. Michelle Bernhardt
Thesis Director

_____
Dr. Gary Prinz
Committee Member

_____
Dr. Clinton Wood
Committee Member

Abstract

The importance of soil-structure interaction (SSI) effects on the seismic response of buildings has been long recognized and has been researched for over 40 years. However, SSI analysis has only been applied in a few building projects because the fixed base condition is considered to provide a conservative estimation for the response of buildings under seismic loads. This assumption of a fixed base condition adopted by practitioners is not always conservative or cost-effective, especially for rigid buildings over soft soils. Additionally, for the case of ductile steel frames with eccentric configurations, the influence of SSI on their seismic performance has not been investigated.

In this study, the seismic performance of eccentrically braced frames (EBFs) considering SSI effects is investigated using analytical models. Background information and modern guidelines available to consider SSI in the seismic analysis of buildings are presented and discussed. Following, a 3-story building with EBFs on shallow foundations is analyzed with and without SSI. The beam on Winkler foundation approach is used to model the linear and nonlinear soil-foundation interface behavior, considering linear-elastic, elastic-perfectly plastic, and nonlinear springs. Inter-story drifts, residual drifts, link rotations, and axial load column demands were similar for frames with flexible base and fixed base conditions when elastic and elastic-perfectly plastic springs were used. However, when nonlinear springs were used, frames with a flexible base showed a significant reduction in their responses in comparison to those observed for the fixed base condition. As a result, a reduction in frame member sizes was possible and justified through SSI analyses.

Acknowledgments

First of all, I would like to express my sincere gratitude to my advisor, Dr. Michelle L. Bernhardt, for believing in me since the very first time I suggested her my research topic. Her guidance, encouragement and support have been very important during my days as a graduate student and for completing this work. I want to also thank Dr. Gary S. Prinz for his clever opinions and suggestions about my research, and for always having opened the door of his office to answer my silly questions.

Special thanks to Dr. José M. Roësset for introducing me to the magic world of "soil-structure interaction." It was a great honor for me to learn from such a smart person and passionate professor. His expertise and advising were very important during my time working on this project.

I thank my parents, grandparents, siblings, and the rest of family for loving and supporting me throughout my life. Their support and encouragement have been very important during my time away from home.

There are no words to express my gratitude to my wife, Gabriela, for her love, support and encouragement during my time as graduate student in the United States, and especially, for giving me the gift of becoming a dad soon.

Lastly, I would like to thank all the faculty members of the Department of Civil Engineering at the University of Arkansas, friends, classmates, and those who have helped me during my journey as a graduate student.

Dedication

I would like to dedicate this work to my grandparents, Narciso and Rosario, humble people who encouraged and helped not only their children but also their grandchildren to go to college. They showed us, from early age, how fantastic learning is. Their unconditional love and kindness are always with me.

Table of Contents

List of Tables

List of Figures

I. Introduction

Soil-structure interaction (SSI) analysis of buildings assesses the combined response of the superstructure, its foundation system, and the soil beneath under seismic excitation. This interaction between a structure and the underlying soil have been a matter of interest and research for many years. This phenomenon is particularly important for massive and stiff structures, such as nuclear power plants, supported on soft soils (Roësset, 1996). Therefore, most of the research conducted in the past on this topic was related to the seismic design of these types of structures. As a result of these research efforts, modern codes related to the design of nuclear facilities require linear time-history analyses considering SSI.

For the case of buildings, SSI has been traditionally thought to be of little benefit for typical seismic analyses. Indeed, for flexible buildings constructed over stiff soils, there is usually no change in their seismic response by including SSI effects in comparison with fixed base conditions. For intermediate and long period buildings; however, period elongation due to the soil flexibility can cause a reduction in the spectral acceleration (i.e., seismic demand) using the response spectrum shape adopted by design codes in the United States. An additional uniform reduction on the response spectrum can also be taken due to the increment of damping in the structure. These reductions in the response spectra, as illustrated in Figure 1, support the conservationism for using a fixed base.

There are also some situations where the seismic demand can increase with the increment of the building period for a specific response spectrum. For instance, ground motions in deep soft soil deposits can be deviated from the motion in the bedrock because the soil column and soil-foundation system act as filters for ground motions. In fact, seismic waves can be amplified at

some frequencies or attenuated at others. Amplification of ground motions in deep soil deposits and the forward fault-rupture directivity can cause an increment in spectral acceleration with building period, as presented in Figure 2. Additionally, elongation of the building period can cause an increase in the ductility demand on buildings constructed over soft soil (Mylonakis and Gazetas, 2000).

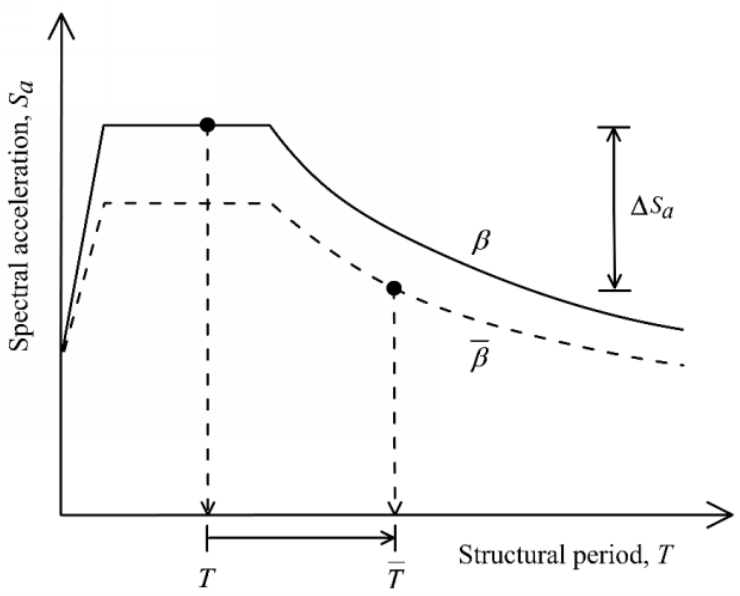

Figure 1. Decrease in spectral acceleration due to SSI effects in a design response spectrum (Bolisetti and Whittaker, 2015)

Despite the limited application of SSI in the seismic design of buildings, reductions in structural member sizes and/or foundation elements has been reported for some buildings projects due to the implementation of this approach (Wilcock et al., 2015). By including SSI effects in the seismic analysis of buildings, a more "realistic" distribution of the strength demands and deformations can be achieved. In addition, base-slab averaging and embedded effects due to the presence of the foundation system and basement levels, respectively, can be taken into account to

modify the input ground motion. This motion at the foundation level, or foundation input motion (FIM), can be applied to the building model as a uniform base excitation instead of using a free-field motion. There are some analytical equations available to evaluate the deviation of the free-field motion due to the presence of shallow foundations (Veletsos and Prasad, 1989; Mylonakys et al., 2006) and basement levels (Elsabee and Morray, 1975; Kausel et al., 1978; Day, 1978).

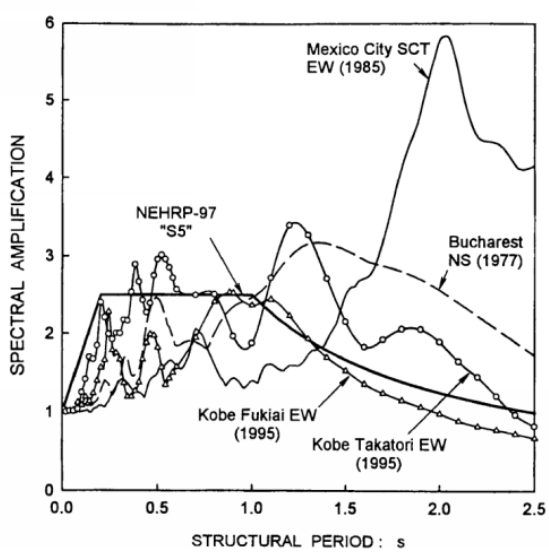

Figure 2. Comparison between a typical design code spectrum and response spectra from recorded earthquakes with strong long-period components (Mylonakis and Gazetas, 2000)

The lack of implementation of SSI analysis can be mainly attributed to the misconception of the conservative approach of using fixed base supports for all types of soil conditions. In addition, the poor understanding of this phenomenon, time-consuming application, and the lack of available technical information support the limited implementation of SSI analysis for building structures. As a consequence, the common support assumption used by structural engineers is the fixed base condition. That is the case of modern design codes such as ASCE/SEI 7-10, *Minimum Design Loads for Buildings and Other Structures* (ASCE, 2010), which contains guidelines to consider SSI for the seismic analysis of buildings using the equivalent lateral force (ELF)

procedure and modal analysis. These guidelines have a bias to always reduce the seismic demand, so neglecting SSI is conservative for structural design. Even the available procedure to account for SSI in ASCE/SEI 7-10 could have a shortcoming because there is no link between the response modification factors, *R*, for considering ductility in linear analysis and SSI (Crouse, 2001). For the case of nonlinear procedures, modern codes remain silent about how to consider SSI effects in nonlinear static analysis (NSA) and nonlinear response history analysis (NRHA) even though there is evidence that these types of analyses are sometimes used in practice for the seismic evaluation of existing buildings and performance-based seismic design of new buildings. Performance-based seismic design is becoming more and more common in practice to evaluate existing or new buildings and its implementation along with SSI effects could be needed, especially, for buildings over soft soils.

In the past five years, there has been an increase in research and the availability of technical information regarding the consideration of SSI in the structural analysis of buildings. ASCE/SEI 41-13, *Seismic Evaluation and Retrofit of Buildings* (ASCE, 2013), adopted the guidelines included in FEMA 440, *Improvement of Nonlinear Static Seismic Analysis Procedures* (FEMA, 2005), for including SSI in the seismic analysis of buildings. These provisions and updated research related to SSI were later included in NIST GCR 12-917-21, *Soil-Structure Interaction for Building Structures* (NIST, 2012). NIST (2012) includes guidelines to incorporate SSI effects in both linear and nonlinear procedures for the seismic analysis of buildings structures. All the information included in the aforementioned documents were used to develop an updated chapter of SSI for buildings in FEMA P-1050, *NEHRP Recommended Seismic Provisions for New Buildings and Other Structures* (FEMA, 2015), and eventually these provisions will be included in the new ASCE/SEI 7-16, *Minimum Design Loads and Associated*

Criteria for Buildings and Other Structures. Although these new provisions state that the implementation of SSI analysis is optional, it is expected that the application of SSI on the seismic analysis of buildings will increase in engineering practice.

With the increased availability of this new technical information and research related to SSI for building structures, linear and nonlinear analysis of new and existing structures can be performed more often. In this context, lateral seismic resisting systems such as ductile braced frames with eccentric configurations can be evaluated considering SSI effects. These types of frames have an advantage over the commonly used concentrically braced frames (CBF) in their ability to accommodate architectural features (e.g., doors, windows, and hallways). Additionally, these frames with eccentric configurations, such as eccentrically brace frames (EBFs), can dissipate energy during severe earthquakes and act as structural fuses to protect the rest of the structure. However, modern design codes (e.g., ANSI/AISC, 2010) suggest that connection testing or prequalified connections are needed for EBFs with link-to-column connections, affecting their economy. The energy dissipation capacity of these types of frames along with SSI have not been the object of previous documented research.

The objectives of this study are summarized as follows:

- Present and discuss approaches to include SSI effects on the seismic analysis of buildings
- Analyze and discuss guidelines included in NIST (2012) and FEMA P-1050/2015 for considering SSI in the seismic analysis of buildings
- Investigate the effects of including SSI on the seismic analysis of low-rise EBFs with link-to-column connections over shallow foundations using numerical modeling
- Compare structural responses of EBFs obtained with fixed base supports and those including SSI effects

II. Background

The seismic design of building structures is typically conducted to satisfy the life safety performance objective implicit in modern design codes. In order to satisfy this objective, deformations need to be limited and enough strength must be assigned to structural elements at certain locations to ensure ductile behavior and sufficient structural capacity under the Design Basis Earthquake (DBE). Additionally, a low probability of collapse must be ensured under the Maximum Considered Earthquake (MCE). For the case of performance-based seismic design, buildings need to behave elastically under an additional hazard level called the Service Level Earthquake (SLE). These types of analyses are usually conducted in practice disregarding the flexibility of the soil beneath the structure (i.e., the fixed base condition).

The assumption of ignoring the flexibility of the soil for the seismic analysis of buildings has been conservative for projects constructed over stiff soils. However, there is evidence of serious damages to buildings and other structures during earthquakes due to the interaction between the soil and the structure or SSI effects at sites with soft soils. For instance, the 1985 Mexico City earthquake caused a lot of damage to many buildings in this area. The deep soft soil deposit at this site and the presence structure-foundation system amplified the ground motions, resulting in a "double-resonance" condition for some buildings (Kramer, 1996). In addition, some studies (Romero and Rix, 2005; Mwafy et al., 2011) have suggested that structures constructed along the Mississippi Embayment in the U.S., close to the New Madrid seismic zone, can experience significant amplification of the ground motions. Based on this evidence, there are some situations when SSI should be taken into account for the seismic analysis of buildings.

Low-rise buildings over soft soils are commonly stiff and supported by shallow foundations; therefore, they are potentially susceptible to SSI effects (Roësset, 1996; Stewart et

al. 1999b; Mylonakis and Gazetas, 2000). Buildings supported by shallow foundations can dissipate energy due to inelastic sliding, settling, and rocking movements under seismic excitation (see Figure 3), so reduction in the seismic demand can be achieved. The rocking mode is of particular interest due to its re-centering mechanism. Therefore, the overall response of buildings can be enhanced by allowing a certain amount of foundation rocking. This energy dissipation capacity of the soil-foundation interface has been studied by many researchers using experimental tests (Rosebrook and Kutter, 2001a, b, c; Gajan et al., 2003a, b; Thomas et al., 2004; Chang et al., 2007; and Ugalde et al., 2007)) and numerical analyses (Cremer et al., 2001; Gajan, 2006; Paolucci et al., 2008).

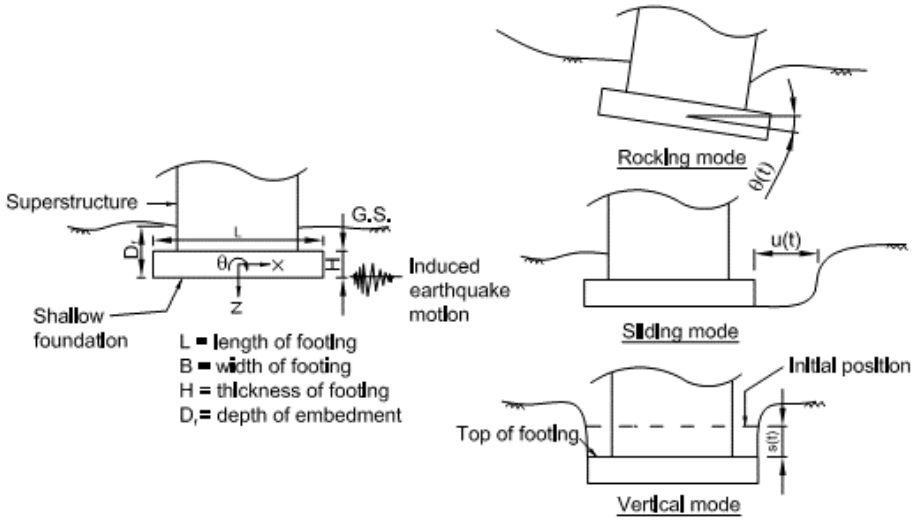

Figure 3. Vibration modes of shallow foundations (Raychowdhury, 2008)

A series of physical tests have been conducted in the past 20 years to evaluate the nonlinear response of shallow foundations under seismic excitation. In this context, centrifuge tests have become very popular for evaluating the performance of soil-foundation systems. For instance, cyclic tests were conducted by Gadre and Dobry (1998) on an embedded square footing

for studying its lateral response under different displacements. Passive and active pressures at the sides of the footing were considered and results showed that the passive pressure provides more than 50% of the lateral resistance of the soil-footing system. Rosebrook and Kutter (2001a,b,c); Gajan et al. (2003a, b); Thomas et al. (2004); Chang et al. (2007), and Ugalde et al. (2007) have also reported a series of tests conducted at the University of California, Davis (UCD) using a 9 m radius centrifuge and a scale factor, N, of 20. These tests were conducted on shallow strip and square footings using a range of vertical factors of safety and different types of loading such as monotonic, vertical and lateral slow cyclic, and dynamic. As result of these tests, the combined effect of structural and soil nonlinearity was observed and the main observations obtained are summarized as follows:

- degradation of rotational stiffness due to the foundation yielding
- the moment-rotation and shear-sliding response showed a significant amount of energy dissipation
- permanent deformations were observed as a result of the soil yielding
- the embedment depth increased both the moment and shear capacity
- soil density, soil type, footing size, aspect ratio, embedment, static vertical factor of safety, and amplitude of cycling loading affected the foundation stiffness degradation and its permanent displacement

Additionally, one-g experiments, using either base input, such as shake table, or inertial load, such as structure-mounted hydraulic jacks, have been used to investigate the seismic performance of the soil-foundation interface using shallow foundations. The first foundation rocking experiments on shallow footings over sand and clay soils for observing their moment-rotation behavior were conducted in New Zealand by Professor Taylor and his students (Barlett,

1976; Wiessing, 1979; Taylor et al., 1981). Results from these studies showed that designing a spread footing capable of yielding the soil beneath at a moment less than the moment capacity of the column can avoid the formation of plastic hinges at the base of the column. One-g experiments were also reported by Negro et al. (1998), Maugeri et al. (2000), and Knapeet et al (2004) on shallow foundations over sand and their main findings were:

- the vertical factor of safety showed a significant effect on the damping and level of distortion
- eccentricity on tests caused a reduction in the seismic bearing capacity and large residual rotations (24°)
- moments effects were significant resulting in a large reduction in bearing capacity due to uplift for structures with a center of mass well above the foundation level

For the case of numerical analysis, there are three common approaches for modeling SSI effects on shallow foundations: continuum finite element and boundary element approaches, macro-element formulations, and Winkler-based approaches. The continuum approach uses a semi-infinite and isotropic or anisotropic soil domain. Macro-element methods evaluate the response of shallow foundations under seismic loading using a single element and a plasticity-based formulation (Cremer et al., 2001; Gajan, 2006; Paolucci et al., 2008). The most utilized approach in practice is Winkler's method (1867). Winkler-based approaches can be used with 1D spring elements or 1D spring elements in combination with 2D or 3D soil elements to model the soil-foundation response. Several publications describe various Winkler-based models used for modeling the seismic response of shallow foundations resting on either an elastic o inelastic soil medium, and these models consider the inelastic behavior of the soil-foundation interface through the effect of foundation uplift due to rocking. The Winkler's approach is further

discussed in detail because it is used in this study to model the soil-foundation interface behavior for shallow foundations.

The first efforts for using Winkler models to assess the rocking response of shallow foundations took place in New Zealand. An analytical model using elastic-perfectly-plastic springs along with Coulomb slider elements to evaluate moment-rotation behavior of rigid footings were developed by Taylor et al. (1981) and Barlett (1976). Psycharis (1981) suggested a model using two different approaches: the two-spring model and the distributed Winkler spring model. Viscous dampers, elastic-perfectly plastic springs, and an impact mechanism allowing dissipation of energy at impact were used as elements to consider nonlinear behavior in the soil-foundation interface. Simplified equations to quantify base shear resistance of flexible structures allowing uplift for single and multi-degree-of-freedom systems were reported by Chopra and Yim (1985) and Yim and Chopra (1985), respectively, using linear springs. Results obtained from analyses suggested that foundation flexibility and uplift have a significant effect on the fundamental period of vibration of multi-story structures, but they have a little effect on higher modes.

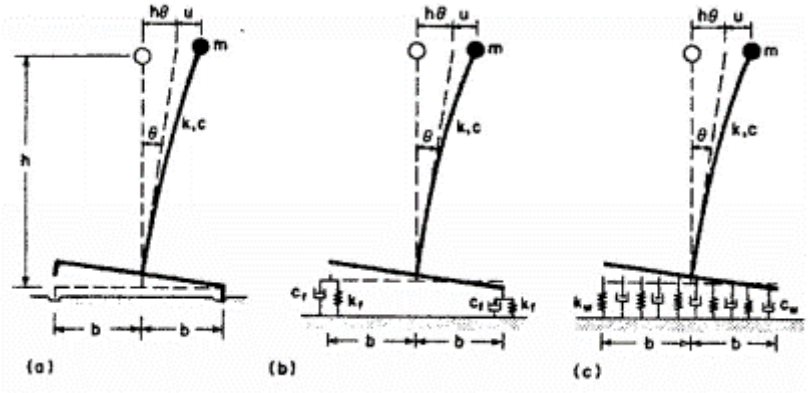

Figure 4. Idealized foundation system by Chopra and Yim (1985): (a) rigid foundation, (b) two-element (spring-dashpot) system, and (c) distributed Winkler (spring-dashpot) system (Harden et al., 2005)

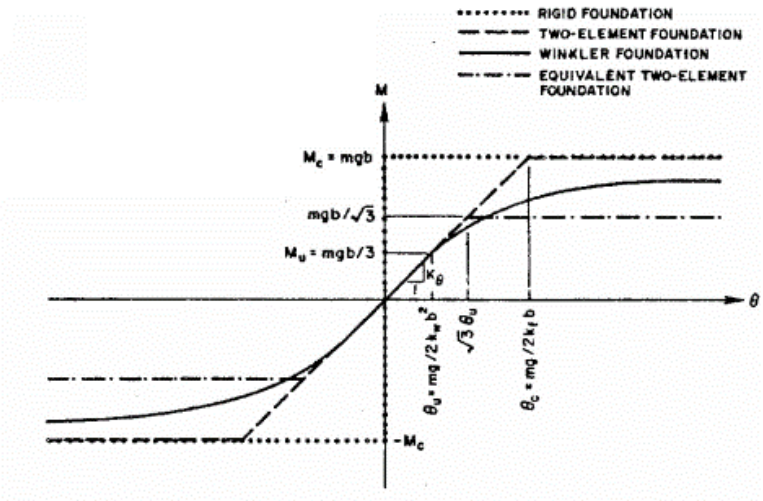

Figure 5. Moment-rotation envelope assuming different idealized foundations after Chopra and Yim (1985)

A shear wall structure was analyzed by Nakaki and Hart (1987) using discretely spaced vertical springs with viscous dampers. This shear wall structure was represented using a nonlinear stiffness degrading hysteretic model while Winkler springs with zero tension capacity and elastic compressive capacity were used. Due to the uplift of the foundation, a considerable reduction in the ductility demands was obtained in comparison with the fixed base condition. A Winkler type finite element model was developed by Harden et al. (2005) to evaluate the nonlinear behavior of shallow strip footings under lateral cyclic loads. Results from this study had good agreement with centrifuge and one-g model tests on shallow foundations subjected to both slow cyclic and dynamic base excitation. In addition, it was shown that the experimental unloading stiffness offered better results than the elastic stiffness computed using equations developed by Gazetas (1991b). Allotey and Naggar (2007) used the Winkler approach and backbone curves previously developed by them for modeling the cyclic response of shallow

foundations. The numerical model developed was able to predict the moment-rotation and settlement response reasonably well, but the sliding response was not well captured.

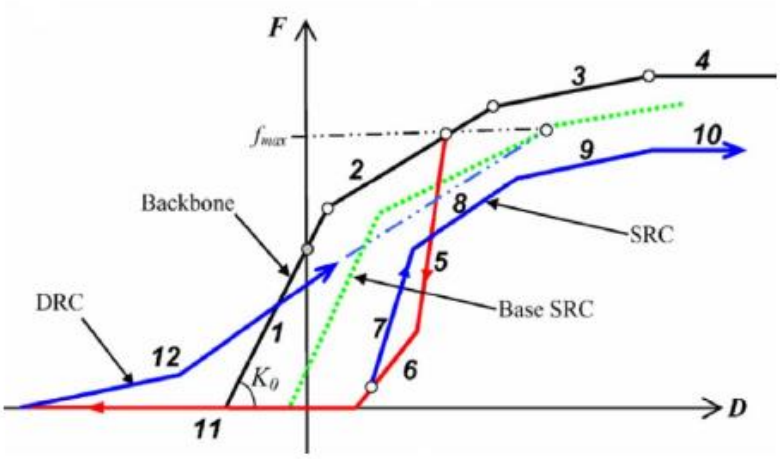

Figure 6. Backbone curves after Allotey and Naggar (2007)

Ductile braced frame systems such as EBFs have been traditionally used to accommodate features in braced spans, offering an advantage over the typically used CBF (Figure 7). However, there are a limited number of EBF configurations due to the poor performance of the link-to-column connections. EBFs dissipate energy during earthquakes through inelastic deformation of beam elements called "links" while the rest of the structural elements remain essentially elastic. Damage to EBF links requires the replacement of entire beams and can be an expensive and time-consuming repair (Prinz, 2010). Consequently, more robust and accurate analyses are needed to better evaluate the performance of EBFs and quantify damage to the EBF links.

One approach that has not been commonly used to assess the seismic performance of EBFs is SSI. The energy dissipation mechanism of EBFs is usually expected to be from specially designed segments of beam called links because these elements act as "structural fuses";

however, the soil-foundation interface can add more energy dissipation capacity to the entire structure-foundation-soil system, thereby reducing the concentrated damage of these ductile elements. In this study, the seismic performance of EBFs with links with column connections considering SSI is investigated since those frames have less inelastic rotation capacity than mid-span links due to the fracture in the flange at the connection (Okazaki et al., 2006).

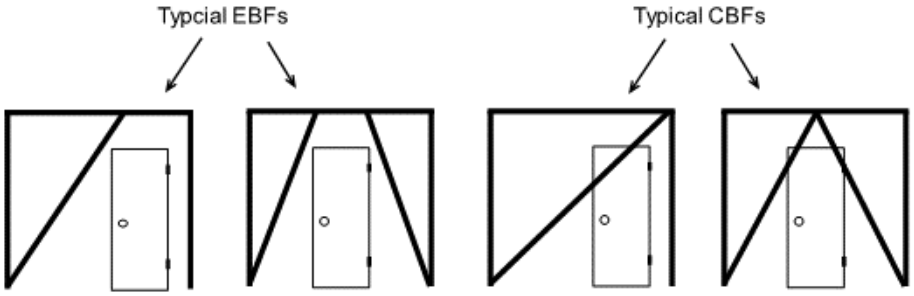

Figure 7. Comparison of EBF and CBF architectural flexibility (Prinz, 2010)

A. Methods to Evaluate SSI

There are two approaches to include SSI in the seismic analysis of structures: the direct approach and the substructure approach. The direct analysis evaluates SSI by modeling a limited soil domain along with the foundation system, superstructure, transmitting boundaries along the perimeter of the soil domain, and interface elements between the foundation system and soil. Therefore, the direct solution considers the complete soil-structure system and solves this problem in one step. For this method, it is necessary to evaluate the input ground motion at the base of the numerical model consistent with the desire seismic design hazard level. This input ground motion is typically obtained using deconvolution or using outcrop motions available. However, since the availability of outcrop motions is limited, site response analyses are usually performed to get this

input ground motion using deconvolution. Commercially available finite element programs such as ABAQUS (Dassault Systemes, 2005), ANSYS (ANSYS Inc., 2013), and LS-DYNA (LSTC, 2013), or the open-source finite element program, OpenSees (Mazoni et al., 2007), can perform nonlinear analysis considering SSI and using the direct approach. Other programs such as SASSI2000 (Ostadan, 2006a) can execute multi-step linear analysis considering SSI with the direct approach.

The substructure approach is a multi-step procedure for which it is necessary to:

1. determine the seismic motion of the foundation or foundation input motion (FIM) without any structure
2. evaluate the dynamic stiffnesses of the foundation as a function of frequency for a steady state harmonic excitation
3. perform dynamic analysis of the structure using the dynamic stiffnesses and the seismic motion applied at the base of the structural model

The first step mentioned above is often referred as kinematic interaction analysis, and it represents the modification of the ground motions due to the presence of the foundation system. The modification of the dynamic properties of the structure due to the flexibility of the soil-foundation interface (second step) is known as inertial interaction. After the analysis of the combined structure-foundation-soil system is conducted, the resulting ground motion at the base will be different from the free-field motion. This modification from the free-field is due to the additional deformations of the soil caused by the base shears, axial forces, and overturning moments resulting from the inertia forces in the structure. It is important to mention that the FIM can vary with depth due to the presence of basement levels. Figure 8 shows the schematic illustration of the direct and the substructure approaches.

By using the direct approach, kinematic and inertial interaction effects are automatically included in the numerical model. Nevertheless, this approach is computationally demanding and time-consuming, so direct analyses for SSI are seldom used in practice. The substructure approach is more often implemented in design offices for the seismic design of buildings considering SSI. Consequently, the substructure approach is used for this study and its implementation is discussed in detail in the following sections.

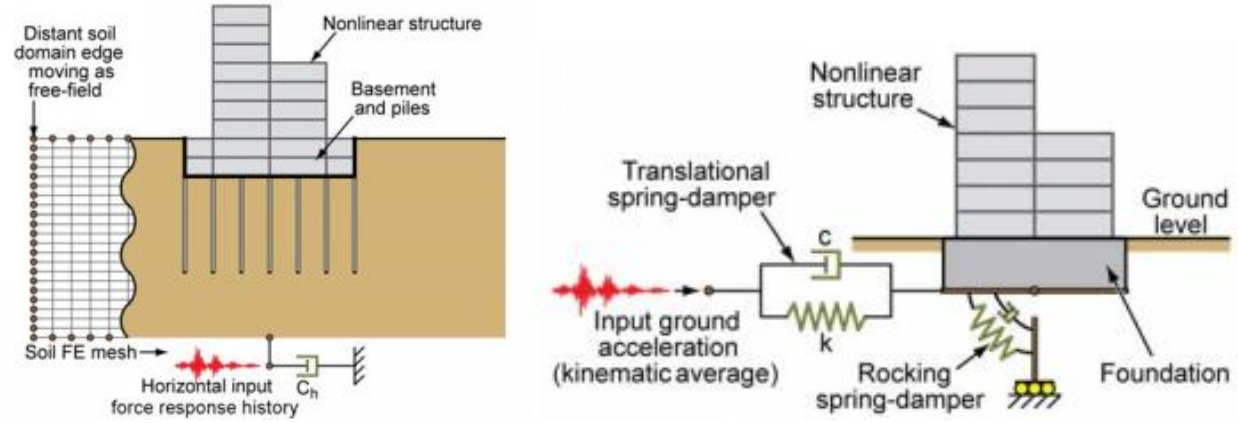

(a) Direct analysis **(b) Substructure approach**

Figure 8. Schematic illustration of the direct and substructure approach (modified from NIST, 2010)

B. Inertial Interaction

Inertial interaction refers to the modification of the dynamic properties of a structure due to the flexibility of the soil-foundation system. As a result, displacements and rotations at the foundation level are caused by inertial forces such as base shears and moments. This effect can be a significant source of flexibility and energy dissipation for the structure-foundation-soil system.

Since the dynamic properties of a structure are affected by its support conditions, the period of vibration is expected to change with the degree of flexibility of its supports. As discussed, a rigid base or fixed base is the most common support assumption used in practice for modeling structures. This support condition assumes that the soil-foundation interface is infinitely rigid. On the other hand, a flexible base considers the deformability of the foundation system and the soil. A schematic illustration of the fixed and flexible base conditions for a single-degree-of-freedom structure with a force concentrated at the top can be seen in Figure 9. The lateral deflection, Δ, of the structure with a fixed base presented in Figure 9a is caused by its translational displacement; however, the lateral deflection, $\tilde{\Delta}$, of this structure with a flexible base (Figure 9b) is not just function of its translational displacement, but also the rotation of the foundation system. The undamped period of vibration, T, for the structure with a fixed base can be calculated as function of the circular frequency, ω, mass, m, and stiffness, k, using the following commonly used equation (Clough and Penzien, 1993):

$$T = \frac{2\pi}{\omega} = 2\pi\sqrt{\frac{m}{k}} \tag{1}$$

For the case of the flexible base, vertical (k_z), horizontal (k_x), and rotational springs (k_{yy}) represent the flexibility of the soil-foundation system (see Figure 9b). The undamped period of vibration, $\tilde{T}$, for a structure with a flexible base can be estimated as a function of the structure height, h, spring constants at the foundation (k_z, k_x, and k_{yy}), k, and T using the equation suggested by Veletsos and Meek (1974):

$$\frac{\tilde{T}}{T} = \sqrt{1 + \frac{k}{k_x} + \frac{kh^2}{k_{yy}}} \tag{2}$$

The ratio $\tilde{T}/T$ is also known as the period lengthening ratio, and it is greater than unity based on the degree of flexibility of the soil-foundation system. Multi-degree-of-freedom structures can be analyzed using Equation 2 by taking the structure height, *h*, as the effective modal height, *h**. This effective modal height applies just for the first-mode shape and is approximately 2/3 of the structure height. ASCE/SEI 7-10 uses Equation 2 to evaluate the period of vibration of buildings with flexible bases, $\tilde{T}$.

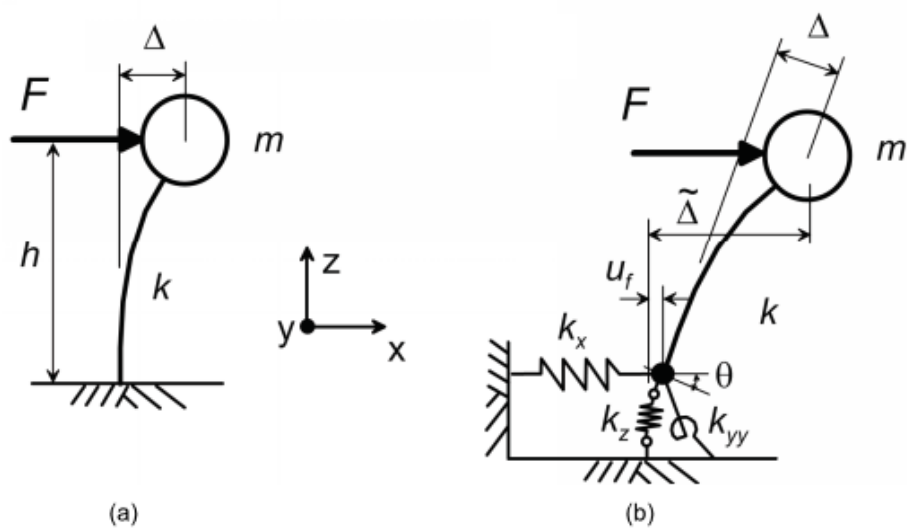

Figure 9. Schematic illustration of deflections caused by a lateral force applied to: (a) structure with a fixed base; and (b) structure with a flexible base (NIST, 2012)

There are some parameters which affect inertial interaction effects for SSI. Veletsos and Nair (1975) and Bielak (1975) studied dimensionless parameters controlling period lengthening due to inertial effects. These two studies found that two of the dimensionless parameters which control period lengthening is the structure-to-soil-stiffness ratio, *h/(Vs.T),* and the mass ratio, *m/(ρ_s.4.B.L.h),* which are function of the shear wave velocity, *Vs*, mass, m, soil mass density, ρ_s, foundation dimensions, *B* and *L*, *h*, and *T*. In a later study, Stewart et al. (1999b) concluded that the period lengthening increases significantly with the structure-to-soil-stiffness ratio, and it is

the most important parameter for inertial SSI effects. This study stated that *h/(Vs.T)* for buildings over soil and weathered rock is less than 0.10 for moment frame structures, and between 0.10 and 0.50 for shear wall and braced frame structures.

Another effect of the inertial interaction on the seismic response of buildings is damping, referred to as foundation damping, β_f. There are two main sources of foundation damping: hysteretic and radiation damping. Hysteretic damping is caused by the hysteretic behavior of soil under seismic excitation while radiation damping is originated by the radiation of the reflected wave-field away from the foundation. Foundation damping is part of the flexible base system damping, β_0:

$$\beta_0 = \beta_f + \frac{1}{(\tilde{T}/T)^n}\beta_i \tag{3}$$

The inherent damping, β_i, is the structural damping assumed for the superstructure using a fixed base, and it is generally assumed to be 5% for typical structural systems. This inherent damping should be based on the material type, configuration, and behavior of the structural and nonstructural elements responding dynamically. PEER/ATC-72-1, *Modelling and Acceptance Criteria for Seismic Design and Analysis of Tall Buildings* (ATC, 2010), suggests more detailed values for β_i based on the structural system type and configuration. The foundation damping can vary from 0 to 25% (Stewart, 1999b), and the exponent n in Equation 3 is taken as 3 for linearly viscous structural damping, and 2 for the other cases (Givens, 2013).

Veletsos and Nair (1975), Bielak (1975 and 1976), Roësset (1980), Wolf (1985), Aviles and Perez-Rocha (1996), Maravas et al. (2007), Givens (2013), among others, developed analytical models for evaluating foundation damping. Most of these analytical models are

frequency-dependent. One exception is the expression suggested by Wolf (1985) using a circular foundation resting on a half-space, which ignores the frequency dependence of the foundation stiffness terms and assumes a linear foundation radiation damping. Similar to a previous study presented by Roësset (1980) considering frequency dependence, the expression initially suggested by Wolf's can be expressed as:

$$\beta_f = \left[\frac{\left(\tilde{T}/T\right)^{n_s} - 1}{\left(\tilde{T}/T\right)^{n_s}}\right]\beta_s + \frac{1}{\left(\tilde{T}/T_x\right)^{n_x}}\beta_x + \frac{1}{\left(\tilde{T}/T_{yy}\right)^{n_{yy}}}\beta_{yy} \tag{4}$$

where β_s is the hysteretic damping, β_x and β_{yy} are damping ratios corresponding to translational and rotational modes and the terms T_x and T_{yy} are fictitious vibration periods, calculated as if the only source of vibration is foundation translation and rotation. These periods can be calculated as follows:

$$T_x = 2\pi\sqrt{\frac{m}{k_x}} \qquad T_{yy} = 2\pi\sqrt{\frac{mh^2}{k_{yy}}} \tag{5}$$

The exponents n_s, n_x, and n_{yy} are assigned based on the specific form of damping corresponding to their components of foundation damping, and Givens (2013) recommended that all exponents can be taken as 2 assuming linear viscous damping.

The soil hysteretic damping, β_s, is strain-dependent, and there are many suggested values for this parameter in the literature. Kramer (1996) summarized classical models for hysteretic damping, and Darendeli (2001) and Menq (2003) presented modern empirical models which consider overburden pressure and shear strain in a consistent way across multiple soil types. FEMA P-1050 suggests values for the soil hysteretic damping as a function of the soil class and shaking intensity (Table 1).

Table 1. Soil Damping Ratio in terms of Effective Peak Acceleration, SDS/2.5[(1)], and Site Class (FEMA, 2015)

Site Class	$S_{DS}/2.5 = 0$	$S_{DS}/2.5 = 0.10$	$S_{DS}/2.5 = 0.40$	$S_{DS}/2.5 = 0.50$
A	0.01	0.01	0.01	0.01
B	0.01	0.01	0.01	0.02
C	0.01	0.01	0.03	0.05
D	0.01	0.02	0.07	0.15
E	0.01	0.05	0.20	(2)
F	(2)	(2)	(2)	(2)

(1) Use straight-line interpolation for intermediate values of $S_{DS}/2.5$
(2) Site-specific geotechnical investigation and dynamic site response analyses shall be performed

As stated by Stewart (1999b) for the period lengthening ratio, $\tilde{T}/T$, the foundation damping, β_f, also increases significantly with the structure-to-soil-stiffness ratio, *h/(Vs.T).* Figure 10 shows the effect of *h/(Vs.T)* on $\tilde{T}/T$ and β_f using different height-to-width ratios, *h/B*, for a specific case of a square footing ($L=B$), soil Poisson's ratio (υ) of 0.33, hysteretic damping (β_s) of 0, and mass ratio of 0.15. Based on Figure 10, $\tilde{T}/T$ increases with *h/(Vs.T)* and decreases with *h/B*. In order to evaluate β_f, Equation 4 was used and the exponents n_s, n_x, and n_{yy} were all taken as 2. Similar to $\tilde{T}/T$, it can be seen in Figure 10 that β_f increases with *h/(Vs.T)* and decreases with *h/B*. The behavior of β_f suggests that lateral movements of the foundation dissipates energy more efficiently than foundation rocking because lateral movements of the foundation dominate at low *h/B* ratios and foundation rocking at high *h/B* ratios.

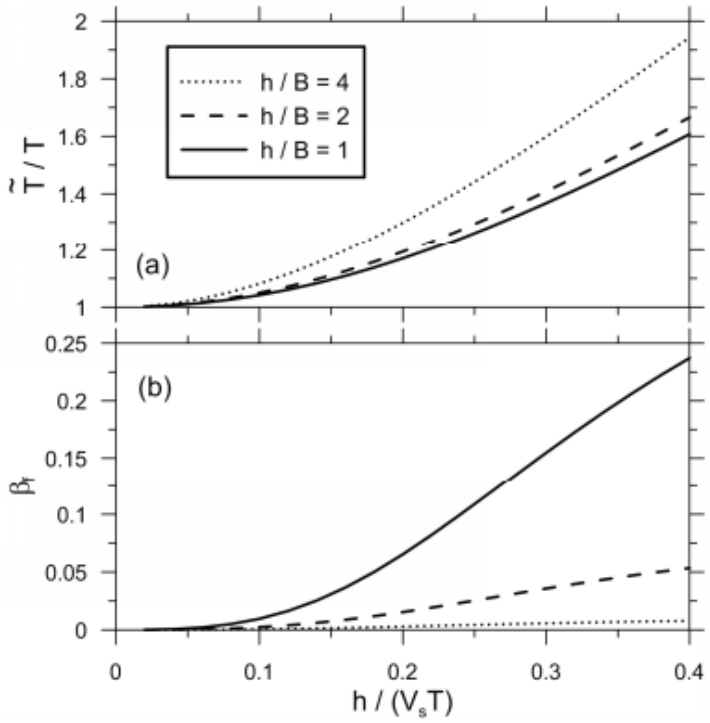

Figure 10. Period lengthening ratio ($\widetilde{T}/T$) and foundation damping (β_f) versus the structure-to-soil-stiffness ratio ($h/(Vs.T)$) for a square footing and different h/B ratios. For this plot, ν=0.33, B/L=1, β_s=0, mass ratio = 0.15, and exponents n_s, n_x, and n_{yy} = 2. (NIST, 2012)

Similar trends to those shown in Figure 10 have been validated by studies conducted on instrumented buildings. For instance, Steward et al. (1999a and 1999b) showed that the most important parameter which controls inertial interaction is $h/(Vs.T)$. Additionally, it was found that inertial SSI effects can be negligible for $h/(Vs.T)$ <0.10, which the typical case of flexible structures such as moment frames over stiff soils or rock. However, as previously mentioned, inertial effects are usually significant for stiff structures such as shear walls and braced frames on soft soils.

B.1 Impedance Functions (Stiffness and Damping) for Shallow Foundations

Impedance functions represent the stiffness and damping characteristics of the foundation-soil system under dynamic loads. For a complete 3-D model, six dynamic impedances are needed, three translational and three rotational, in order to evaluate the dynamic equilibrium equation of a rigid foundation. These impedances are a function of the foundation geometry, the soil properties, and frequency of the structure-foundation-soil system. The general procedure to calculate dynamic impedances for a rigid shallow foundation can be summarized as follows:

1. Model a massless and infinitely rigid foundation on a soil domain with elastic properties
2. Apply a harmonic force or moment at a specific frequency and with unit magnitude (e.g., $P(t) = P_0e^{i\omega t}$ or $M(t) = M_0e^{i\omega t}$) to the underlying soil domain
3. Obtain the steady state vibration amplitude ($U(t) = U_0e^{i\omega t+i\phi}$ or $\theta(t) = \theta_0e^{i\omega t+i\phi}$) of the foundation under harmonic excitation
4. Calculate the dynamic impedance $K(\omega)$ as the ratio between the harmonic force acting on the foundation and its vibration amplitude as follows:

$$K(\omega) = \frac{P(t)}{U(t)} = \frac{P_0e^{i\omega t}}{U_0e^{i\omega t+i\phi}} = \frac{P_0}{U_0}e^{-i\phi} \tag{6}$$

5. Write the classical solution for complex-valued impedance (Luco and Westman, 1971; Veletsos and Wei, 1971) to associate the real and imaginary parts with a dynamic (frequency-dependent) spring and dashpot

$$K(\omega) = \bar{k} + i\omega C \; or \; K(\omega) = \bar{k}(1 + 2i\beta) \tag{7}$$

$$\bar{k}(\omega) = Re\big(K(\omega)\big) = \frac{P_0}{U_0}\cos\phi \tag{8}$$

$$C(\omega) = \frac{Im(K(\omega))}{\omega} = -\frac{P_0}{U_0}\sin\phi \tag{9}$$

$$\beta = \frac{\omega C}{2\bar{k}} \tag{10}$$

6. Repeat this procedure to the range of frequencies of interest

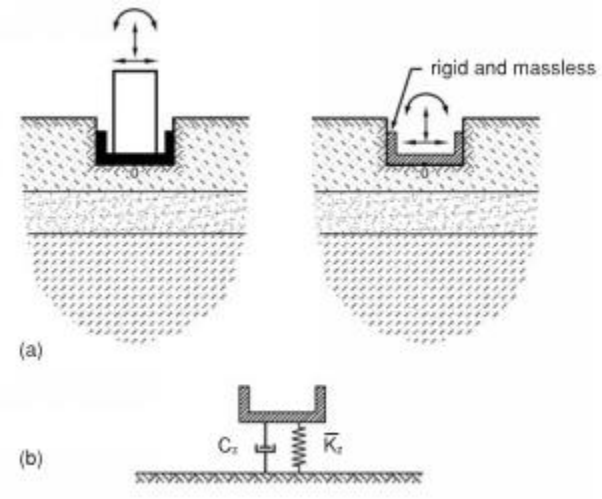

Figure 11. Physical interpretation of dynamic spring and dashpot in vertical mode of vibration (Mylonakis et al., 2006)

Many analytical solutions for impedance functions have been developed for rigid circular and rectangular footings on the surface or embedded within the soil. These solutions were evaluated for a uniform, elastic, or visco-elastic half space. Pais and Kausel (1988), Gazetas (1991b), and Mylonakis et al. (2006) reviewed impedance functions for rigid rectangular footings resting on the surface of a half-space and suggested equations for evaluating the stiffness and damping parameters shown in Equation 7. These analytical solutions describe translational stiffness and damping along axes x, y, and z, and rotational stiffness and damping about those axes. These equations for stiffness and damping are a function of the foundation dimensions, soil shear modulus, *G*, Poisson's ratio of the soil, ν, dynamic stiffness modifiers, α_j,

and the embedment modifiers, η_j. The general expression for evaluating the dynamic stiffness, k_j, can be expressed as:

$$k_j = K_j \alpha_j \eta_j \tag{11}$$

In Equation 11, K_j represents the static foundation stiffness at zero frequency for mode j. Equations for evaluating stiffness, damping, embedment factors, and dynamic correction factors suggested by Pais and Kausel (1988) are shown in Figure 12, 13, and 14. To evaluate K_j using the equations shown in Figure 12, the large strain shear modulus of the soil, G, needs to be computed. The following equation is typically used to evaluate the low strain shear modulus, G_0, as a function of the shear wave velocity, V_s, and the soil mass density, ρ_s:

$$G_0 = \rho_s V_s^2 \tag{12}$$

As mentioned above, the shear modulus, G, used to calculate the foundation stiffness should reflect the effects of modulus reduction with the increment of shear strain amplitude. ASCE/SEI 7-10 and FEMA P-1050 provide G/G_0 ratios as a function of the site class and shaking intensity, and these ratios are presented in Table 2.

In order to consider the variability of the shear wave velocity measured in the free-field, V_s, and the additional weight of the structure in a soil profile, an average effective shear wave, $V_{s,avg}$, needs to be calculated. Consequently, the added weight of the structure can be considered by calculating the overburden-corrected shear wave, $V_{s,F}$, at a depth z using the following equation:

$$V_{s,F}(z) = V_s(z)\left(\frac{\sigma'_v(z) + \Delta\sigma'_v(z)}{\sigma'_v(z)}\right)^{\frac{n}{2}} \tag{13}$$

The overburden-corrected shear wave velocity at a depth, $V_{s,F}$, evaluated in Equation 13 is a function of the shear wave velocity measured in the free-field at depth z, $V_s(z)$, effective stress from the self-weight of the soil at depth z, $\sigma'_v(z)$, the increment of vertical stress due to weight of the structure at depth z, $\Delta\sigma'_v(z)$,and the exponent n related to the soil type. The exponent n varies from 0.50 for granular soils (Hardin and Black, 1969; and Marcuson and Wahls, 1972) to 1.0 for cohesive soils with the plasticity index (PI) greater than 6.5 (Yamada et al., 2008).

Degree of Freedom	Pais and Kausel (1988)	Pais and Kausel (1988)
Translation along z-axis	$K_{z,sur}=\frac{GB}{1-\nu}\left[3.1\left(\frac{L}{B}\right)^{0.75}+1.6\right]$	$\eta_z=\left[1.0+\left(0.25+\frac{0.25}{L/B}\right)\left(\frac{D}{B}\right)^{0.8}\right]$
Translation along y-axis	$K_{y,sur}=\frac{GB}{2-\nu}\left[6.8\left(\frac{L}{B}\right)^{0.65}+0.8\left(\frac{L}{B}\right)+1.6\right]$	$\eta_y=\left[1.0+\left(0.33+\frac{1.34}{1+L/B}\right)\left(\frac{D}{B}\right)^{0.8}\right]$
Translation along x-axis	$K_{x,sur}=\frac{GB}{2-\nu}\left[6.8\left(\frac{L}{B}\right)^{0.65}+2.4\right]$	$\eta_x\approx\eta_y$
Torsion about z-axis	$K_{zz,sur}=GB^3\left[4.25\left(\frac{L}{B}\right)^{2.45}+4.06\right]$	$\eta_{zz}=\left[1+\left(1.3+\frac{1.32}{L/B}\right)\left(\frac{D}{B}\right)^{0.9}\right]$
Rocking about y-axis	$K_{yy,sur}=\frac{GB^3}{1-\nu}\left[3.73\left(\frac{L}{B}\right)^{2.4}+0.27\right]$	$\eta_{yy}=\left[1.0+\frac{D}{B}+\left(\frac{1.6}{0.35+(L/B)^4}\right)\left(\frac{D}{B}\right)^2\right]$
Rocking about x-axis	$K_{xx,sur}=\frac{GB^3}{1-\nu}\left[3.2\left(\frac{L}{B}\right)+0.8\right]$	$\eta_{xx}=\left[1.0+\frac{D}{B}+\left(\frac{1.6}{0.35+L/B}\right)\left(\frac{D}{B}\right)^2\right]$

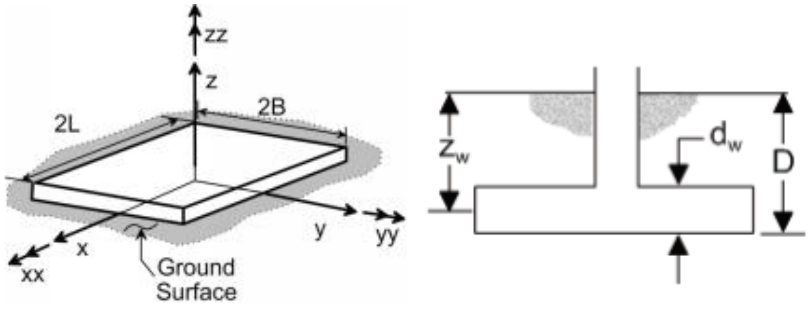

Figure 12. Elastic solutions for static stiffness of rigid footings at the ground surface and embedment correction factors (NIST, 2012)

Degree of Freedom	Surface Stiffness Modifier
Translation along z-axis	$\alpha_z = 1.0 - \left[\frac{\left(0.4 + \frac{0.2}{L/B}\right) a_0^2}{\left(\frac{10}{1+3(L/B-1)} \right) + a_0^2} \right]$
Translation along y-axis	$\alpha_y = 1.0$
Translation along x-axis	$\alpha_x = 1.0$
Torsion about z-axis	$\alpha_{zz} = 1.0 - \left[\frac{\left(0.33 - 0.03\sqrt{L/B-1}\right) a_0^2}{\left(\frac{0.8}{1+0.33(L/B-1)} \right) + a_0^2} \right]$
Rocking about y-axis	$\alpha_{yy} = 1.0 - \left[\frac{0.55 a_0^2}{\left(0.6 + \frac{1.4}{(L/B)^3} \right) + a_0^2} \right]$
Rocking about x-axis	$\alpha_{xx} = 1.0 - \left[\frac{\left(0.55 + 0.01\sqrt{L/B-1}\right) a_0^2}{\left(2.4 - \frac{0.4}{(L/B)^3} \right) + a_0^2} \right]$

Notes: Orient axes such that $L \geq B$.

Soil hysteretic damping, β_s, is additive to foundation radiation damping, β_j.

$a_0 = \omega B / V_s$; $\psi = \sqrt{2(1-\nu)/(1-2\nu)}$; $\psi \leq 2.5$

Figure 13. Dynamic stiffness modifiers for rigid footings suggested by Pais and Kausel (1988) (NIST, 2012)

After computing $V_{s,F}$, the average effective shear wave velocity, $V_{s,avg}$, is calculated for the appropriate depth interval. Stewart et al. (2003) suggested the depth interval, z_p, for computing $V_{s,avg}$. The following equation can be used for evaluating $V_{s,avg}$:

$$V_{s,avg} = \frac{z_p}{\sum_{i=1}^{n}\left(\Delta z_i \Big/ \left(V_{s,F}(z)\right)_i\right)} \tag{14}$$

$$Horizontal\ (x\ and\ y):\ z_p = B_e^A, B_e^A = \sqrt{A/4} = \sqrt{BL} \tag{15}$$

$$Rocking\ (xx):\ z_p = B_e^I, xx: B_e^I = \sqrt[4]{0.75 I_x} = \sqrt[4]{B^3 L} \tag{16}$$

$$Rocking\ (yy):\ z_p = B_e^I, yy: B_e^I = \sqrt[4]{0.75 I_y} = \sqrt[4]{B L^3} \tag{17}$$

Degree of Freedom	Radiation Damping
Translation along z-axis	$\beta_z = \left[\frac{4\left[\psi(L/B)+(D/B)(1+L/B)\right]}{\left(K_{z,emb}/GB\right)}\right]\left[\frac{a_0}{2\alpha_z}\right]$
Translation along y-axis	$\beta_y = \left[\frac{4\left[L/B+(D/B)(1+\psi L/B)\right]}{\left(K_{y,emb}/GB\right)}\right]\left[\frac{a_0}{2\alpha_y}\right]$
Translation along x-axis	$\beta_x = \left[\frac{4\left[L/B+(D/B)(\psi+L/B)\right]}{\left(K_{x,emb}/GB\right)}\right]\left[\frac{a_0}{2\alpha_x}\right]$
Torsion about z-axis	$\beta_{zz} = \left[\frac{(4/3)\left[3(L/B)(D/B)+\psi(L/B)^3(D/B)+3(L/B)^2(D/B)+\psi(D/B)+(L/B)^3+(L/B)\right]a_0^2}{\left(\frac{K_{zz,emb}}{GB^3}\right)\left[\left(\frac{1.4}{1+3(L/B-1)^{0.7}}\right)+a_0^2\right]}\right]\left[\frac{a_0}{2\alpha_{zz}}\right]$
Rocking about y-axis	$\beta_{yy} = \left[\frac{(4/3)\left[\left(\frac{L}{B}\right)^3\left(\frac{D}{B}\right)+\psi\left(\frac{D}{B}\right)^3\left(\frac{L}{B}\right)+\left(\frac{D}{B}\right)^3+3\left(\frac{D}{B}\right)\left(\frac{L}{B}\right)^2+\psi\left(\frac{L}{B}\right)^3\right]a_0^2}{\left(\frac{K_{yy,emb}}{GB^3}\right)\left[\left(\frac{1.8}{1+1.75(L/B-1)}\right)+a_0^2\right]}+\frac{\left(\frac{4}{3}\right)\left(\frac{L}{B}+\psi\right)\left(\frac{D}{B}\right)^3}{\left(\frac{K_{yy,emb}}{GB^3}\right)}\right]\left[\frac{a_0}{2\alpha_{yy}}\right]$
Rocking about x-axis	$\beta_{xx} = \left[\frac{(4/3)\left[\left(\frac{D}{B}\right)+\left(\frac{D}{B}\right)^3+\psi\left(\frac{L}{B}\right)\left(\frac{D}{B}\right)^3+3\left(\frac{D}{B}\right)\left(\frac{L}{B}\right)+\psi\left(\frac{L}{B}\right)\right]a_0^2}{\left(\frac{K_{xx,emb}}{GB^3}\right)\left[\left(\frac{1.8}{1+1.75(L/B-1)}\right)+a_0^2\right]}+\frac{\left(\frac{4}{3}\right)\left(\psi\frac{L}{B}+1\right)\left(\frac{D}{B}\right)^3}{\left(\frac{K_{xx,emb}}{GB^3}\right)}\right]\left[\frac{a_0}{2\alpha_{xx}}\right]$
Notes:	Soil hysteretic damping, β_s, is additive to foundation radiation damping, β_f. $\alpha_{emb} = \alpha_{sur}$; from Table 2-3a $a_0 = \omega B / V_s$; $\psi = \sqrt{2(1-\nu)/(1-2\nu)}$; $\psi \le 2.5$

Figure 14. Radiation damping for embedded rigid footings suggested by Pais and Kausel (1988) (NIST, 2012)

In practice, the impedance functions are not adjusted for non-rigid foundation conditions. Alternatively, springs and dashpots are distributed along elements with the same stiffness as the

foundation component. These distributed springs and dashpots allow the foundation to deform in a natural manner due to the loads imposed by the structure and the spring and dashpot reactions (i.e., similar to the Winkler's approach). In order to do this with vertical springs, k_z is normalized by the foundation area to compute the stiffness intensity or coefficient of subgrade reaction, k_z^i, as follows:

$$k_z^i = \frac{k_z}{4BL} \tag{18}$$

Similarly, the dashpot intensity can be calculated as:

$$c_z^i = \frac{c_z}{4BL} \tag{19}$$

Table 2. Soil Modulus Reduction in terms of Effective Peak Acceleration, SDS/2.5[(1)], and Site Class (ASCE, 2010)

	Reduction Factor (G/G_0)		
	S_{DS}[(1)]/2.5		
Site Class	≤0.10	0.40	≥0.80
A	1.00	1.00	1.00
B	1.00	0.95	0.90
C	0.95	0.75	0.60
D	0.90	0.50	0.10
E	0.60	0.05	(2)
F	(2)	(2)	(2)

(1) SDS is the short period spectral response acceleration parameter defined ASCE/SEI 7-10; use straight-line interpolation for intermediate values of S_{DS}/2.5
(2) Value should be evaluated from site-specific response analyses

B.2 Beam-on-Nonlinear Winkler Foundation

The beam-on-nonlinear Winkler foundation (BNWF) model was introduced with the pioneering work of McClelland and Focht (1958), and this approach has been broadly used for

the lateral analysis of piles under static loads (Matlock, 1970; and Cox et al. 1974) and dynamic loads (Penzien, 1970; Nogami et al., 1992; Boulanger et al., 1999). In addition to the lateral analysis of piles, the Winkler's approach has been implemented with linear-elastic springs, similar to those presented in the previous section, in conjunction with gapping and damper elements (Chopra and Yim, 1985). Recently, BNWF models have been used for modeling the two-dimensional (2D) seismic behavior of shallow foundations with nonlinear springs allowing gapping and dashpot elements by Allotey and Naggar (2003 and 2007) as well as Raychowdury (2008). For the case of shallow foundations, BNWF models have the following attributes:

- The soil-structure interaction phenomena can be described by one-dimensional nonlinear springs and dashpots distributed along the soil-foundation interface.
- This model can represent the behavior of the soil-foundation system due to inelastic soil behavior (material nonlinearity) and uplift (geometric nonlinearity). In this context, a nonlinear material can follow a nonlinear load-displacement path, but it may not return along the same path due to permanent plastic deformations and cyclic degradation effects. Inelastic behavior refers to the development of gaps during cyclic loading. Thus, the BNWF can capture rocking, sliding, and permanent settlement of the footing. Hysteretic energy dissipation and radiation damping can also be evaluated.
- A variable stiffness distribution and spring spacing can be used at the end of footings to account for larger reactions at the end of rigid foundations and to include the effect of rotational stiffness.
- This model is numerically efficient to perform linear and nonlinear analyses

Despite the aforementioned advantages of BNWF models, a limitation of this approach is its one-dimensional nature. Springs and dashpots respond only to loads parallel to their axes, so

loads acting in a perpendicular direction have no effect on the response of these elements. Therefore, plastic potential and flow rules cannot be explicitly incorporated in this model. Although BNWF models can have issues during implementation, this approach is frequently used in research and practice because of its simplicity and its ability to capture the experimental response of different soil-structure interaction problems.

As mentioned above, the Winkler's approach can be used with either linear or nonlinear materials. These two types of materials are used to model the spring constitutive behavior. Linear-elastic materials use an initial elastic stiffness and have an infinite capacity; however, this is not a realistic assumption for load demands during moderate earthquakes based on experimental work on shallow foundations (Gajan, 2006). Another material which is frequently used in practice is the elastic-perfectly-plastic (EPP) material. This material model has an initial elastic stiffness and it reaches its maximum stress capacity at a certain level of strain called "yielding strain." After the yielding point, this material enters into a plastic region where it can strain without any increment in stress. For the seismic analysis of shallow footings, the maximum capacity of EPP materials used for the vertical springs is usually limited by the unfactored bearing capacity of the footing, while the maximum capacity for the lateral springs is limited by both the unfactored frictional resistance and the passive resistance of the footing. Since the transition between the elastic and plastic regions for EPP materials is very abrupt, this material model is an idealization of the real soil behavior.

There are also some nonlinear materials available to model the constitutive behavior of springs. Boulanger (2000) developed nonlinear material models for the seismic analysis of pile foundations. These models were then adapted and calibrated by Raychowdhury (2008) for the seismic analysis of shallow foundations. The nonlinear models used for shallow foundations

simulate the vertical load-displacement behavior, horizontal passive load-displacement behavior against one side of the footing, and horizontal shear-sliding behavior at the base of the footing, and they are denoted in Raychowdhury (2008) as QzSimple2, PxSimple1, TxSimple1, respectively. The original versions of these nonlinear materials presented by Boulanger (2000) are called QzSimple1, PySimple1, and TzSimple1. These materials are able to capture the "far-field" elastic behavior and the "near-field" permanent displacements. A dashpot is used in parallel with the far-field elastic component to account for radiation damping, as can be seen in Figure 15.

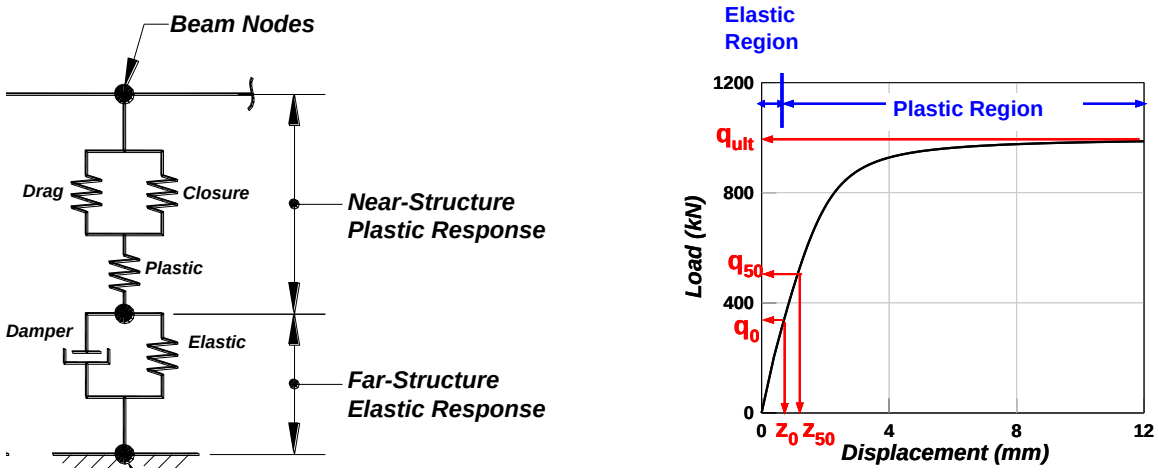

(a) **(b)**

Figure 15. (a) Idealization of nonlinear springs material models and (b) parameters of the backbone for the q-z material (Boulanger, 1999)

The equations and parameters used to describe the QzSimple1 and TzSimple1 materials are similar to those for the PySimple1 material presented in Boulanger (1999). The elastic portion of the backbone curve of these materials can be described using the following equation:

$$q = k_{in} z \tag{20}$$

Then, the range of the elastic portion can be defined by

$$q_0 = C_r q_{ult} \tag{21}$$

where the instantaneous load, q, in Equation 20 is obtained as the product of the initial elastic stiffness (tangent), k_{in}, and the instantaneous displacement, z. The load at the yield point, q_0, described in Equation 21 is a function of the parameter controlling the range of the elastic portion, C_r, and the ultimate load, q_{ult}.

The nonlinear portion of the backbone curve is described by

$$q = q_{ult} - (q_{ult} - q_0)\left[\frac{cz_{50}}{cz_{50} + \left|z^p - z_0^p\right|}\right]^n \tag{22}$$

where the instantaneous load, q, in Equation 22 is a function of the previously defined parameters q_{ult} and q_0, and the displacement at which 50% of ultimate load is mobilized, z_{50}, displacement at the yield point, z_0, c and n are the constitutive parameters controlling the shape of the post-yielding portion of the backbone curve. A closure and drag spring in parallel are used to represent the gap component of the near-field spring. The closure component (q^c - z^g) is a simple bilinear spring, which is relatively rigid in compression and very flexible in tension. The nonlinear drag component (q^d - z^g) of the backbone curve is characterized by

$$q_d = C_d q_{ult} - (C_d q_{ult} - q_0^d)\left[\frac{z_{50}}{z_{50} + 2\left|z^g - z_0^g\right|}\right] \tag{23}$$

Equation 23 describes the drag force on the closure component, q_d, as a function of the previously defined parameters q_{ult} and z_{50}, and the load at the start of the loading cycle, ($q_0^d = q^d$), displacement at the start of the current loading cycle, ($z_0^g = z^g$), and the ratio of the maximum drag (suction) force to q_{ult}, C_d.

Equations 20, 21, 22, and 23 were originally developed for pile foundations, but they can be used for the nonlinear springs developed by Raychowdhury (2008) for shallow foundations (i.e., QzSimple2, PxSimple1, and TxSimple1) using different values for the constants *n*, *c*, and C_r. Suggested values for the constants *n*, *c*, and C_r obtained from physical tests are summarized in Table 3, for pile and shallow foundations. A comparison between the backbone curves of the nonlinear springs developed for pile and shallow foundations is presented in Figure 16. The cyclic response of the QzSimple2, PxSimple1, and TxSimple1materials is shown in Figure 17.

Table 3. Parameters for defining the spring material backbone curves (Raychowdhury, 2008).

Material Type	Soil Type	OpenSees recommended value (calibrated from pile tests)			References	Values used suggested by Raychowdhury (2008) (calibrated from shallow footing tests if available)		
		C_r	n	c		C_r	N	c
QzSimple1	clay	0.2	1.2	0.35	*Reese & O'Neill (1988)*	0.22	1.2	0.5
	sand	0.3	5.5	12.3	*Vijayvergiya (1977)*	0.36	5.5	9.29
PySimple1	clay	0.35	5	10	*Matlock (1970)*	-	-	-
	sand	0.2	2	0.5	*API (1993)*	0.33	2	1.1
TzSimple1	clay	0.5	1.5	0.5	*Reese & O'Neill (1988)*	-	-	-
	sand	0.5	0.85	0.6	*Mosher (1984)*	0.48	0.85	0.26

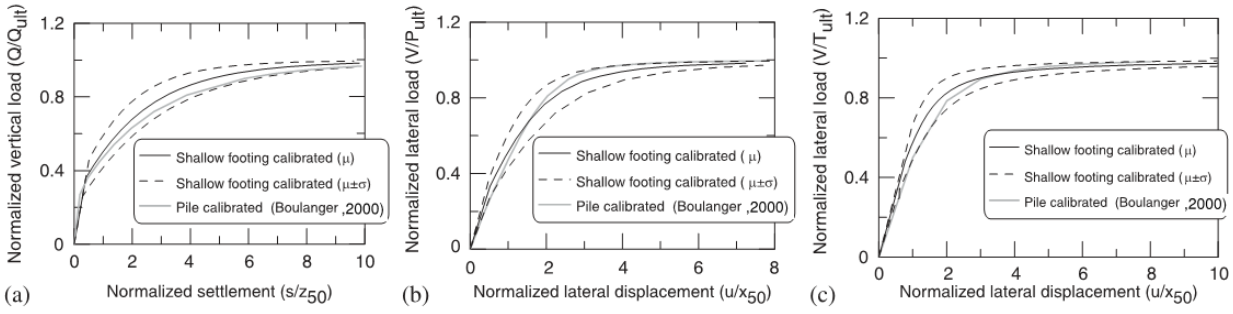

Figure 16. Backbone curves for: (a) q-z spring (QzSimple1 and QzSimple2); (b) p-x spring (PySimple1 and PxSimple1); and (c) t-x spring (TzSimple1 and TxSimple1 (adapted from Raychowdhury and Hutchinson, 2009)

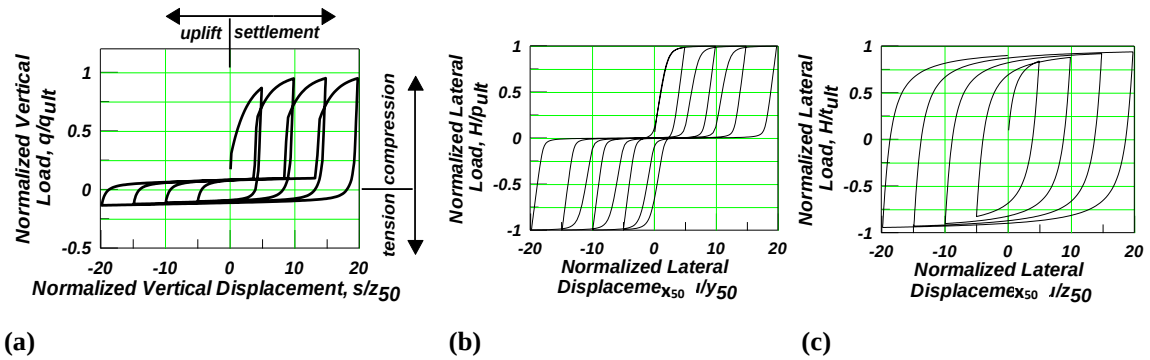

Figure 17. Cyclic response of: (a) q-z spring (QzSimple2); (b) p-x spring (PxSimple1); and (c) t-x spring (TxSimple1) (adapted from Raychowdhury and Hutchinson, 2009)

The nonlinear spring materials discussed above can reasonably capture results obtained with physical tests. For instance, Figure 18 shows a comparison of the BNWF model of Raychowdhury and Hutchinson (2009) with results obtained from centrifuge test SSG04-06 reported by Thomas et al. (2005). The test conducted was a slow, cyclic test on a medium aspect ratio shear wall structure, with a vertical factor of safety, FS_v = 2.3, resting on a dense sand with D_r = 80%. In general, the numerical model was able to capture the responses for moment versus rotation, settlement versus rotation, shear force versus sliding, and settlement versus sliding histories obtained from the centrifuge test.

All the previously defined linear-elastic, elastic-perfectly plastic, and nonlinear material models used to model the flexibility of the soil using springs and dashpots can be implemented in OpenSees, *Open System for Earthquake Engineering Simulation*, (OpenSees, 2016) using 2D or 3D models and either the direct or substructure approach for SSI.

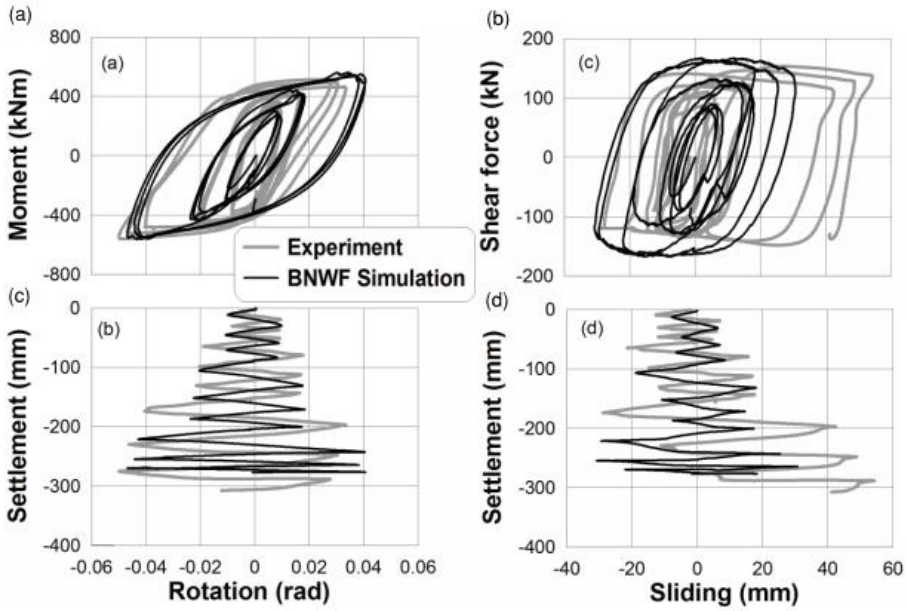

Figure 18. Comparison of the BNWF model response with a centrifuge test for a medium aspect ratio shear wall structure on dense sand, with *Dr* = 80% and FS_v = 2.3: (a) moment-rotation; (b) settlement-rotation; (c) shear-sliding; and (d) settlement-sliding (Raychowdhury and Hutchinson, 2009)

C. Kinematic Interaction

Motions at the free surface or free-field motions (FFMs) can deviate from this condition due to the presence of a foundation system on or in the soil. This phenomenon is called "kinematic interaction" and the resulting motion at the foundation level is detonated foundation input motion (FIM). These deviations from the FFM can be attributed to three main mechanisms: base-slab averaging, embedment effects, and wave scattering. The stiffness of the foundation systems causes the averaging of the FFMs related to inclined and/or incoherent waves and this effect is known as "base-slab averaging." Embedment effects result in the reduction of seismic ground motions with depth for embedded foundations, while wave scattering is caused by the scattering of seismic waves off of corners and asperities of the foundation. These three mechanisms resulting from kinematic interaction can be described by complex-valued transfer

functions relating free-field and foundation motions. In the following sections, base-slab averaging and embedment effects are explained and discussed. Wave scattering is not included because its effects on base-slab motions have been barely investigated and are usually ignored.

C.1 Base-Slab Averaging

For vertically propagated coherent waves**,** the motion of a rigid foundation on the surface is the same as the FFM. On the other hand, motions of foundations at the surface are modified relative to the free-field motion when seismic waves are incoherent. The incoherence of incident waves at two different points refers to variations in their phase angle. This effect is also greater at higher frequencies. This phenomenon is caused by different ray paths and local heterogeneities in the geologic media through which seismic waves travel. Therefore, base-slab averaging is caused by waves which have an incidence angle relative to the vertical, α_v, or which are incoherence in time and space.

Some incoherence is predictable because it results from the wave passage. The wave passage effect is related to the presence of non-vertical incident waves which arrive at different points along the foundation of a building at different times. In this context, the apparent propagation velocity, V_{app}, can be used to relate non-vertical incident waves with an apparent horizontal velocity using α_v, as shown in Figure 19a.

Lagged coherence models are used to quantify the incoherence that remains when waves are aligned to have common arrival times, which is stochastic in nature. Stochastic incoherence results from source-to-site heterogeneities in the seismic path of travel, which scatters seismic waves. Array studies such as Abrahamson et al. (1991) and Ancheta et al. (2011) explained and discussed this phenomenon of lagged coherency.

Translational base-slab motions are reduced relative to the free field, and torsional rotation of the base slab takes place due to the presence of incoherent or non-vertically incident waves (Stewart et al, 1998). The base-slab translation decrement as well as the appearance of torsion and rocking increases with the frequency. This frequency-dependent behavior is mainly a product of the effective size of the foundation relative the seismic wavelengths at higher frequencies.

The reduction of base-slab translation as well as the introduction of torsion and rocking are more significant with increasing frequency. The frequency-dependence of these effects is mainly associated with the increment of the effective size of the foundation relative the seismic wavelengths at higher frequencies.

There are many analytical equations for predicting the relationship between the foundation input motion (FIM) and the free-field motion (FFM) for the case of inclined, otherwise coherent, shear waves. A model was suggested by Mylonakis et al. (2006) which considers wave passage effects to evaluate transfer functions, H_u. This model relates the acceleration, velocity, or displacement of the foundation input motion, u_{FIM}, and the free-field motion, u_g, as follows:

$$u_{FIM} = H_u u_g \tag{24}$$

$$H_u = \frac{\sin\left(a_0^k\left(\frac{V_s}{V_{app}}\right)\right)}{a_0^k\left(\frac{V_s}{V_{app}}\right)}, a_0^k \leq \frac{\pi}{2}\frac{V_{app}}{V_s} \tag{25}$$

$$H_u = \frac{2}{\pi}, a_0^k > \frac{\pi}{2}\frac{V_{app}}{V_s} \tag{26}$$

$$a_0^k = \frac{\omega B_e^A}{V_s} \tag{27}$$

In Equation 27 the term B_e^A is related to the foundation area and was defined in the previous section. From arrays studies (Ancheta et al., 2011), V_{app} ranges from approximately 2.0 km/s to 3.5 km/s, so a reasonable estimation of the velocity ratio, V_{app}/V_s, for typical soils is approximately 10. The transfer function obtained using the equations 24 to 27 is shown in Figure 19b and labeled as "wave passage only." This model for wave passage alone produces modest base-slab reductions in ground motions. Indeed, transfer functions obtained from recorded foundation input motions and free-field motions are commonly lower at high frequencies than those predicted by wave passage models.

A semi-empirical model was developed based on the analytical solutions proposed by Veletsos and Prasad (1989) and Veletsos et al. (1997). In these studies, spatially variable ground motions were applied to a rigid foundation perfectly bonded to the soil. These studies evaluated the responses of rigid, massless, circular and rectangular foundations on the surface of an elastic half-space to incoherent S-waves propagating either vertically or at an angle α_v using numerical modeling. These results showed that the transfer function, H_u, obtained is independent of the foundation geometry, but it is strongly dependent upon a parameter, κ_a, related to the lagged coherency and wave inclination. The resulted transfer function for vertically propagating waves (adapted from Veletsos and Prasad, 1989) can be expressed as:

$$H_u = \left\{\frac{1}{b_0^2}[1 - \exp(-2b_0^2)(I_0(2b_0^2) + I_1(2b_0^2)]\right\}^{\frac{1}{2}} \tag{28}$$

$$b_0 = \left(\sqrt{4/\pi}\right)\kappa_a a_0^k \tag{29}$$

where I_0 and I_1 are modified Bessel functions, zero and first order, respectively. The Bessel function summation in Equation 28 can be represented in terms of power series and exponential functions (Watson, 1995) as follows:

$$\left(I_0(2b_0^2) + I_1(2b_0^2)\right) = \begin{cases} 1 + b_0^2 + b_0^4 + \frac{b_0^6}{2} + \frac{b_0^8}{4} + \frac{b_0^{10}}{12} & for\ b_0 \le 1 \\ \exp(2b_0^2)\left[\frac{1}{\sqrt{\pi}b_0}\left(1 - \frac{1}{16b_0^2}\right)\right] & for\ b_0 > 1 \end{cases} \quad (30)$$

Kim and Stewart (2003) developed a semi-empirical model for κ_a by matching model predictions to observed variations between foundation input and free-field motions from instrumented buildings. This model can be written as:

$$\kappa_a = 0.00065V_s, \qquad 200 < V_s < 500\,m/s \quad (31)$$

Values of κ_a obtained from Equation 31take into account the combined effects of incoherence from wave passage and stochastic processes as well as Fourier amplitude variability. Transfer functions calculated with this semi-empirical approach for upper and lower limits of κ_a are shown in Figure 19b.

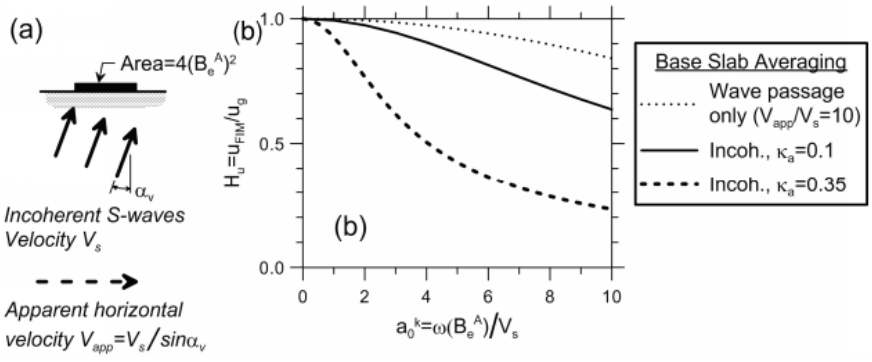

Figure 19. Base-slab averaging effects: (a) schematic geometry of a foundation subjected to inclined shear waves; (b) H_u using wave passage only and the semi-empirical method for incoherent waves (NIST, 2012)

C.2 Embedment Effects

For embedded foundations with lateral walls, such as buildings with basement levels, foundation-level motions experience a reduction as a result of the ground motion reduction with depth below the surface. Analytical solutions are available to consider embedment effects for rigid cylinders embedded in a uniform soil of finite or infinite thickness (i.e., half-space). Elsabee et al. (1977) and Dominguez and Roësset (1978) presented analytical solutions in the form of transfer functions for circular and rectangular embedded foundations subjected to vertically propagating coherent shear waves. Other studies conducted by Kausel et al. (1978) and Day (1978) describe FIM at the base of embedded cylinders as a function of FFMs. The FFM for these cylinders showed a reduction in its translation mode when subjected to vertically propagating coherent shear waves because of ground motion reductions with depth and wave scattering. In addition, as a result of differential displacements imposed to the cylinders over their embedment depth, rotations in the vertical plane developed. As a result of the aforementioned studies, transfer functions for translational and rotational motions, H_u and H_{yy}, were adapted for rectangular foundations as follows:

$$H_u = \frac{u_{FIM}}{u_g} = \cos\left(\frac{D}{B_e} a_0^k\right) = \cos\left(\frac{D\omega}{V_s}\right), \quad \frac{D\omega}{V_s} < 1.1 \tag{32}$$

$$H_u = 0.45, \qquad \frac{D\omega}{V_s} > 1.1 \tag{33}$$

$$H_{yy}(\omega) = \frac{\theta L}{u_g} = 0.26\left[1 - \cos\left(\frac{D\omega}{V_s}\right)\right], \quad \frac{D\omega}{V_s} < \frac{\pi}{2} \tag{34}$$

$$H_{yy}(\omega) = 0.26, \qquad \frac{D\omega}{V_s} > \frac{\pi}{2} \tag{35}$$

where D is the embedment depth and V_s is the average effective profile velocity, $V_{s,avg}$. The above equations suggested for evaluating translational and rotational transfer functions are plotted in Figure 20b. It can be seen in Figure 20b that there is a significant reduction in the FFM at high frequencies, at approximately 70% of the fundamental frequency of the soil column, f_E. By further inspection of Figure 20b, it is seen that the effect of the embedment on the de-amplification of the ground motions is greater in comparison with base-slab averaging. On the other hand, the rotational transfer function, H_{yy}, increases with frequency. Predictions for cylinder models using the previously developed transfer functions for this case showed good agreement with records from nuclear reactor structures and embedded buildings (Stewart and Tileylioglu, 2007).

All the equations previously presented in this section need to be carefully used. Most of these equations were calibrated for specific foundation conditions, soil types, and wave propagation directions, so their application is limited to those unique scenarios.

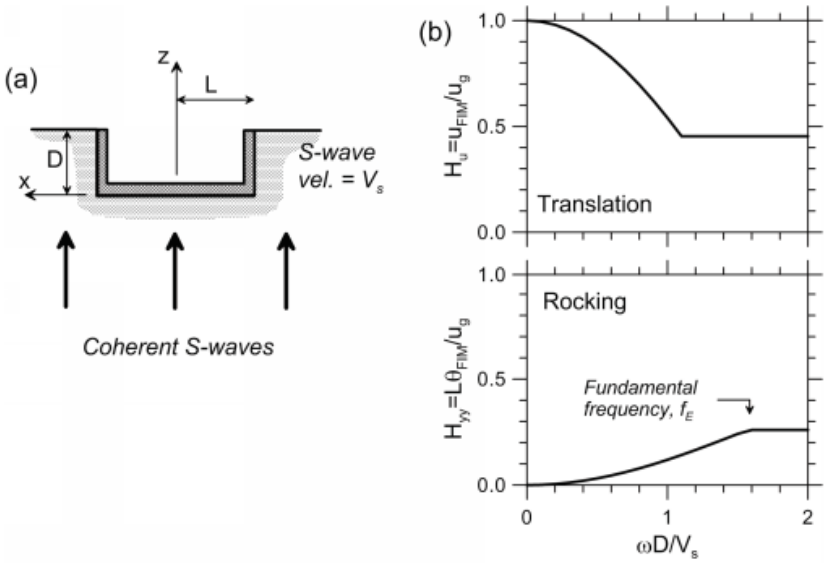

Figure 20. Foundation subjected to vertically incident shear waves: (a) schematic geometry; (b) transfer functions for foundation translation and rocking (NIST, 2012)

D. Eccentrically Braced Frames

Eccentrically braced frames (EBFs) are a hybrid lateral force-resisting systems which combine the lateral stiffness of steel concentrically braced frames and the ductility of steel moment resisting frames. Therefore, EBFs have high elastic stiffness, stable inelastic response under cyclic lateral loading, and excellent ductility and energy dissipation capacity. Since these types of ductile frames have been successfully implemented in regions of high seismicity, they have been a matter of research for many years. Research related to EBFs started in the mid-1970s (Roeder and Popov, 1978), continued through the 1980s (Engelhardt and Popov, 1989, 1992; Kasai and Popov, 1986a, 1986b; Ricles and Popov, 1987; Whitaker, Uang, and Bertero, 1987), and it is still currently active (Chao and Goel, 2006, Richards and Uang, 2006; Okazaki et al., 2006; Prinz and Richards, 2009; Richards, 2009).

EBFs use special segments beam called links which act as structural fuses under severe earthquakes, experiencing inelastic deformations while other structural elements behave essentially elastic. The typical arrangement of links in EBFs are at the middle of beams, between two braces, and at the end of beams, adjacent to columns (Figure 21). Links either yield in shear or flexure (Figure 22); however, the links that yield in shear typically have a greater rotational capacity than those that yield in flexure. Links that yield in shear are called “short links” and are typically used in the design of EBFs.

In the U.S., provisions for the analysis, design, and detailing of EBFs are included in the ANSI/AISC 341-10, *Seismic Provisions for Structural Steel Buildings* (ANSI/AISC, 2010). For these types of ductile structures, ANSI/AISC 341-10 requires that columns, braces, and beams be designed following capacity design principles; therefore, the full strength and deformation capacity can be developed without failure of any individual column, brace, or beam and without

the formation of a soft story. For this purpose, structural elements must be designed using the expected shear capacity of the links. In addition, ANSI/AISC 341-10 limits the rotation of short links to 0.08 radians. This limitation is primarily based on experiments conducted at the University of California at Berkeley in the 1980s (Hjelmstad and Popov, 1983; Malley and Popov, 1984; Kasai and Popov, 1986a; Ricles and Popov, 1989; Engelhardt and Popov, 1992). Special considerations are needed for EBFs with link-to-column connections since they have less inelastic rotation capacity than those with mid-span links (Okasaki et al., 2006).

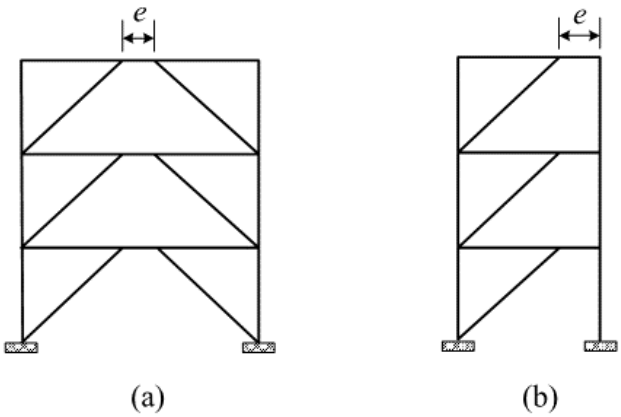

Figure 21. Typical eccentrically braced frames with (a) mid-span links and (b) links with column connections

To achieve the goals of the EBF design, it is necessary for the connections between the structure and the foundation, as well as the foundation itself to develop the full resistance and deformation capacity of the EBF. Unfortunately, current foundation design criteria do not require foundations to develop that same capacity, and uplift can occur if the foundation is underdesigned. If uplift is expected, this effect needs to be considered in the analysis of EBFs along with SSI in order to ensure that the assumed energy dissipation capacity is achieved. In addition, as mentioned before, including SSI effects on the seismic analysis of EBFs can enhance the accuracy of the analytical simulations.

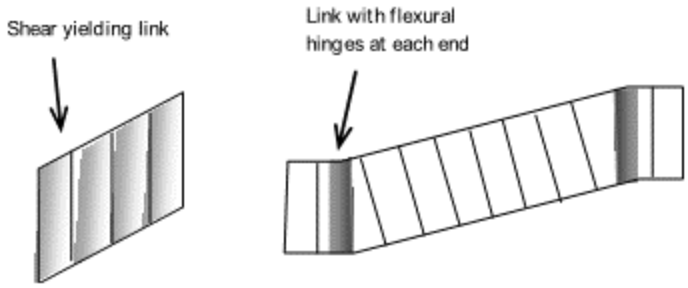

Figure 22. Typical link inelastic behavior (adopted from Prinz, 2010)

III. Methodology

As mentioned before, EBFs are sometimes used as the lateral load-resisting system of buildings in high seismic regions due to their efficient seismic performance and ability to accommodate architectural features. Nevertheless, achieving an economical and efficient design for this type of steel frame is challenging. In EBF design, the size of structural members depends on the expected shear capacity of the links, which usually have the same size as the beam. To achieve good seismic performance, beam sizes need to vary at each floor (Popov et al., 1992), so a balance between economy and performance is difficult to obtain.

In addition to the design considerations for the superstructure, connections between the foundation system and the foundation itself for EBFs need to be designed to develop the full capacity and deformation of these structures. This means that uplift can occur if the foundation system is underdesigned, so this effect needs to be taken into account. Therefore, studying the interaction between the structure, foundation system, and soil beneath has the advantage of being able to evaluate the collective performance of the system and include the additional energy dissipation capacity of the foundation-soil interface.

In this study, the seismic performance of EBFs considering SSI effects is investigated and compared with the commonly used support assumption of a fixed base. To achieve this goal, a 3-story office building is analyzed and evaluated using both the fixed base and flexible base. The building geometry and mass was slightly modified from a SAC study (Gupta and Krawinkler, 1999). A specific site in California was chosen to conduct the analyses due to the availability of site characterization data and its high seismic demand. The 3-story EBF was preliminary sized using the Equivalent Lateral Force (ELF) procedure according to ASCE/SEI7-10 and ANSI/AISC 341-10. In addition, the same frame was redesigned following the guidelines available in Chapter 19 of ASCE/SEI 7-10 for considering SSI along with the ELF procedure. Therefore, two frames were analyzed using the preliminary design with both a fixed and flexible based, and then the frame re-designed considering SSI was also evaluated with a flexible base. Nonlinear static analysis (NSA) and nonlinear response history analysis (NRHA) were conducted to evaluate the seismic performance of the EBFs described. Inter-story drifts, residual drifts, link rotations, and column demands were computed for each frame and then compared.

A. Building Description

Because SSI effects can be significant for stiff structures, a 3-story building was chosen for this study. The building prototype is similar to the one used in Prinz (2010). The EBFs were placed around the perimeter of the building. The typical bay width and story height of this building were 30 ft and 13 ft; respectively (Figure 23). A link length of 4 ft was used at every story. The building was assumed to be used for offices, and its importance factor (I) was taken as 1 according to ASCE/SEI 7-10. Accidental torsion for the linear analyses was also considered by assuming an eccentricity of 5% of the building plan between the center of mass and the center of

rigidity (ASCE, 2010). The total seismic weight of the 3-story EBF is 9,755 kips, and the weights of each story can be seen in Figure 23.

The Gilroy 2 site in California was used for the design of the 3-story EFBs. This site has site classification D with a design spectral acceleration at 0.20 seconds, S_{DS}, of 1.002 and a design spectral acceleration at 1.0 seconds, S_{D1}, of 0.654 in terms of gravity. Therefore, the seismic design category of the building used for this study is D, thus EBFs can be use as the lateral load-resisting system for this building (ASCE, 2010). A response modification coefficient, *R*, of 8 and a deflection amplification factor, C_d, of 4.0 were used for the design of the EBFs based on ASCE/SEI 7-10.

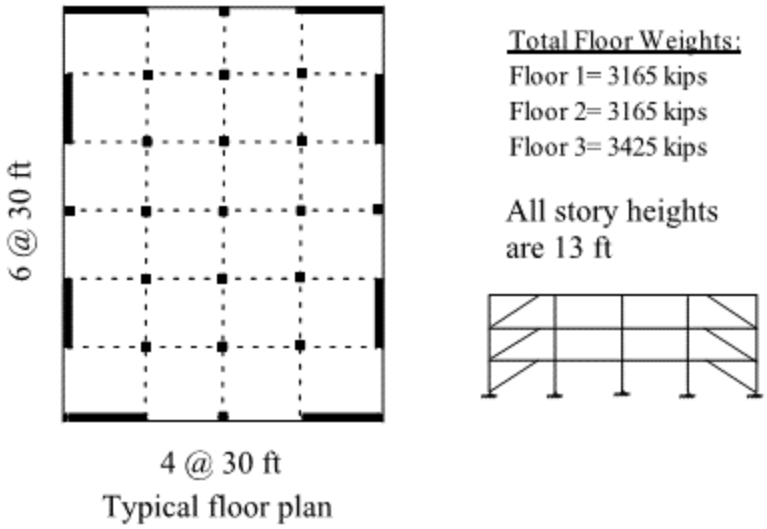

Figure 23. Frame configuration, dimensions, and floor weights for the 3-story EBFs (modified from Prinz, 2010)

B. Site Characterization

The location plan for the Gilroy 2 site is shown in Figure 24. The soil parameters (Table 4) and the geophysical (Figure 25) were obtained from Curras (2000). The foundations of the 3-

story building were placed on the topmost sand layer with a soil unit weight of 19 kN/m3 and an effective friction angle of 38 degrees. The water table was located at a depth of 22.5 m. The shear wave velocity profile is presented in Figure 25. Based on this profile, the average shear wave velocity for the first 30 m, $\bar{V}_{s30}$, is 283.10 m/s, so the site class according to ASCE/SEI 7-10 is D. Additionally, the average shear wave velocity for the entire soil profile, $\bar{V}_s$, is 467.3 m/s, and the shear wave velocity, V_s, of the sand layer where the foundations were placed is 200 m/s.

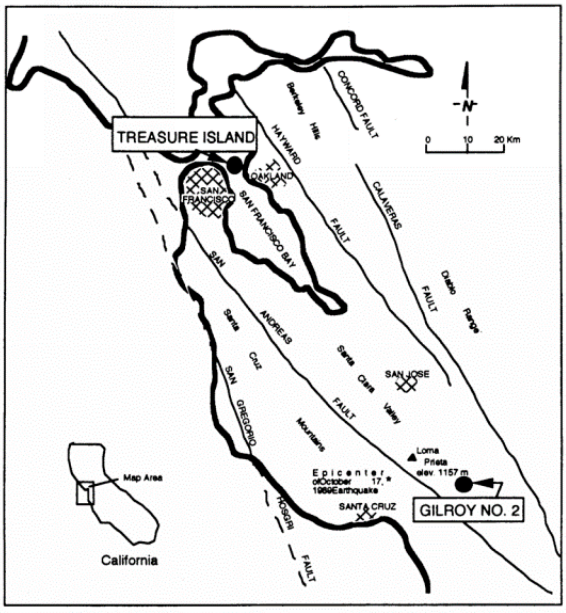

Figure 24. Map of the San Francisco Bay area locating the Gilroy 2 site

The shear modulus degradation curves and the damping curve for the Gilroy 2 site are shown in Figure 26. This figure shows curves for the sand and clay soils existing in this site as well as for the bedrock.

Table 4. Soil strength parameters for the Gilroy site 2 (Curras, 2000)

Depth (m)	Soil Type	γ (kN/m^3)	ϕ' (deg)	k (MN/m^3)	S_u/σ'_{vo}	OCR	ε_{50}
0-7.5	Sand	19	38	42.7	-	-	-
7.5-10.5	Clay	19	-	-	$0.35.OCR^{0.80}$	3.0	0.005
10.5-22.5	Sand	19	42	61.0	-	-	-
22.5*-42	Clay	19	-	-	$0.35.OCR^{0.80}$	4.0	0.005

*Ground water table at 22.5 m

Where:

γ = total unit weight,

ϕ' = effective friction angle,

k = soil modulus,

Su = undrained shear strength of the soil,

σ'_{vo} = initial effective vertical stress,

OCR = over-consolidation ratio,

ε_{50} = strain corresponding to 50% of the maximum principal stress difference on triaxial test

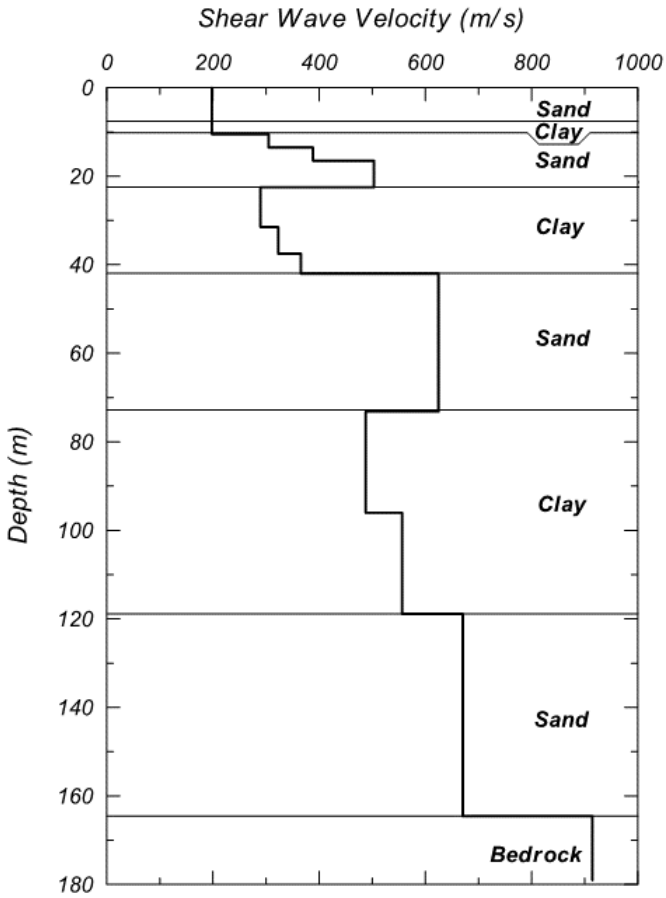

Figure 25. Shear wave velocity profile for the Gilroy 2 site (Curras, 2000)

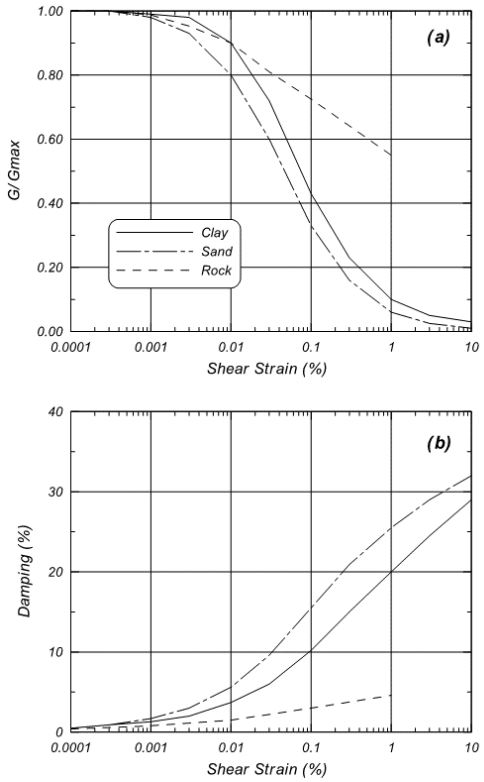

Figure 26. (a) Shear modulus and (b) damping curves for the different soils at Gilroy site 2 (Curras, 2000)

C. Eccentrically Braced Frame Designs

Because the gravity system of the building was assumed to be pin-connected to the lateral load-resisting system, the EBFs were decoupled from the spatial building structure and analyzed using 2-D models. Subsequently, the EBFs were designed using the factored forces obtained from the structural analysis conducted in SAP2000 (Computers and Structures Inc., 2009), and then those forces were used to design the structural elements according to ANSI/AISC 341-10. The load factor used to amplify the seismic forces was the ratio of the expected shear capacity of the link to the shear force in the link obtained from the structural analysis. This was done in order to follow the capacity based approach required for this type of steel frame.

Two sets of equivalent lateral forces were obtained for designing the EBFs. One set of forces was calculated to perform the structural analysis without SSI ($EBF1_{FB}$) and the other set of forces was used to conduct the structural analysis considering SSI ($EBF1_{SSI}$) based on ASCE/SEI 7-10. The equivalent lateral forces applied at each level for the two static analyses conducted are presented in Table 5, and the EBF designs are shown in Figure 27. The procedure for considering SSI according to ASCE/SEI 7-10 just reduces the static seismic forces due to the period elongation using the response spectrum approach, and then the structural analysis is conducted using a fixed base. To account for the effects of SSI, the base shear (V) according to ASCE/SEI 7-10 can be reduced as follows:

$$\tilde{V} = V - \Delta V \tag{36}$$

$$\Delta V = \left[C_s - \tilde{C}_s \left(\frac{0.05}{\tilde{\beta}} \right)^{0.4} \right] \overline{W} \leq 0.3V \tag{37}$$

$$\tilde{\beta} = \beta_0 \frac{0.05}{\left(\frac{\tilde{T}}{\overline{T}} \right)^3} \tag{38}$$

where $\tilde{V}$ is the base shear considering SSI and ΔV is the reduction in V due to SSI. The terms C_s, $\tilde{C}_s$, $\tilde{\beta}$, and $\overline{W}$ in Equation 37 and 39 are the seismic design coefficient for a fixed base, seismic design coefficient for a flexible base, fraction of critical damping for the structure foundation system, and the effective seismic weight of the structure, respectively.

Table 5. Equivalent lateral forces for the EBFs

Equivalent Lateral Force (kips)		
Floor	Without SSI ($EBF1_{FB}$)	Including SSI ($EBF1_{SSI}$)
1	177.99	148.40
2	106.25	88.60
3	50.34	42.00

D. Foundation Design

The foundation system was designed using the capacity of the structural elements from the superstructure. The bearing capacity was calculated using the soil parameters of the topmost sand layer presented in Table 4. Equations initially proposed by Terzaghi (1943) and later modified by Meyerhoff (1963) were used for evaluating the ultimate bearing capacity. The ultimate lateral capacity of the proposed foundation was evaluated using both its passive and friction resistance. Combined footings were used as a foundation for the EBFs while isolated footings were adopted as foundations for the gravity columns. The top of the foundation system was assumed to be at the grade level of the building. In addition, the slab on grade was designed to act as a rigid diaphragm at the grade level. Resistance factors for bearing capacity for seismic design suggested by FEMA P-750, *NEHRP Recommended Seismic Provisions for New Buildings and Other Structures* (FEMA, 2009), were applied to the ultimate bearing capacity calculated. Figure 28 shows the foundation plan for the building analyzed.

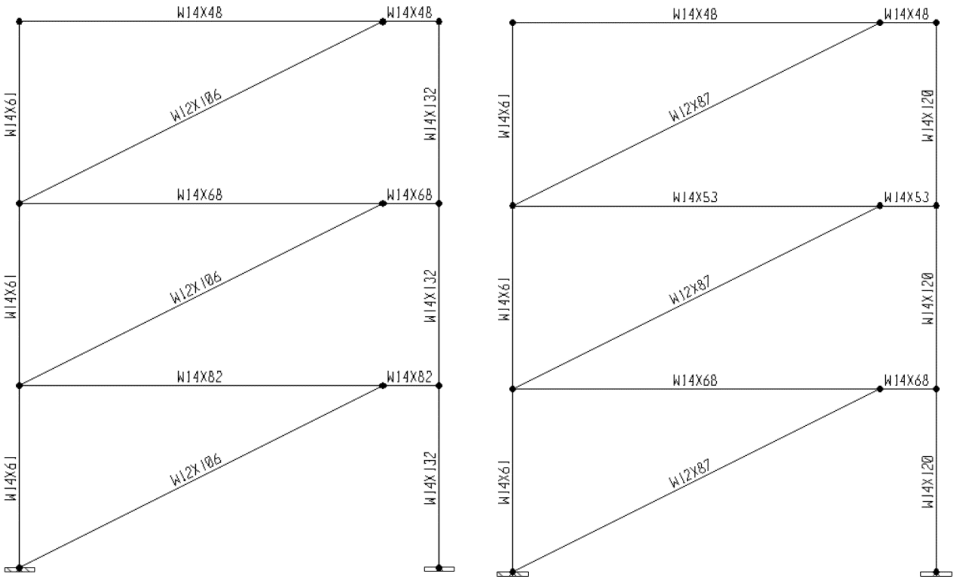

(a) (b)

Figure 27. EBF designs based on ASCE/SEI 7-10 and ANSI/AISC 341-10 (a) EBF without SSI (EBF1$_{FB}$); and (b) EBF considering SSI (EBF1$_{SSI}$)

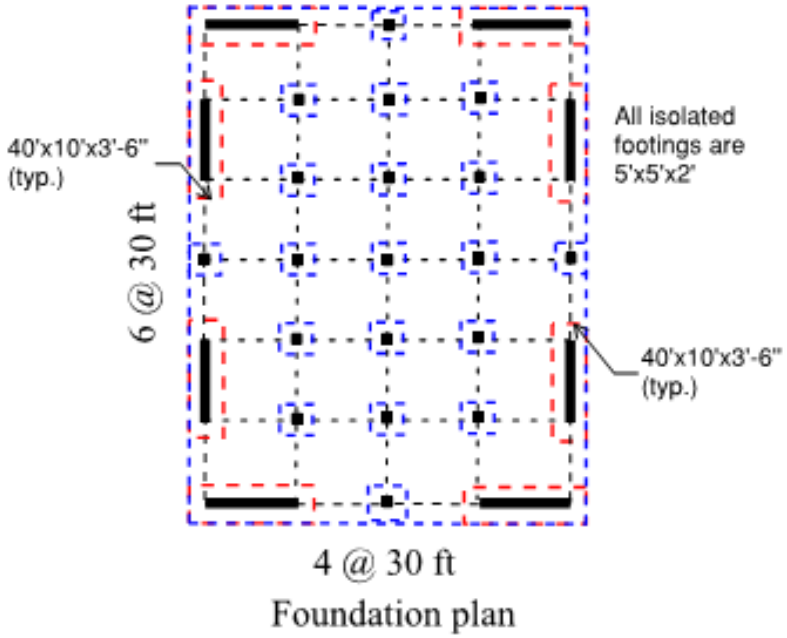

Figure 28. Foundation plan for the building analyzed

E. Evaluation of Foundation Springs and Dashpots

The foundation system designed for the building used in this study consists of shallow footings interconnected through the slab on grade. The methodologies described for inertial interaction were used to develop the foundation springs and dashpots for the EBFs. Parameters such as foundation dimensions, soil properties, embedment depth, and the fundamental period of the structure were used to compute the foundation impedances. The equations proposed by Pais and Kausel (1988) were chosen to evaluate the foundation springs and dashpots. Modeling of the EBF foundation and site conditions included the following:

- Determination of the average effective profile velocity for the shallow foundation of the EBFs, considering foundation dimension and overburden pressures from the structures
- Determination of the structure-to-soil stiffness ratio for estimating the importance of inertial interaction effects
- Calculation of the combined footing stiffness and damping in the vertical and horizontal directions, as well as the rotational component for stiffness and damping
- Distribution of springs and dashpots along the foundation in the numerical model
- Evaluation of the limiting spring forces

For the typical case of soil profiles that vary with depth, foundation stiffness and damping coefficients should be based on an average effective profile velocity evaluated over an effective profile depth, z_p. Using z_p and considering the overburden pressure due to the weight of the building, $\Delta\sigma'_v(z)$, the average effective profile velocity, $V_{s,avg}$, is calculated using Equation 14. The $\Delta\sigma'_v(z)$ was calculated using the classical Boussinesq stress distribution theory. Table 6 shows the values of z_p and $V_{s,avg}$ for the different vibration modes used for modeling the EBFs.

Table 6. Effective profile depths and average effective profile velocities

Vibration Mode	z_p (ft)	Depth Range (ft)	$V_{s,avg}$ (ft/s)	Equation
Horizontal Translation (x)	10.0	3.5 to 13.5	708.40	15
Rocking along y-axis (yy)	14.10	3.5 to 17.6	694.30	17

In order to anticipate whether inertial interaction effects are significant for the building analyzed, the structure-to-soil stiffness ratio (*h/(Vs.T))* proposed by Stewart (1999b) was calculated. The effective height (*h*) and the fundamental period of vibration (*T*) with a fixed base were obtained from the modal analysis conducted for the EBF without considering SSI. The value of *Vs* used for this calculation was $V_{s,avg}$ for the rocking vibration mode. The parameters *h*, V_s, and *T* used to calculate *h/(Vs.T)* were 29.95 ft, 694.3 ft/s, and 0.72 sec, respectively, and the value obtained for *h/(Vs.T)* was 0.06. Because *h/(Vs.T)* < 0.10, inertial interaction effects are not expected to be considerable for the building analyzed (Stewart et al., 1999a, 1999b).

To incorporate the flexibility of the soil in the numerical models of the EBFs, the foundation stiffness and dashpot were computed, and they are shown in Table 6. Before computing the foundation impedances, the low strain shear modulus, G_0, was evaluated using the unit weight of soil for the uppermost sand layer and the values of $V_{s,avg}$ presented in Table 6. The large strain shear modulus, *G*, was calculated using a ratio G/G_0 of 0.50 as suggested in Table 2, for the S_{DS} and site class of the site analyzed.

For the case of the dynamic stiffness, k_{dyn} , the dynamic stiffness modifier, α, was evaluated using the frequency corresponding to the first-mode period of the EBF with a flexible base ($\tilde{T}$=0.80 sec) originally designed without considering SSI effects. The period of vibration for the flexible base condition was calculated using Equation 2 along with the static springs and dashpots calculated with the equations suggested by Pais and Kausel (1988). Then, the k_{dyn} was

evaluated as the product of α and the embedded static stiffness, k_{emb}. In addition, the soil damping, β_s, was taken as 0.07 from Table 1, for the S_{DS} and site class corresponding to the Gilroy site 2. The dynamic stiffness was computed using Equation 11 while the dashpot constant was evaluated as follows:

$$c = 2k_{dyn}\left(\frac{\beta_{emb} + \beta_s}{\omega}\right) \tag{39}$$

The terms β_{emb} and ω in Equation 39 are the damping as a ratio considering the embedment depth of the footing and the angular frequency of the soil-foundation system, respectively.

Table 7. Foundation stiffness and damping parameters for the EBF1SSI

Vibration mode	G (ksf)	k_{emb} (kip/ft(1); kip-ft/rad(2))	α	β_{emb}	c (kip-s/ft)
Vertical Translation, z-direction (k_z, c_z)	913.70	87,764.80	1.0	0.065	2,978.50
Horizontal Translation, x-direction (k_x, c_x)	913.70	74,574.60	1.0	0.057	2,366.55
Rocking along y-axis, yy –direction (k_{yy}, c_{yy})	898.30	28,949,064.90	1.0	0.001	512,830

(1) Units for translational stiffness
(2) Units for rotational stiffness

As shown in Table 7, the α is 1.0; therefore, k_{dyn} is equal to k_{emb}. Subsequently, the intensity of the vertical stiffness, k_z, and dashpot, c_z, were calculated using Equation 18 and 19; respectively. A value of 219.4 kip/ft^3 was obtained for k_z while c_z was estimated as 7.45 kip-s/ft^3.

The intensity of the vertical stiffness cannot be used along the entire length of the footing without including the effect of the rotational stiffness because the vertical soil reaction is not uniform. The vertical soil reaction tends to increase at the edges of the foundation, so assigning a uniform value of k_z underestimates the vertical stiffness at these locations. Using a similar procedure of assigning a uniform c_z would overestimate the radiation damping due to rocking. To correct for the underestimation of rotational stiffness, stiffer springs are assigned along the foundation edge, as shown in Figure 29. These springs with higher stiffness along with the springs the interior reproduce the effect of the rotational stiffness. The distance where the springs with higher stiffness are assigned is denoted as R_eL, where R_e is called the end length ratio. ATC 40 (1996) suggests that *Re* should be *B/6* (B = footing width) while Harden et al. (2005) suggests values for *Re* as a function of the footing aspect ratio, *B/L*. NIST (2012) suggests that R_e can vary between 0.30 to 0.50 and presents the following equation to evaluate the stiffness intensity ratio, R_k, for springs at the edges of footings:

$$Rocking\ (yy): R_{k,yy} = \frac{\left(\frac{3k_{yy}}{4k_zBL^3}\right) - (1-R_e)^3}{1-(1-R_e)^3} \tag{40}$$

To correct for overestimation of rotational damping, the dashpot intensities over the full length and width of the foundation are scaled down by a factor, R_c, as follows:

$$Rocking\ (yy): R_{c,yy} = \frac{\frac{3c_{yy}}{4c_zBL^3}}{R_{k,yy}(1-(1-R_e)^3) + (1-R_e)^3} \tag{41}$$

For this study, R_e was used as 0.375 and the resulting values for R_{kyy} and R_{cyy} were 2.95 and 0.52, respectively.

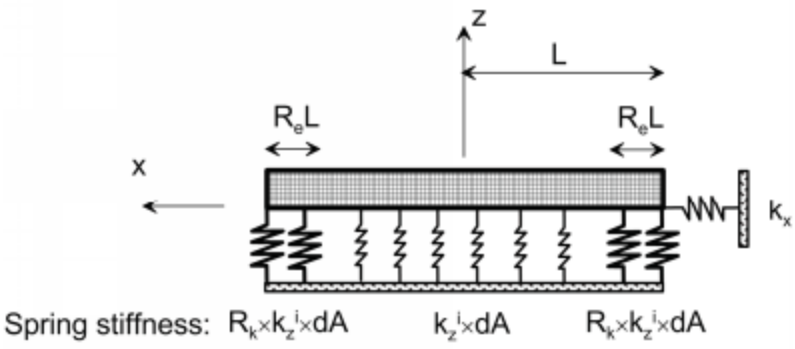

Figure 29. Vertical spring distribution to reproduce the rotational stiffness k_{yy} (NIST, 2012)

The foundation stiffness and dashpot were used for constructing linear-elastic (LE), elastic-perfectly plastic (EPP), and nonlinear springs (NL). Linear-elastic springs were estimated using only the foundation stiffness calculated and they were modeled along with dashpots by using a parallel material. For the case of elastic-perfectly plastic springs, the foundation stiffness evaluated was used as the slope of the force-displacement relationships. The ultimate capacity of EPP springs in the vertical direction was taken as the ultimate bearing capacity times the area of each spring ($q_u.dA$). Once the maximum capacity of the spring is calculated, the yielding displacement can be evaluated. The same process was followed to evaluate EPP springs in the horizontal direction, where the maximum capacity of these springs was taken as the sum of the ultimate passive and frictional resistance of the footing. The EPP springs were combined with dashpots in a parallel material.

The ultimate bearing capacity, ultimate passive resistance, and ultimate frictional resistance used for calculating the maximum capacity of EPP springs were computed using the equations suggested in AASHTO 2010, *AASTHO LRFD Bridge Design Specifications* (AASHTO, 2010). Figure 30 shows the force-displacement relationship evaluated for vertical EPP springs for this study. Lower and upper bounds for the force-displacement relationships

were also included in Figure 30 following the recommendations of NIST (2012) and ASCE/SEI 41-13. These documents state that lower and upper bounds need to be evaluated for accounting for variability of the soil properties. Since there is no information about differences for the soil tests conducted at the site, upper and lower bound were estimated as two times and half the spring stiffness and maximum capacity computed (NIST, 2012; ASCE, 2013), respectively. These upper and lower bounds are shown as an illustration of the suggested presentation of these types of load-deformation relationships, and only the expected curve was used for this study.

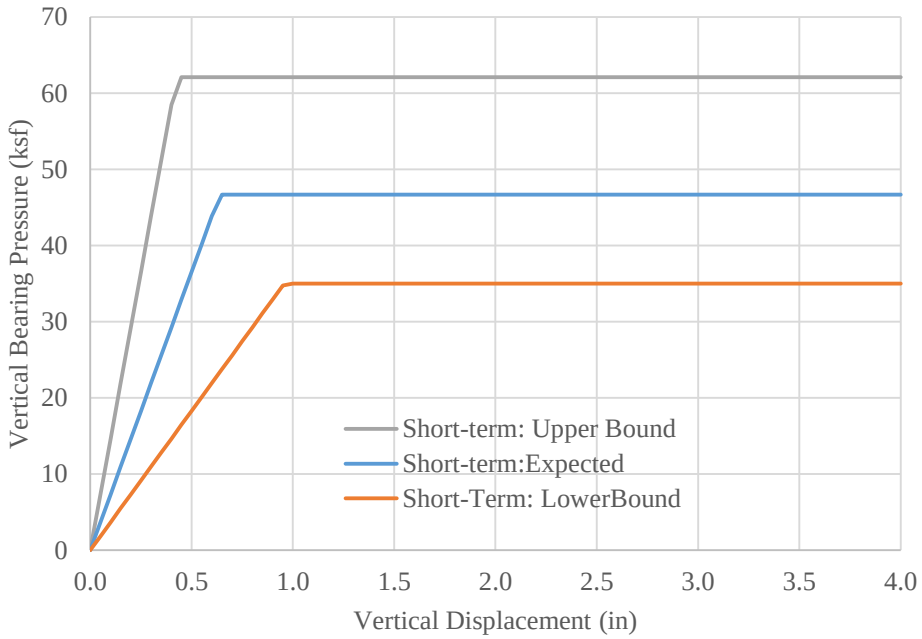

Figure 30. Force-displacement relationship for interior vertical springs

Nonlinear springs were also used for the numerical simulations in this study. The nonlinear springs used for modeling SSI were those developed by Boulanger (2000) for pile foundations and later calibrated by Raychowdhury (2008) for the seismic analysis of shallow foundations. Parameters for the backbones curve for the springs QzSimple2, PxSimple1, and TxSimple1 were taken from Table 3. For the QzSimple2 material, the backbone curve for sands

suggested by Vijayvergiya (1977) was used. The ultimate vertical capacity (q_{ult}) of individual springs and the foundation damping ratio in the vertical direction previously computed were also used. A suction of 0.10 times q_{ult} was adopted. As the last parameter needed for this material, the displacement at which 50% of q_{ult} is mobilized in monotonic loading, z_{50}, was evaluated using a relationship suggested by Boulanger (2000):

$$z_{50} = \frac{1.39 q_{ult}}{k_{zi}} \tag{42}$$

The term k_{zi} in Equation 42 refers to the vertical stiffness of a single spring. The backbone curve proposed for sands in API (1993) was used for the material Pxsimple1. The passive resistance (p_{ult}) of the footing and the foundation damping ratio in the horizontal direction computed were used. A drag resistance factor, C_d, of 0.10 times p_{ult} was applied. The displacement at which 50% of p_{ult} is mobilized in monotonic loading, y_{50}, was computed using the following relationship (Boulanger, 2000):

$$y_{50} = \frac{0.542 p_{ult}}{k_x} \tag{43}$$

The backbone curve for sands suggested by Mosher (1984) was used for the TxSimple1 material. The friction resistance (t_{ult}) of the footing and the foundation damping ratio in the horizontal direction computed were used. The displacement at which 50% of t_{ult} is mobilized in monotonic loading, z_{50}, was also assessed using a relationship suggested by Boulanger (2000):

$$y_{50} = \frac{2.05 t_{ult}}{k_x} \tag{43}$$

All the spring materials evaluated above were used along with the Winkler's approach for considering inertial interaction in numerical models with a flexible base.

F. Numerical Modeling

For the nonlinear analyses, two-dimensional models were used to analyze the EBFs using OpenSees Navigator (Schellenberg and Yang, 2016). OpenSees Navigator is a MATLAB-based graphical user interface (GUI) which is used for pre- and post-processing OpenSees files. All columns, beams, and braces were modeled using nonlinear beam-column elements with inelastic fiber sections (i.e., elements with distributed plasticity). Floor masses were lumped into the column nodes at each story. Full dead load plus 25% of the unreduced live load were assigned to the columns nodes at each story (ASCE, 2010; PEER, 2010). Braces were assumed to have fully-restrained end connections. All beam-column connections were also assumed to be fully restrained. Columns were oriented to resist lateral forces through strong-axis bending.

The material behavior for all beams, columns, and braces was modeled using a Giuffre-Menegotto-Pinto material model (Menegotto and Pinto, 1973) with isotropic strain hardening and yield strength of 50 ksi, called Steel 02 in OpenSees. The dynamic behavior of the EBF shear links was idealized using the analytical model proposed by Ramadan and Ghobarah (1995) and modified slightly by Richards (2004). In order to use this material model in OpenSees Navigator, EBF links were idealized as an elastic beam element with lumped plasticity and translational springs in parallel at each end. These springs were modeled using an elastic-perfectly-plastic material, and then they were combined into a single uniaxial parallel material model. The parallel material was then applied to a zero-length elements. Figure 31a and 31b show the proposed link element and its constitutive behavior, respectively. The validation of the experimental test conducted on EBF links following the protocol outlined in the 2002 AISC Seismic Provisions (ANSI/AISC, 2002) is shown in Figure 31c and 31d.

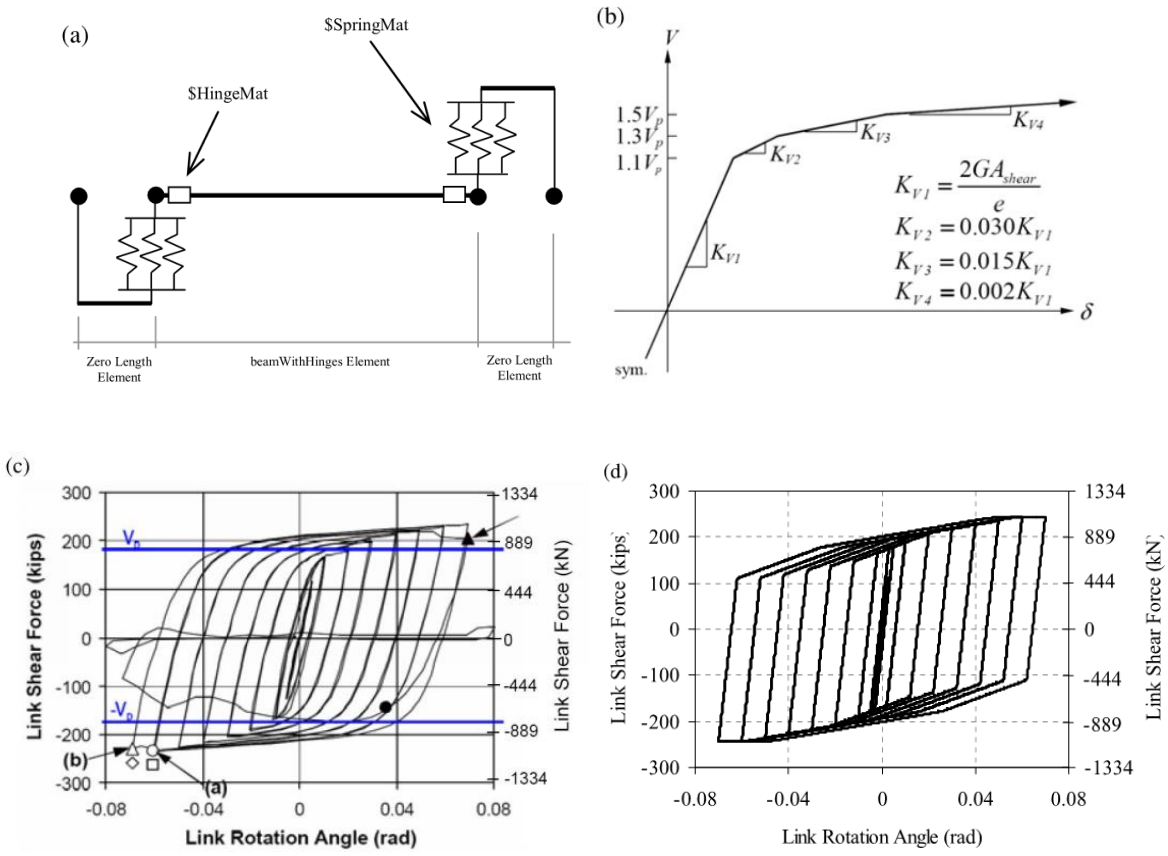

Figure 31. Description of the EBF link model used: (a) EBF link element; (b) constitutive behavior of the parallel springs; (c) hysteretic link behavior – experimental test; and (d) hysteretic link behavior – OpenSees Model (adapted from Prinz, 2010)

A co-rotational formulation was used to simulate large deformations and P-delta effects. The effect of the gravity system was accounted for using a leaning column, which was pinned at the base and assumed to be axially rigid but without any lateral strength. Therefore, the lateral stiffness and strength of the gravity system were not considered for the EBF models. This column was constrained laterally to have the same lateral displacements of the EBF columns. The full dead load plus 25% of the unreduced live load for one-quarter of the building was subtracted from the gravity load assigned to the EBF columns and then applied to this leaning column at each story. Additionally, for models with a flexible base, the gravity load needed to

equalize the design gravity load for the foundation was applied at the base of columns. This was done to ensure that the springs beneath the footing have the correct ratio between the ultimate bearing capacity (V_{ult}) and the design gravity load (V_d) (i.e., vertical factor of safety, FS_v). Figure 32 shows the description of the two-dimensional models developed in OpenSees Navigator with the leaning column using the fixed and flexible base conditions.

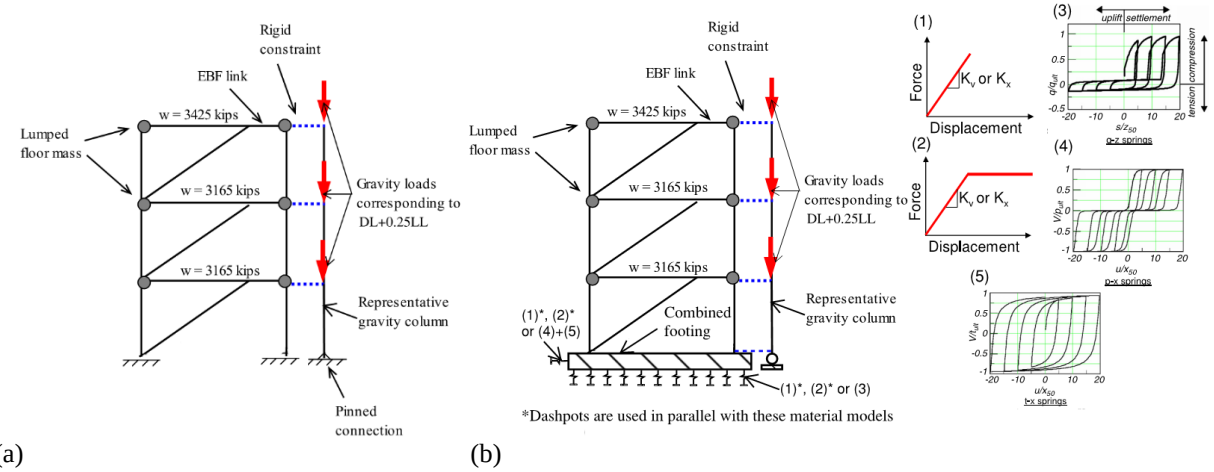

Note: Gravity loads on the EBF columns and the foundation are not shown for clarity

Figure 32. Two-dimensional models for EBFs with a leaning column: (a) fixed base; and (b) flexible base

Three different models were evaluated using nonlinear analyses. Firstly, a preliminary fixed base model was designed ($EBF1_{FB}$). Secondly, the same preliminary designed model ($EBF1_{SSI}$) was analyzed using a flexible base. Finally, the EFB was re-designed and analyzed according to the guidelines for considering SSI ($EBF2_{SSI}$) in ASCE/SEI 7-10. LE, EPP, and NL springs were used along with the Winkler's approach to model the flexible base conditions, and the material models used for these springs are shown in Figure 32b.

G. Nonlinear Static Analyses

Nonlinear static analyses or pushover analyses were conducted to characterize the load-deformation capacity of the EBFs under static lateral loads. The gravity load was applied first to the models and then the EBFs were pushed using the lateral force distribution suggested by the equivalent lateral force (ELF) procedure in ASCE/SEI 7-10. Figure 33 shows a schematic illustration of a pushover analysis considering the flexibility of the soil. In addition to the pushover analyses, modal analyses (MA) were performed to determine the periods of vibration of the EBF models with the fixed and flexible base conditions and their other dynamic properties.

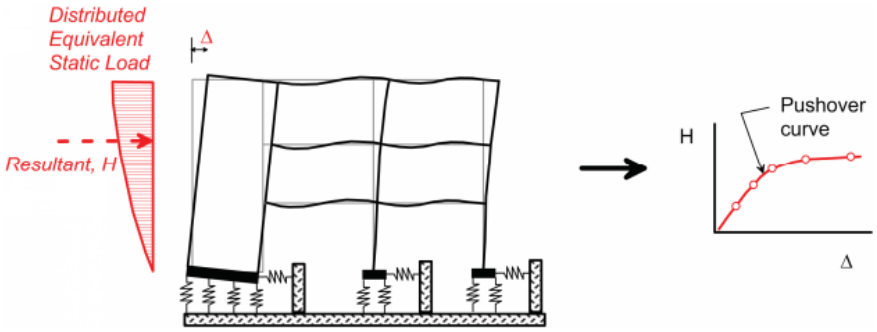

Figure 33. Schematic illustration of a pushover analysis and the resulting pushover curve for a building with a flexible base (NIST, 2012)

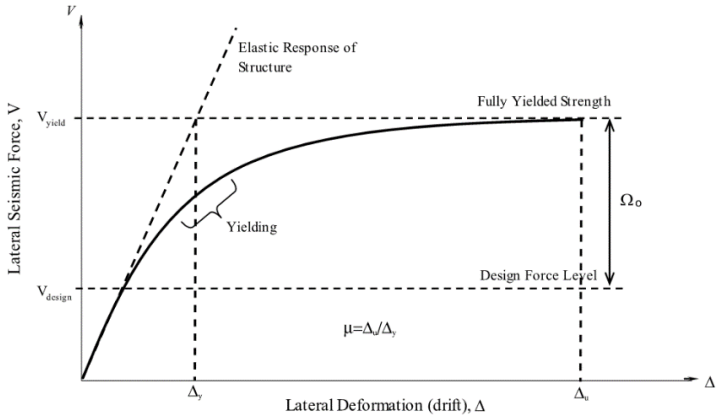

Figure 34. Determination of system overstrength factor (Ω_0) and global ductility (μ) (adapted from Prinz, 2010)

H. Nonlinear Response History Analyses

Dynamic analyses were also conducted on the EBFs with the fixed and flexible base conditions. A set of ten ground motions was selected to perform the dynamic analyses. The strongest component of each ground motion pair was used because two-dimensional analyses were performed (ASCE, 2010). In order to choose these ten ground motions, the deaggregation of the seismic hazard corresponding to the peak acceleration and site class of the Gilroy 2 site was used for a return period of 2475 years (MCE). This deaggregation was obtained from the USGS Unified Hazard Tool, *United States Geological Survey* (2008), and it was implemented to gain some understanding of the combination of magnitudes (M_w) and rupture distances from the fault (R_{rup}) which contribute most to the seismic hazard at the Gilroy 2 site. The deaggregation for a return period of 2475 years obtained using the USGS Hazard Tool is shown in Figure 35. As can be seen in Figure 35, the seismic hazard at the Gilroy 2 site is controlled by events located about 11 km from the site with an associated magnitude range between 6 and 7.

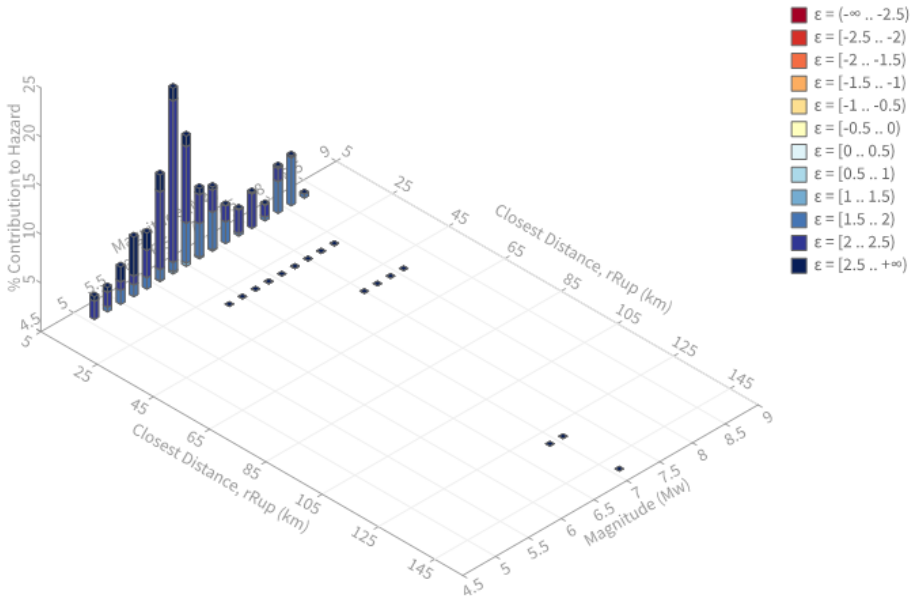

Figure 35. USGS total component deaggregation (return period of 2475 years) for the Gilroy 2 site

Before choosing the set of ten ground motions, the 5% damped design response spectrum according to ASCE/SEI 7-10 was constructed. This response spectrum was used as the target spectrum to perform the amplitude scaling process and match it with the average scaled response spectrum of the records over a period range from 0.2T to 1.5T (T=fundamental period of the structure). Finally, the results from the deaggregation (magnitude and distance), site class, target response spectrum shape, tectonic regime, and scale factors were considered to choose the ground motions. The ten records chosen are presented in Table 8 along with the scale factors used for each numerical model. The unscaled and scaled spectra along with the target spectrum for the $EBF1_{FB}$, $EBF1_{SSI}$, and $EBF2_{SSI}$ are shown in Figure 35, 36, and 37, respectively.

Table 8. Selected ground motion records

Event	Station/Component	R_{rup} (km)	Site Class	Mechanism	Scale Factor-Fixed Base ($EBF1_{FB}$)	Scale Factor-Flexible Base ($EBF1_{SSI}$)	Scale Factor-Flexible Base ($EBF2_{SSI}$)
Loma Prieta	Gilroy Array No.2/000	11.07	D	Reverse/Oblique	1.59	1.82	2.33
Loma Prieta	Gilroy Array No.3/000	12.82	D	Reverse/Oblique	2.3	2.07	2.03
Loma Prieta	Hollister Differential Array/255	24.82	D	Reverse/Oblique	1.83	1.51	1.28
Loma Prieta	Capitola/000	15.23	D	Reverse/Oblique	1.24	1.51	1.53
Northridge	Beverly Hills-14145 Mulhol/279	17.15	D	Reverse	1.33	1.03	0.77
Northridge	Canyon Country-W Lost Cany/270	12.44	D	Reverse	0.94	1.36	1.47
Northridge	Pacoima Kagel Canyon/360	7.26	C	Reverse	1.16	1.25	1.22
Coalinga	Pleasant Valley P.P.-yard/045	16.05	D	Reverse	1.06	1.02	1.15
Kobe-Japan	Amagasaki/090	11.34	D	Reverse	1.05	0.85	0.79
Christchurch -New Zealand	Papanui High School /33W	9.06	D	Reverse/Oblique	1.23	1.66	1.70

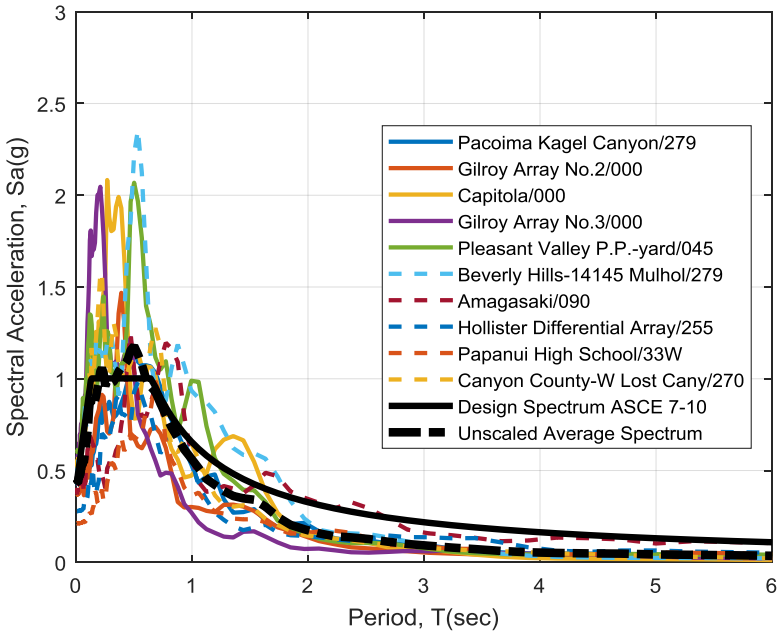

(a)

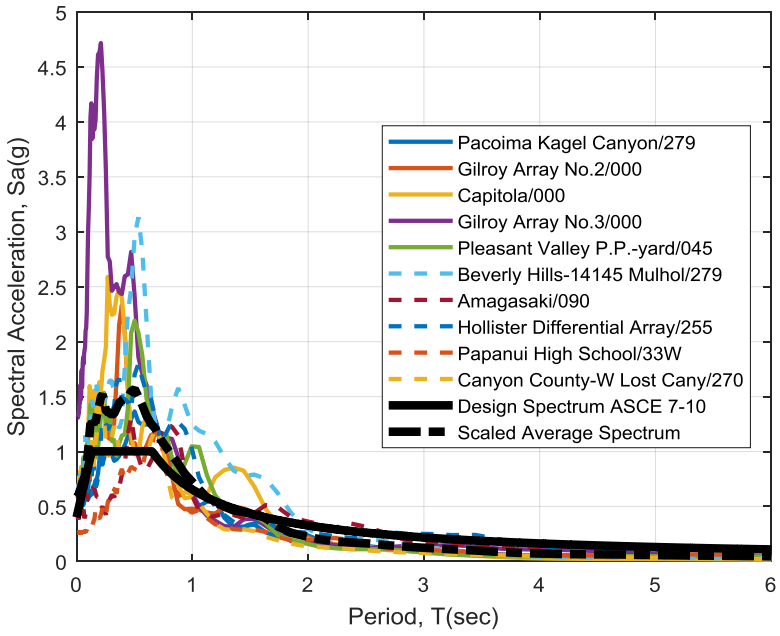

(b)

Figure 36. Design spectrum and spectra of selected ground motions for the EBF1$_{FB}$ model: (a) unscaled spectra; (b) scaled spectra

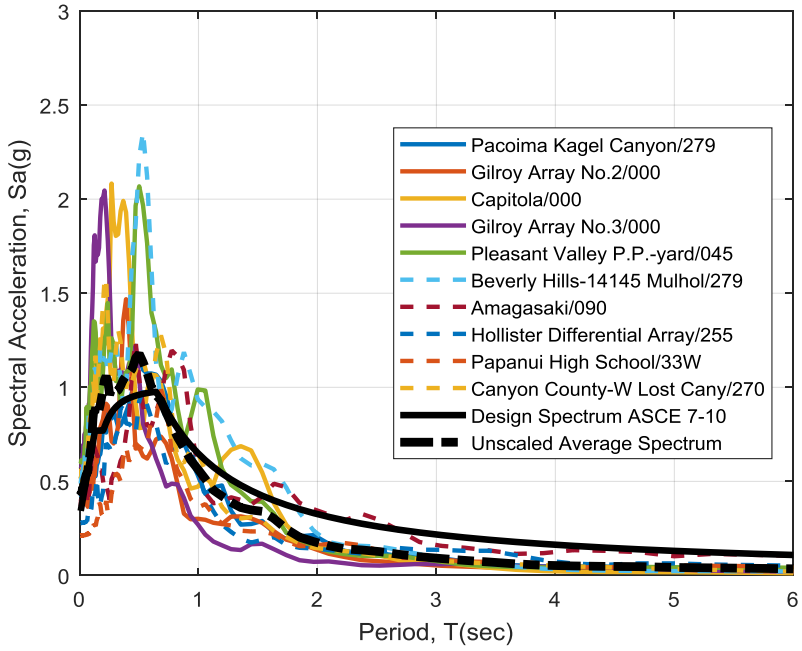

(a)

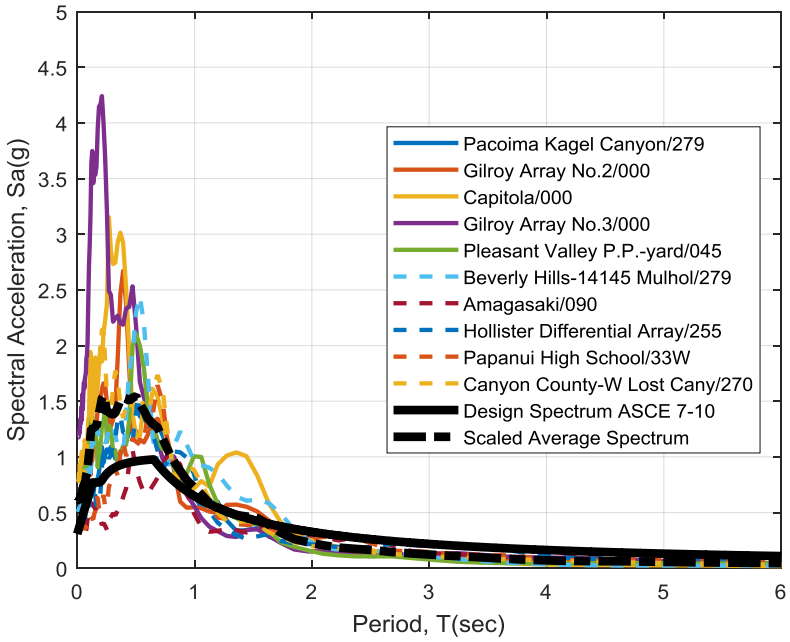

(b)

Figure 37. Design spectrum and spectra of selected ground motions for the EBF1$_{SSI}$ model: (a) unscaled spectra; (b) scaled spectra

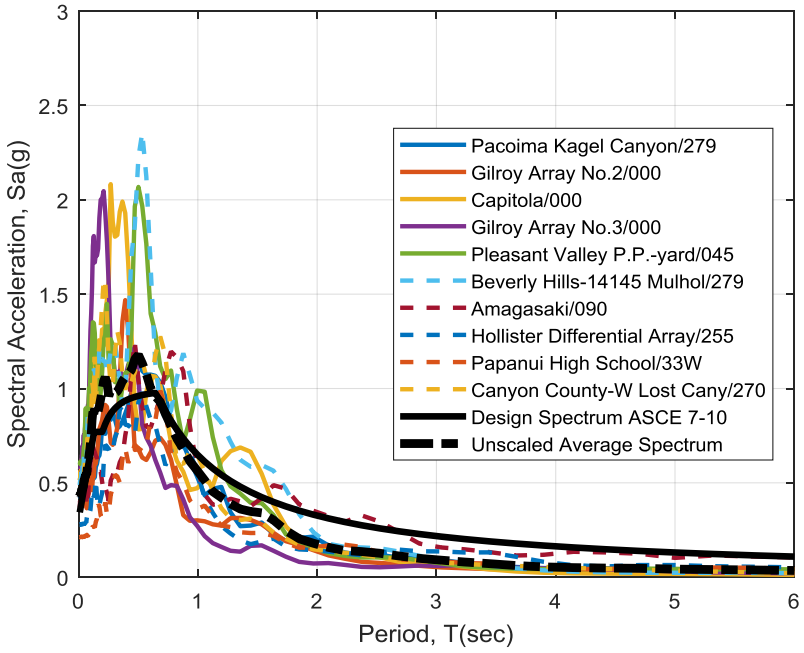

(a)

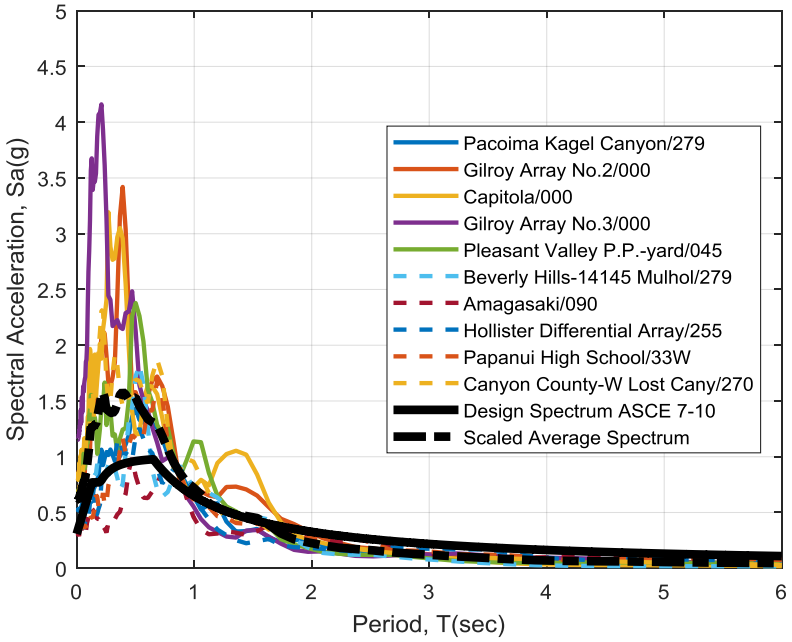

(b)

Figure 38. Design spectrum and spectra of selected ground motions for the EBF2$_{SSI}$ model: (a) unscaled spectra; (b) scaled spectra

The ground motions presented in Table 8 were selected from PEER Ground Motion Database considering the aforementioned procedure. A reduction on the design response spectrum was implemented for models considering SSI (see Figure 36 and 37). This reduction was due to the kinematic interaction effects; specifically, base-slab averaging effects. Embedment effects were not considered since the building prototype has no basement levels. Base-slab averaging was accounted for following FEMA P-1050. Kinematic effects in FEMA P-1050 were considered by using the response spectra reduction factors RRS_{bsa} and RRS_e, for base-slab averaging and embedment, respectively. These reduction factors multiply the spectral acceleration ordinates on the design response spectrum at each period. The product of RRS_{bsa} and RRS_e shall not be less than 0.60 (FEMA, 2015). The reduction due to base-slab averaging is allowed for structures located on site class C, D, or E soils, and for structures having structural mats or interconnected foundation elements. The reduction factor for base-slab averaging, RRS_{bsa}, was determined in the form of a transfer function using the following equations for each period:

$$RRS_{bsa} = 0.25 + 0.75\left\{\frac{1}{b_0^2}[1 - (\exp(-2b_0^2))B_{bsa}]\right\}^{1/2} \tag{44}$$

$$B_{bsa} = \begin{cases} 1 + b_0^2 + b_0^4 + \dfrac{b_0^6}{2} + \dfrac{b_0^8}{4} + \dfrac{b_0^{10}}{12} & for\ b_0 \leq 1 \\ \exp(2b_0^2)\left[\dfrac{1}{\sqrt{\pi}b_0}\left(1 - \dfrac{1}{16b_0^2}\right)\right] & for\ b_0 > 1 \end{cases} \tag{45}$$

$$b_0 = 0.00071\left(\frac{b_e}{T}\right) \tag{46}$$

$$b_e = \sqrt{A_{base}} \leq 260\ ft \tag{47}$$

The term A_{base} in Equation 47 refers to the area of the base of the building. All the above equations are very similar to Equation 28 to Equation 31, which were previously discussed in this document.

A 2% Rayleigh damping value was used in the dynamic analyses with consideration of its potential problems. Ricles and Popov (1994), Hall (2006), and Charney (2008) have demonstrated that Rayleigh damping may result in unrealisticly high damping forces in some structural elements during nonlinear response history analyses. The sensitivity of the Rayleigh damping was investigated by comparing it with the stiffness proportional damping. As a result of the sensitivity analysis, a mass-stiffness-proportional Rayleigh damping of 2% with stiffness at the last committed state was used over a period range between 0.2T and 1.5T, following the recommendations included in PEER/ATC 72-1, *Modelling and Acceptance Criteria for Seismic Design and Analysis of Tall Buildings* (PEER/ATC, 2010). As mentioned before, soil hysteretic and radiation damping was explicitly modeled using dashpots in models with a flexible base.

IV. Results and Discussion

A. Modal and Nonlinear Static Analyses

The nonlinear static analyses indicate a similar capacity and overstrength factor, Ω_0, for the EBFs designed with a fixed base ($EBF1_{FB}$) and then analyzed with flexible base ($EBF1_{SSI}$). Nevertheless, the global ductility, μ, is slightly greater for $EBF1_{SSI}$ with NL springs in comparison the other two $EBF1_{SSI}$ models and with $EBF1_{FB}$, while the $EBF1_{FB}$ model and $EBF1_{SSI}$ models with EPP springs have similar μ. Figure 34 presents a description of how Ω_0 and μ are determinated, while Figure 38 shows the pushover curves (V/V_e vs roof drift) obtained for all models, where V_e is the design base shear. In fact, the overstrength factors for all

models are very close to 2, which is the value assumed in design (ASCE, 2010). For the case of global ductility, values of μ in Table 8 are similar to the approximation of 4 ($\mu \approx R/\Omega_0$) for this parameter, according to FEMA P-1050.

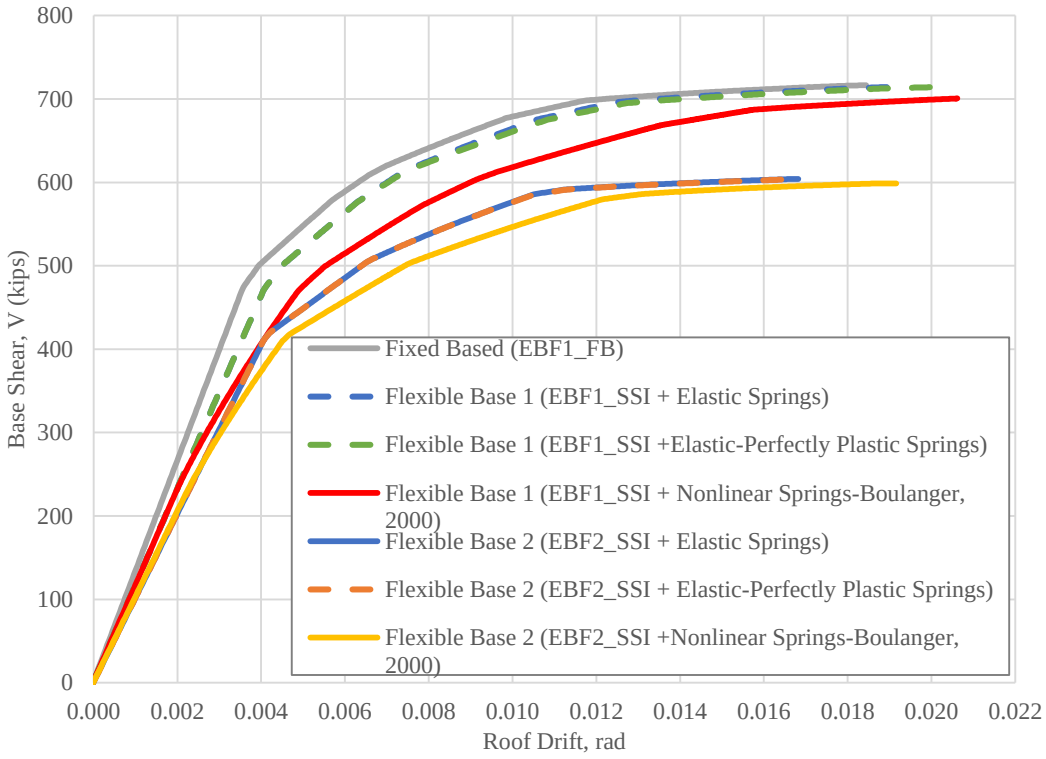

Figure 39. Pushover curves for the EBF models with the fixed and flexible base conditions

Table 9. Results from pushover analyses

Model	Vmax (kips)	Ω_0	μ
$EBF1_{FB}$	716.50	2.14	3.52
$EBF1_{SSI}$+LE springs	714.62	2.13	3.22
$EBF1_{SSI}$+EPP springs	714.06	2.13	3.35
$EBF1_{SSI}$+NL springs	700.60	2.09	3.77
$EBF2_{SSI}$+LE springs	604.04	2.13	2.86
$EBF2_{SSI}$+EPP springs	603.81	2.13	2.84
$EBF2_{SSI}$+NL springs	598.68	2.11	3.45

For the case of the EBF model re-designed ($EBF2_{SSI}$) considering SSI based on ASCE/SEI 7-10, the Ω_0 is also similar for all models and very close to 2. The μ for the $EBF2_{SSI}$ with NL springs is approximately 1.20 times greater than those for $EBF2_{SSI}$ models with LE and EPP springs. Indeed, for the $EBF2_{SSI}$ models, μ is similar to the expected value only for the model using NL springs. In general, the EBF1 models have a greater capacity in comparison with EBF2, but their performance under lateral static monotonic load is similar.

As expected, the fundamental period of vibration for the model with a fixed base, *T*, is clearly stiffer than the fundamental periods of vibration for models with flexible base, $\tilde{T}$. This fact shows the effect of the inertial interaction on the dynamic properties of models with a flexible base. The periods of vibration for each frame are presented in Table 10. As can be seen in Table 10, there is period elongation due to the inertial interaction for the two EBFs designed (EBF1 and EBF2) with and without SSI, so SSI affected the dynamic properties of the flexible base frames, contrary to the prediction obtained using the empirical ratio *h/(Vs.T)* suggested by Stewart et al. (1999a, 1999b). The ratio $\tilde{T}/T$ was also calculated using Equation 2 (Veletsos and Meek, 1974) and the results were very similar (less than 2% of difference) to those obtained with the modal analyses.

Table 10. Fundamental periods of vibration for models with the fixed and flexible base

Model	T, $\tilde{\mathbf{T}}$ (seconds)	$\tilde{T}/T$
$EBF1_{FB}$	0.72	-
$EBF1_{SSI}$+LE springs	0.80	1.11
$EBF1_{SSI}$+EPP springs	0.80	1.11
$EBF1_{SSI}$+NL springs	0.81	1.125
$EBF2_{FB}$	0.78	-
$EBF2_{SSI}$+LE springs	0.86	1.10
$EBF2_{SSI}$+EPP springs	0.86	1.10
$EBF2_{SSI}$+NL springs	0.86	1.10

B. Nonlinear Response History Analyses

After application of the gravity load, ten records were applied at the base of the EBF models as a uniform base excitation, and the average of the ten records was used to evaluate the performance of the frames according to ASCE/SEI 7-10. Results from the dynamic analyses of the EBFs with the fixed and flexible conditions base are presented in three parts: peak average inter-story drifts and residual drifts, peak average link rotation, and peak average column demands.

Peak inter-story drifts were evaluated to estimate if the nonstructural elements of the building will suffer damage under the Design Basis Earthquake (DBE) and they were limited to 1.25 times the limit for linear procedures (ASCE, 2010). For the case of residual drifts, they were evaluated to estimate the permanent drift after earthquake events, and they were limited to a value of 2/3 the limit (0.0067) suggested by PEER (2010) for the MCE hazard level. Residual drifts were computed by allowing 10 seconds of free vibration (i.e., analyses with zero acceleration) to the frames after the end of each record. In order to evaluate the rotational capacity of the EBF links during the earthquakes, link rotations were calculated and compared with the limit of 0.08 radians suggested by ANSI/AISC 341-10. Finally, the column demands due to the combined effect of gravity and seismic loads (P) were assessed and compared with the design column demands (P_d) to validate the design conducted using the equivalent lateral load procedure.

B1. Peak Inter-Story and Residual Drifts

In general, EBFs with the fixed and flexible base conditions met the inter-story limit criterion required by ASCE/SEI 7-10 for nonlinear dynamic analysis. The maximum inter-story

drift demand occurs at the second level, but only a few individual records do not meet the drift limit at this level. There is a significant reduction at all levels in the inter-story drift for the $EBF1_{SSI}$ model with NL springs in comparison with the other cases. In addition, the unscaled Gilroy Array 2 record, which was the record measured at that site, meets the drift limit for all cases. Figures 39 to 42 show the individual and the average peak inter-story responses for the $EBF1_{FB}$ and for $EBF1_{SSI}$ with LE, EPP, and NL springs; respectively

For the frames re-designed considering SSI ($EBF2_{SSI}$), similar trends to the EBF1s were obtained, but the Capitola ground motion showed a higher inter-story drift demand at the first floor. Only three individual records do not meet the drift limit at the first and second story; however, the peak average inter-story drift is below the limit for all cases. Figures 43 to 45 show the individual and the average peak inter-story responses for the $EBF2_{SSI}$ with elastic, EPP, and NL springs, respectively. Figure 46 shows a summary of all the drift responses for all EBFs.

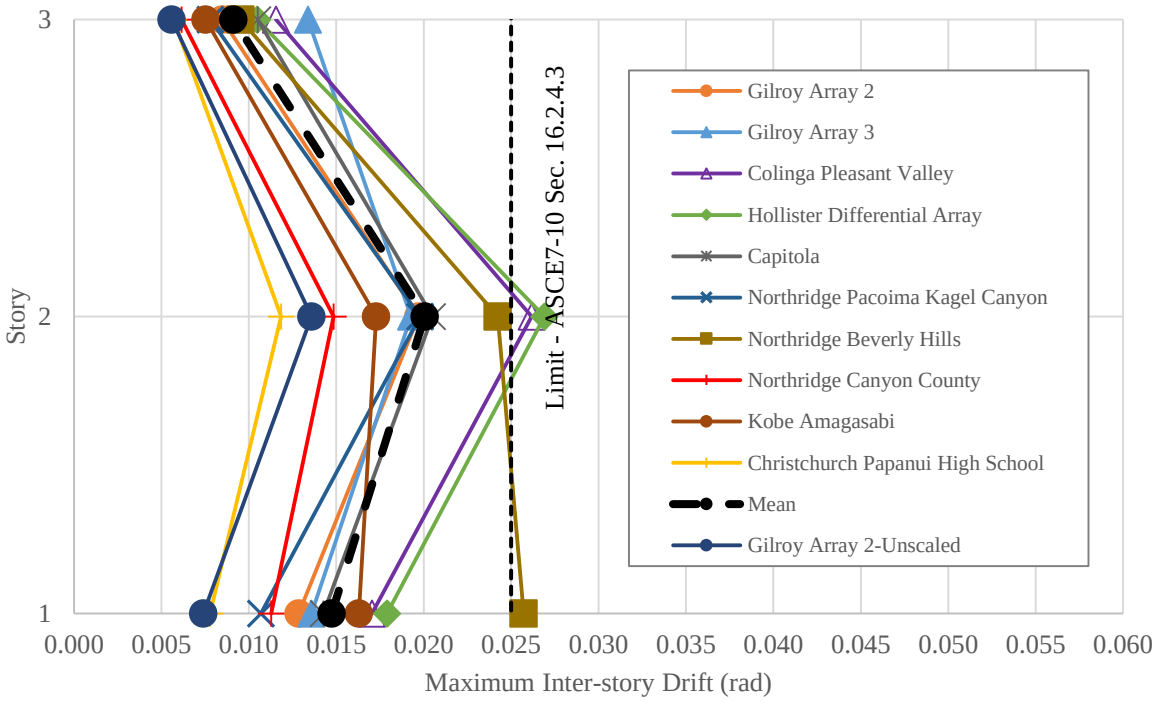

Figure 40. Individual and average inter-story drifts for the $EBF1_{FB}$

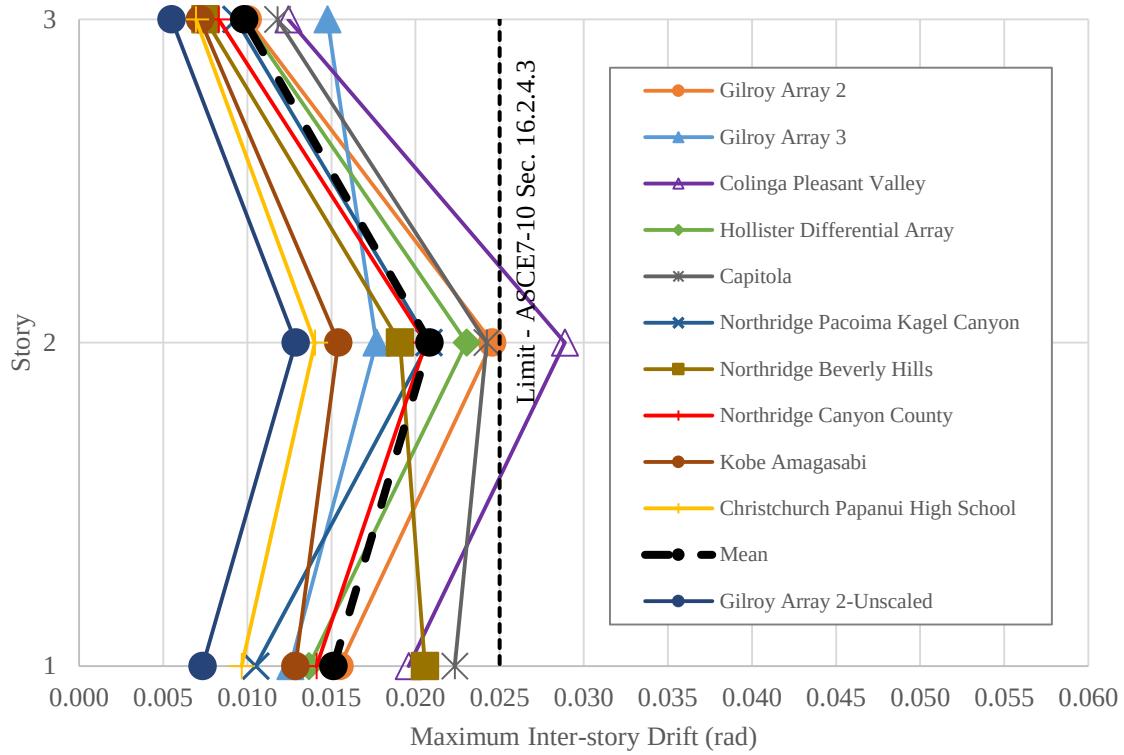

Figure 41. Individual and average inter-story drifts for the EBF1SSI with LE springs

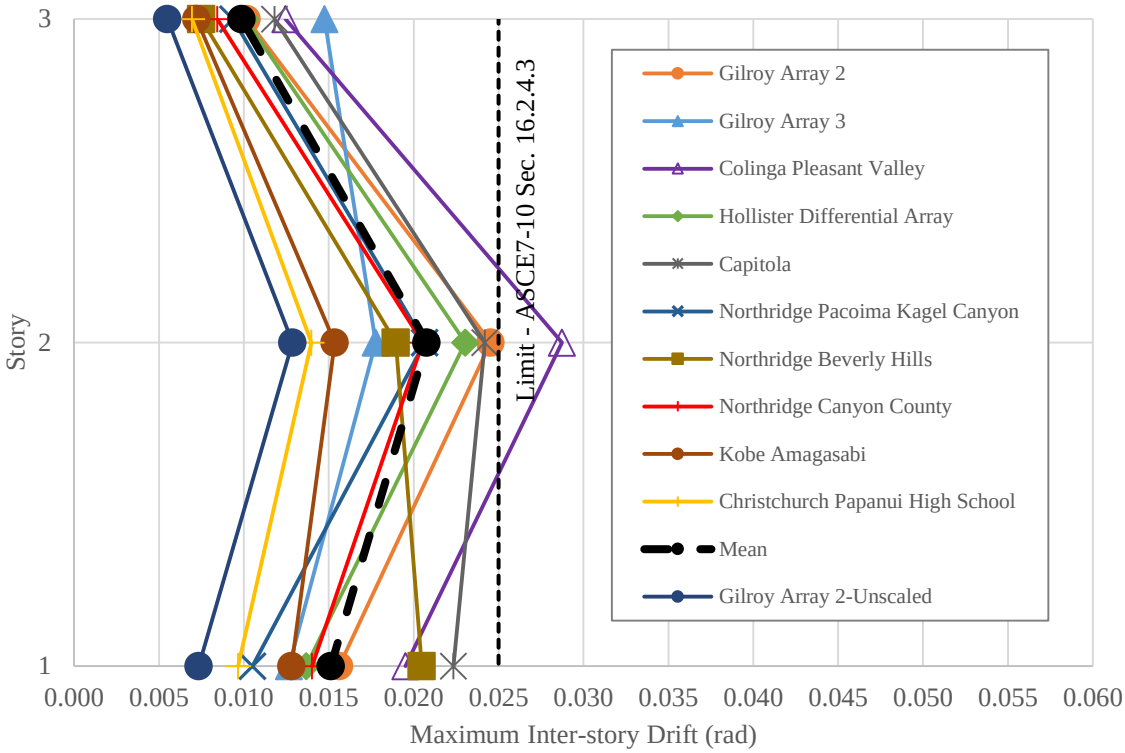

Figure 42. Individual and average inter-story drifts for the EBF1SSI with EPP springs

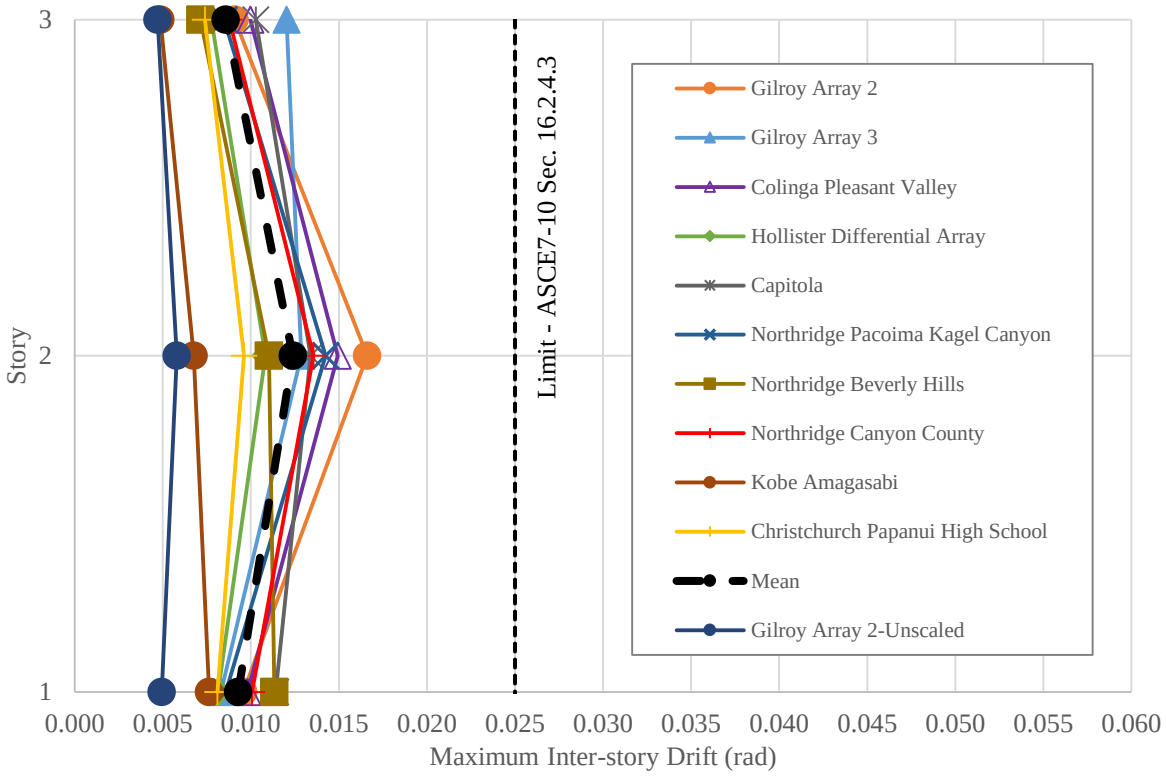

Figure 43. Individual and average inter-story drifts for the EBF1$_{SSI}$ with NL springs

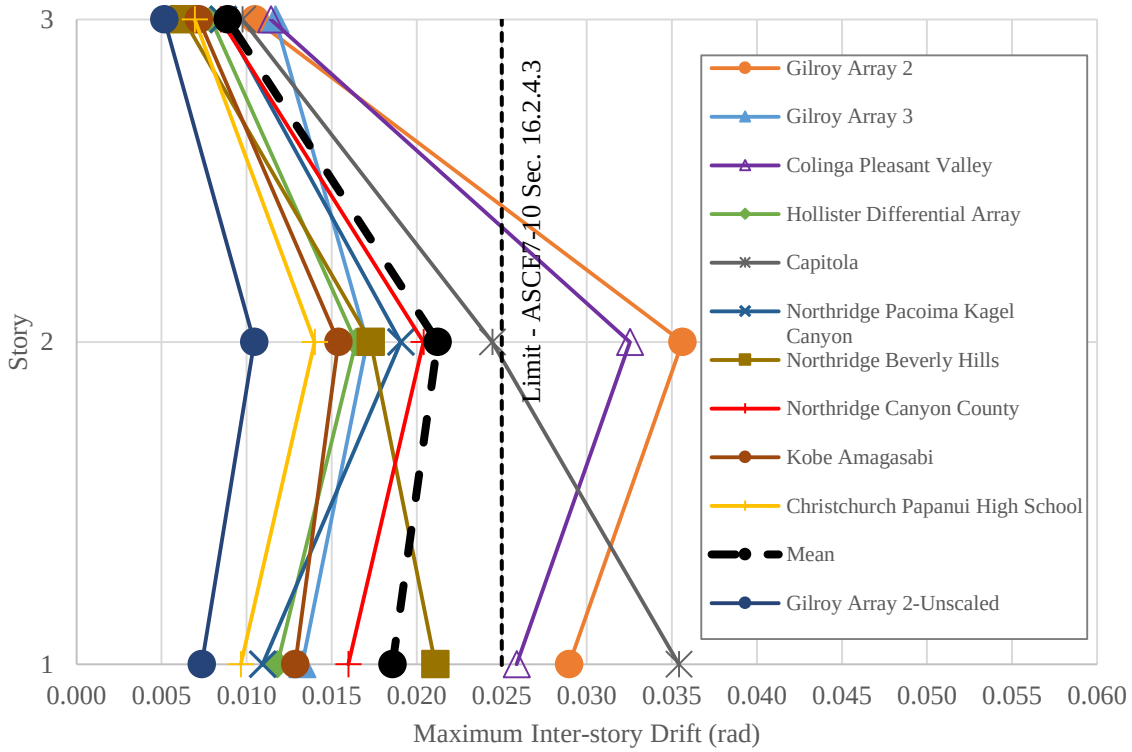

Figure 44. Individual and average inter-story drifts for the EBF2$_{SSI}$ with LE springs

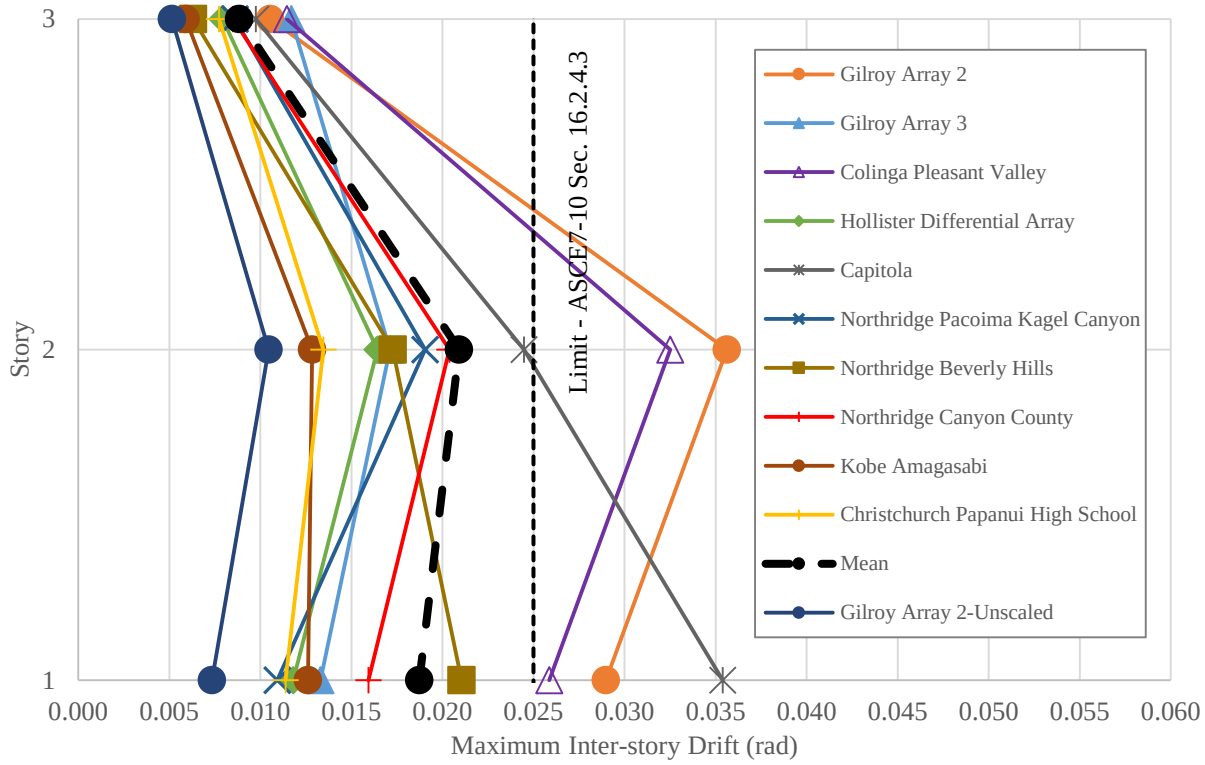

Figure 45. Individual and average inter-story drifts for the EBF2$_{SSI}$ with EPP springs

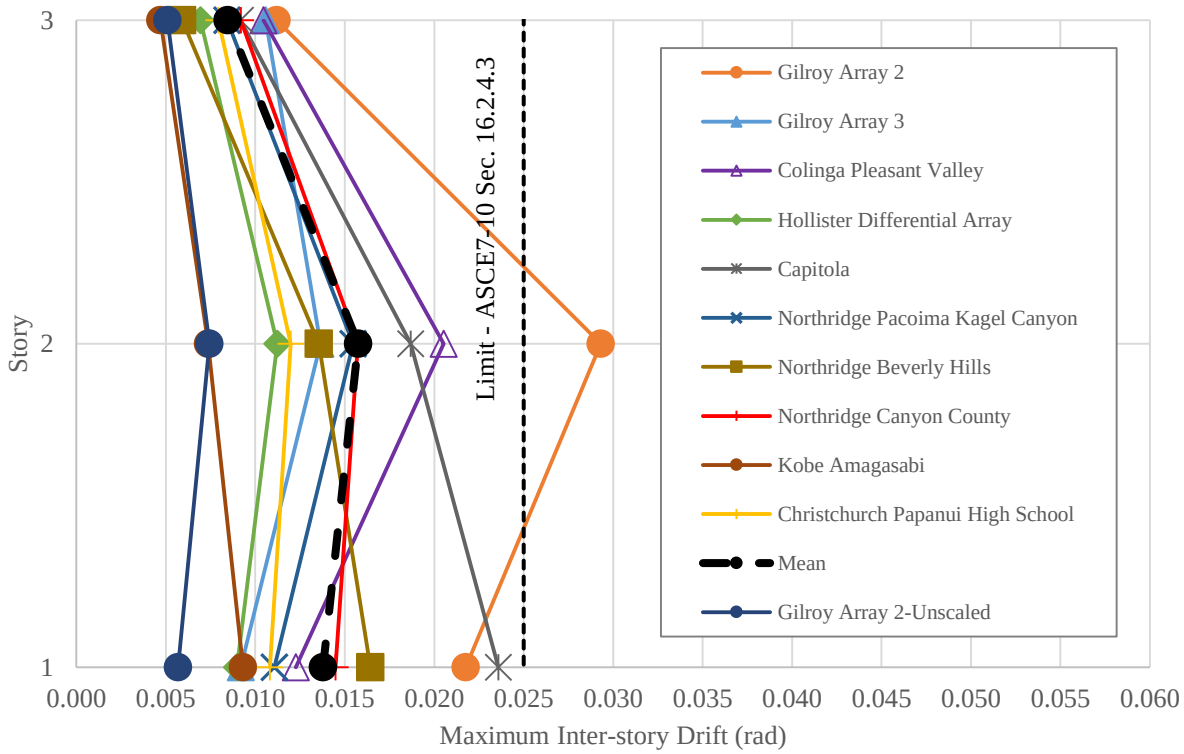

Figure 46. Individual and average inter-story drifts for the EBF2$_{SSI}$ with NL springs

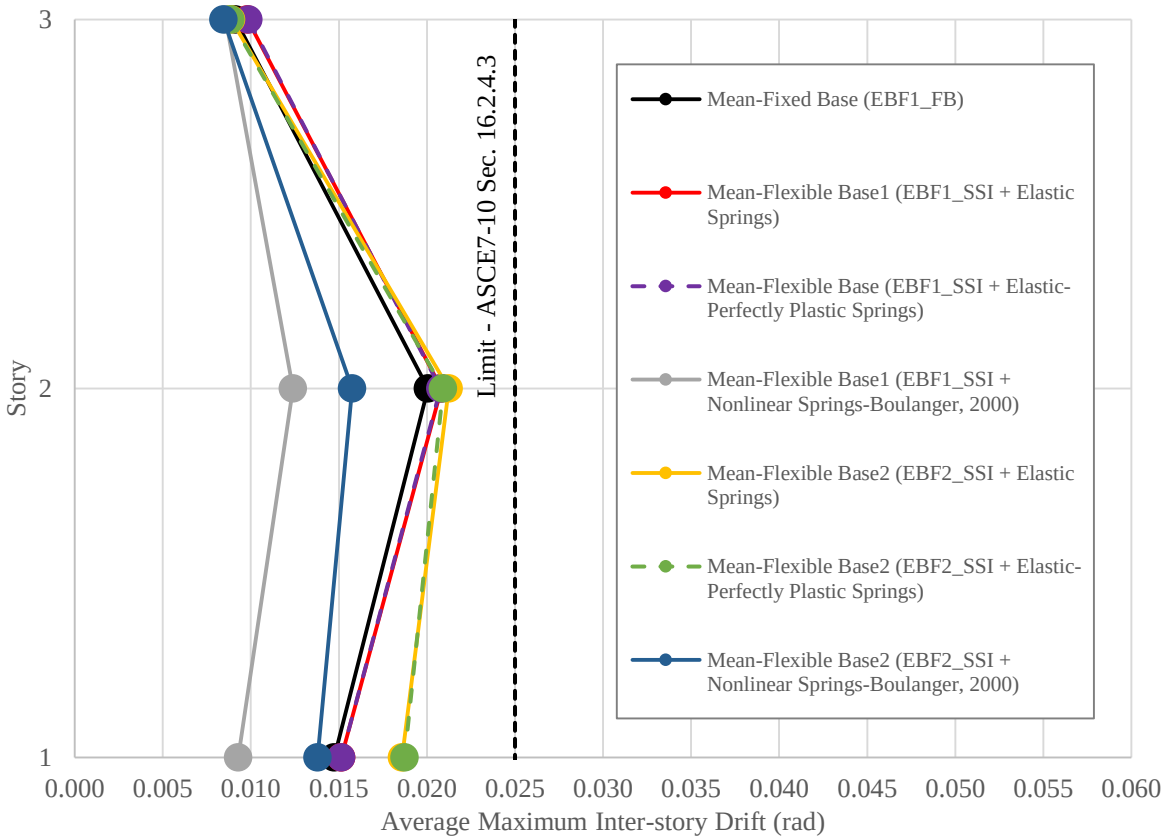

Figure 47. Average maximum inter-story drifts for all the EBF models

Residual drifts showed similar trends to the inter-story drift responses. In general, the residual drifts for all EBFs met the limit criterion of 0.0067 (PEER, 2010). FEMA 356, *Prestandard and Commentary for the Seismic Rehabilitation of Buildings* (FEMA, 2000b), suggests a limit of 0.005 for ensuring realignment of the structural frame and economical structural repairs after earthquakes. Even with the limit suggested by FEMA (2000b), all EBFs can be considered as meeting the limit criterion. Figure 47 shows the average maximum residual drifts for the EBFs with the fixed and flexible base conditions. As for the case of the inter-story drift, the maximum residual drift demand is at the second floor, and the $EBF1_{SSI}$ and $EBF2_{SSI}$ models with NL springs showed a significant reduction (approximately 4.25 and 2 times at the

second floor, respectively) in the residual drifts at all levels. This can be an important fact for deciding whether this building behaves acceptably after earthquakes according to the residual drift limit suggested in FEMA 356. Using NL springs along with the Winkler's approach can make a significant difference for meeting the residual drift limit not only for new buildings but also existing ones.

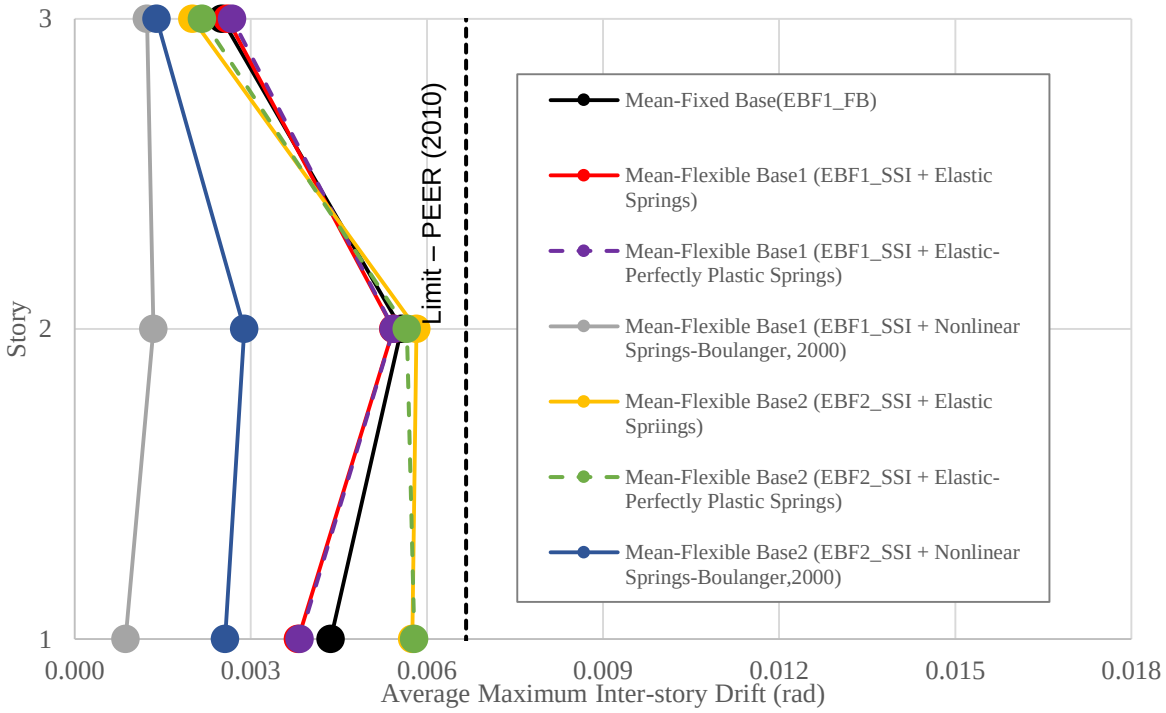

Figure 48. Average maximum residual drifts for all the EBF models

B2. Link Rotation

Frames with the fixed and flexible base conditions showed link rotation demands below the limit (0.08 rad) suggested by ANSI/AISC 341-10 at all levels. Similar to the inter-story and residual drift responses, the maximum link rotation demand was at the second story. In addition, a significant reduction in the link rotation demand was also obtained for the $EBF1_{SSI}$ and $EBF2_{SSI}$ models with NL springs. For instance, the $EBF1_{SSI}$ and $EBF2_{SSI}$ models with NL

springs showed a reduction in the link rotations at the second story of approximately 2.3 and 1.58 times in comparison with the other cases. These results suggest that the EBF links evaluated with column connections have an adequate performance. Reductions in the link rotations at all levels were obtained from models considering SSI with NL springs. The average maximum link rotations are presented in Figure 48.

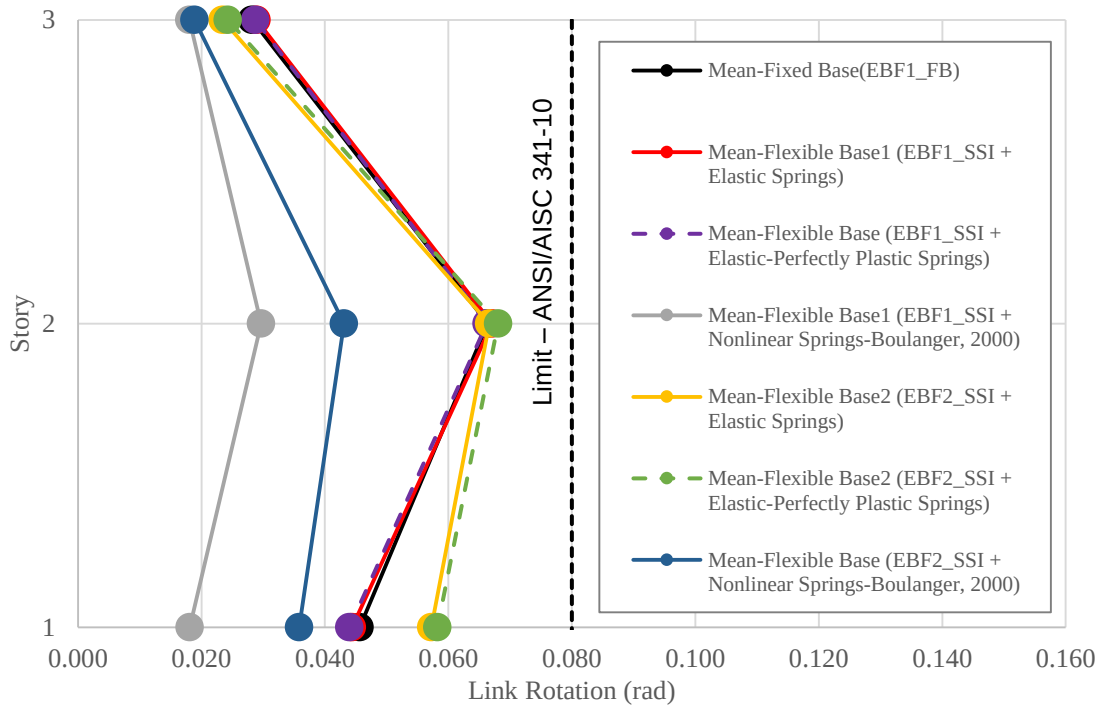

Figure 49. Average maximum link rotations for all the EBF models

B3. Column Demands

Column demands in the left and right columns of the EBFs at each story were evaluated by normalizing the axial load, P, from the set of ground motions by the design load, P_d. As a result of the capacity-based design conducted to size the members of the EBFs, P_d was obtained assuming simultaneous yielding of all ductile structural elements throughout the frame height.

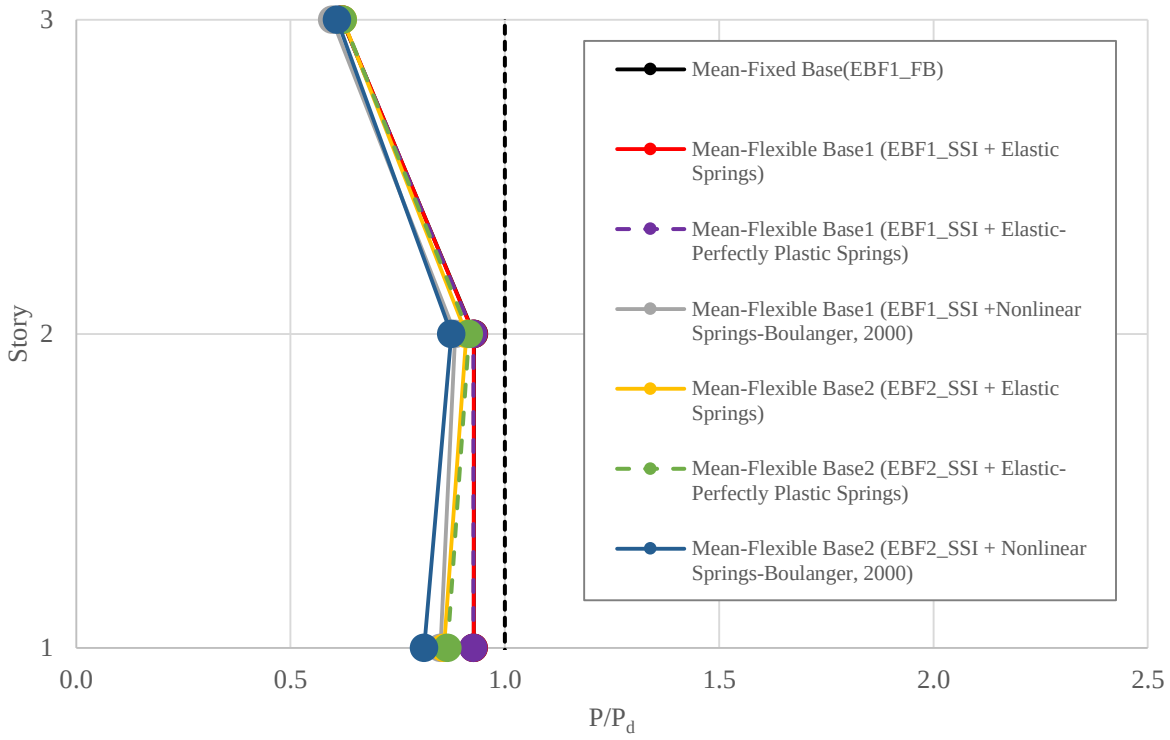

Figure 50. Normalized (P/P_d) average maximum column demands (left column) for all the EBFs

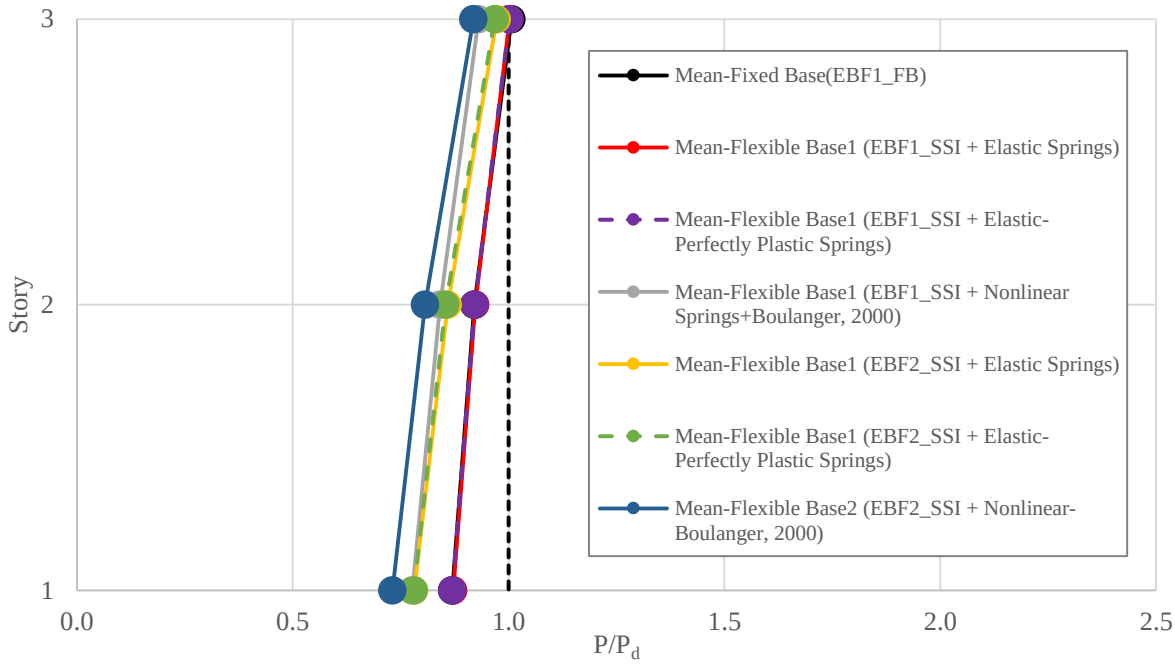

Figure 51. Normalized (P/P_d) average maximum column demands (right column) for all the EBFs

The normalized column demands, P/P_d, are shown in Figures 49 and 50 for the left and right column, respectively. In Figures 49 and 50, the dashed vertical line at $P/P_d=1$ shows that the peak average column demand is equal to the design load of the frame assuming simultaneous yielding of the EBF links. The left column has very similar P/P_d ratios throughout the entire frame height. Indeed, P/P_d ratios are close to unity at the first and second floor but approximately 0.60 at the third floor for the EBFs with fixed and flexible bases. Results for the left column show that the link at the third floor does not yield simultaneously with the links at the first and second floor, and this indicates that the size of the column at the third floor can be reduced for the EBFs designed (EBF1 and EBF2). On the contrary, the right column showed a different load demand due to the yielding pattern of the EBF links. The right column at the third story reached its capacity while the right columns at the first and second level have a remaining capacity of approximately 20% on average. Unlike the inter-story drift, residual drift, and link rotation demands, the normalized column demands are slightly affected by the type of spring used for EBF models with a flexible base.

B4. EBF Weight Comparison

Two different EBFs were designed to validate the methodology suggested in ASCE/SEI 7-10 for considering SSI in the seismic analysis of building using the equivalent lateral force (ELF) procedure. One frame was designed using the ELF procedure ignoring SSI effects (EBF1) while the other EBF was designed using the ELF procedure considering SSI (EBF2). Based on the results shown in this section, the reduction in the size of some elements was justified trough the nonlinear static analyses (NSA) and nonlinear response history analysis (NRHA). As expected from the NSA, the lateral load capacity of the EBF2 models is greater than the capacity of the EBF1 models, but the performance of the EBF1 models is similar to the

EBF2 models. Average maximum inter-story and residual drifts, average peak link rotations, and average peak column demands met the criteria for the dynamic analyses conducted on EBFs designed considering SSI effects (EBF2). For the weight computations, a constant steel density of 490 lb/ft^3 was assumed. As a result, EBF1 is 13.2% heavier than EBF2, thus considering SSI effects on the seismic analysis of the building used for this study reduced the weight of the EBF and therefore its cost.

IV. Conclusions

The ability to accommodate architectural features makes EBFs an attractive seismic lateral load-resisting system; however, the lack of studies about more efficient numerical analyses, such as those considering SSI effects, has hindered its broader used. In addition, the lower rotation capacity of EBF links with column connections in comparison with mid-span links have reduced The benefits in performance and cost-savings were shown by evaluating the seismic response of a prototype building having EBFs with and without the inclusion of SSI. Based on the results obtained from the MA, NSA, and NRHA, the conclusions for this study are:

- EBFs with fixed and flexible base conditions showed similar lateral load capacities using the Winkler's approach along with linear, EPP, and NL springs
- EBFs modeled with a flexible base using NL springs showed similar Ω_0 and greater μ when compared to the model with a fixed base
- EBFs modeled with a flexible base using LE and EPP springs showed similar Ω_0 and lower μ when compared to the model with a fixed base

- EBFs experienced period elongation ratios, $\tilde{T}/T$, of 1.10 on average which was contrary to the insignificant effect of the inertial interaction predicted using the relationship suggested by Stewart et al. (1999a, 1999b)
- NRHA showed that both the EBF designed ignoring SSI (EBF1) and the EBF designed considering SSI (EBF2) met the design criteria for inter-story drifts, residual drifts, link rotations, and columns demands
- EBF1 and EBF2 modeled using a flexible base with NL springs showed significant reductions in inter-story drift, residual drift, and link rotation demands
- Reductions in the link rotation demands obtained from models using NL springs suggest that the 3-story EBFs with link-to-column connections performed well under the seismic demand for the site studied, so connection testing or prequalified connections could be avoided
- The reduction of the sizes of some structural elements obtained for the EBF2 using the methodology for considering SSI available in ASCE/SEI 7-10 was justified through the MA, NSA, and NRHA results
- By considering SSI in the seismic analysis of the building analyzed, the weight of the EBF was reduce by 13.2%
- Kinematic interaction effects were not significant for the building analyzed because there were no basement levels for consideration of embedment effects and soft soil conditions

V. Recommendations for Future Work

The results obtained in this study suggest that using SSI for the seismic analysis of buildings could offer cost savings and a better understanding of their performance. However,

more research is needed in order to improve the application and understanding of SSI effects. It is suggested that future research efforts can focus on the following areas:

- More experimental and numerical validation of the equations used for obtaining foundation impedances in non-homogenous soils
- Revision of the effects of SSI on the R factors used for the seismic design of buildings to avoid over-conservatism
- More validation of the existing equations for considering base-slab averaging and embedment effects using instrumented buildings
- Development of additional nonlinear material models for non-uniform soil conditions to incorporate the energy dissipation capacity of shallow foundations
- Evaluation of different lateral load-resisting systems considering SSI effects using the substructure as well as the direct approach, with and without basement levels
- Perform SSI analyses on buildings with different lateral systems using soft soil conditions (soil types E and F)
- Conduct experimental and analytical validations of the rotation capacity of EBF links considering SSI

References

Abrahamson, N. A., Schneider, J. F., and Stepp, J. C., 1991. Empirical spatial coherency functions for application to soil-structure interaction analyses, *Earthquake Spectra* **7(1)**, 1-27.

American Association of State Highway and Transportation Officials (AASHTO), 2010. *AASHTO Bridge Design Specifications*, AASHTO 2010, 5th Edition, Washington, DC.

American Institute of Steel Construction (AISC), 2002. *Seismic Provisions for Structural Steel Buildings*, ANSI/AISC 341-02, Chicago, IL.

American Institute of Steel Construction (AISC), 2010. *Seismic Provisions for Structural Steel Buildings*, ANSI/AISC 341-10, Chicago, IL.

American Petroleum Institute (API), 1993. *Recommended practice for planning, designing and constructing fixed offshore platforms – Working stress design*. 20th Edition, Washington, DC.

American Society of Civil Engineers (ASCE), 2010. *Minimum Design Loads for Buildings and Other Structures*, ASCE/SEI 7-10, Reston, VA.

American Society of Civil Engineers (ASCE), 2013. *Seismic Evaluation and Retrofit of Existing Buildings*, ASCE/SEI 41-13, Reston, VA.

Ancheta, T. D., Stewart, J. P., and Abrahamson, N.A., 2011. Earthquake characterization of earthquake ground motion coherency and amplitude variability. *Proceedings, 4th International Symposium on Effects of Surface Geology on Seismic Motion*, IASPEI/IAEE, University of California Santa Barbara, CA.

ANSYS Inc., 2013. *ANSYS 13.0*, software, Canonsburg, PA.

Allotey, N., and Naggar, M. H. E., 2003. Analytical moment-rotation curves for rigid foundations based on a Winkler model, *Soil Dynamics and Earthquake Engineering* **23**, 367-381.

Allotey, N., and Naggar, M. H. E., 2007. An investigation into the Winkler modeling of the cyclic response of rigid footings, *Soil Dynamics and Earthquake Engineering* **28**, 44-57.

Applied Technology Council (ATC), 1996. *Seismic Evaluation of Concrete Buildings*, ATC-40, Redwood City, CA.

Aviles, J., and Perez-Rocha, L. E., 1996. Evaluation of interaction effects on system period and the system damping due to foundation embedment and layer depth, *Soil Dynamics and Earthquake Engineering* **15**, 11-27.

Barlett, P. E., 1976. Foundation rocking in clay soil, Master's Thesis, University of Auckland, New Zealand.

Bielak, J., 1975. Dynamic behavior of structures with embedded foundations, *Earthquake Engineering and Structural Dynamics* **3**, 259-274.

Bielak, J., 1976. Modal analysis for building-soil interaction, *Journal of Engineering Mechanics*, **102**, 771-786.

Bolisetti, C., and Whittaker, A. S., 2015. Site Response, Soil-Structure Interaction and Structure-Soil-Structure Interaction for Performance Assessment of Building and Nuclear Structures, *Report No. MCEER-15-0002,* Multidisciplinary Center for Earthquake Engineering Research, University at Buffalo, The State University of New York, Buffalo, NY.

Boulanger, R. W., Curras, C. J., Kutter, B. L., Wilson, D. W., and Abghari, A., 1999. Seismic soil-pile-structure interaction experiments and analyses, *Journal Geotechnical and Geoenvironmental Engineering* **125**, 750-759.

Boulanger, R. W. (2000a). *The PySimple1 Material, Document for the OpenSees platform*. http://opensees.berkeley.edu.

Boulanger, R. W. (2000b). *The QzSimple1 Material, Document for the OpenSees platform*. http://opensees.berkeley.edu.

Boulanger, R. W. (2000c). *The TzSimple1 Material, Document for the OpenSees platform.* http://opensees.berkeley.edu.

Chang, B., Thomas, J. M., Raychowdhury, P., Gajan, S., L., K. B., and Hutchinson, T. C., 2007. Soil-Foundation Structure Interaction: Shallow Foundations, *Data Report No.SSRP 07/24*, Center for Geotechnical Modeling, University of California, Davis, CA.

Chao, S.-H., and Goel, S. C., 2006. Performance-Based Seismic Design of Eccentrically Braced Frames Using Target Drift and Yielding Mechanism as Performance Criteria, *Engineering Journal **3***, 173-200.

Charney, F. A., 2008. Unintended Consequences of Modeling Damping in Structures, *Journal of Structural Engineering* **134(4)**, 581-592.

Chopra, A., and Yim, S. C., 1985. Simplified earthquake analysis of structures with foundation uplift, *Journal of Structural Engineering* **111(4)**, 906-930.

Clough, R. W., and Penzien, J., 1993. *Dynamics of Structures*, McGraw Hill, New York.

Computers and Structures Inc., 2009. *SAP2000 – Structural Analysis Program, Version 14.0*, Berkeley, CA.

Cremer, C., Pecker, A., and Davenne, L., 2001. Cyclic macro-element for soil-structure interaction: Material and geometrical nonlinearities, *International Journal for Numerical and Analytical Methods in Geomechanics* **25(12)**, 1257-1284.

Crouse, C. B., 2001. Commentary on soil-structure interaction in U.S. seismic provisions, *Proceedings, 2nd UJNR Workshop on Soil-Structure Interaction*, Tsukuba, Japan.

Curras, C. J., 2000. Seismic soil-pile-structure interaction for bridge and viaduct structures, Ph.D. Dissertation, University of California, Davis.

Darendeli, 2001. Development of a New Family of Normalized Modulus Reduction and Material Damping Curves, Ph.D. Dissertation, University of Texas at Austin, TX.

Day, S.M., 1978. Seismic response of embedded foundations, Preprint No. 3450, *Preprints of Conference Proceedings of ASCE Convention and Exposition*, Chicago, IL, American Society of Civil Engineers.

Dessault Systemes, 2005. *ABAQUS – Finite Element Analysis Software*, Providence, RI.

Dominguez, J., and Roësset, J. M., 1978. Response of Embedded Foundations to Travelling Waves, *Report No. R78-24*, Dep. of Civil Engineering, Massachusetts Institute of Technology, Cambridge, MA.

Elsabee, F., Morray, J.P., and Roësset, J. M., 1977. Dynamic behavior of embedded foundations, *Report No. R77-33*, Dep. of Civil Engineering, Massachusetts Institute of Technology, Cambridge, MA.

Engelhardt, M. D., and Popov, E. P., 1989. On design of Eccentrically Braced Frames, *Earthquake Spectra* **5(3)**, 495-511.

Engelhardt, M. D., and Popov, E. P., 1992. Experimental Performance of Long Links in Eccentrically Braced Frames, *Journal of Sructural Engineering, ASCE* **118(11)**, 3067-3088.

Federal Emergency Management Agency (FEMA), 2000d. *Prestandard and Commentary for the Seismic Rehabilitation of Buildings*, *FEMA 356*, Washington, D.C.

Federal Emergency Management Agency (FEMA), 2005. *Improvement of Nonlinear Static Seismic Analysis Procedures*, *FEMA 440*, Washington, D.C.

Federal Emergency Management Agency (FEMA), 2009. *Recommended Seismic Provisions for New Buildings and Other Structures*, *FEMA P-750/2009*, Washington, D.C.

Federal Emergency Management Agency (FEMA), 2015. *Recommended Seismic Provisions for New Buildings and Other Structures*, *FEMA P-1050-1/2015*, Washington, D.C.

Gadre, A., and Dobry, R., 1998. Lateral cyclic loading centrifuge tests on square embedded footing, *Journal of Geotechnical and Geoenvironmental Engineering* **120(11)**, 1128-1138.

Gajan, S., Palen, J., and Kutter, B., 2003a. Soil-Foundation Structure Interaction: Shallow Foundations, *Data Report No.UCD/CGMDR-02*, Center for Geotechnical Modeling, University of California, Davis, CA.

Gajan, S., Palen, J., and Kutter, B., 2003b. Soil-Foundation Structure Interaction: Shallow Foundations, *Data Report No.UCD/CGMDR-03*, Center for Geotechnical Modeling, University of California, Davis, CA.

Gajan, S., 2006. Physical and numerical modeling of nonlinear cyclic load-deformation behavior of shallow foundations supporting rocking walls, Ph.D. Dissertation, University of California Davis.

Gazetas, G., 1991b. Formulas and charts for impedances of surface and embedded foundations, *Journal of Geotechnical Engineering* **117 (9)**, 1363-1381.

Givens, M. J., 2013. Dynamic Soil-Structure Interaction of Instrumented Buildings and Test Structures, Ph.D. Dissertation, University of California, Los Angeles, CA.

Gupta, A., and Krawinkler, H., 1999. Prediction of seismic demands for SMRFs with ductile connections elements, *Report No. SAC/BD-99/06.* SAC Joint Venture, Sacrament, CA.

Hall, J. F., 2005. Problems encountered from the use (or misuse) of Rayleigh damping, *Earthquake Engineering and Structural Dynamics* **35**, 525-545.

Harden, C. W., Hutchinson, T., Martin, G. R., and Kutter, B. L., 2005. Numerical modeling of nonlinear cyclic response of shallow foundations, *Report No. PEER-2005/04*, Pacific Earthquake Engineering Research Center, University of California, Berkley, CA.

Hardin, B. O., and Black, W. L., 1968. Vibration modulus of normally consolidated clay, *Journal of the Soil Mechanics and Foundation Division* **94(2)**, 353-369.

Hardin, B. O., and Black, W. L., 1968. Vibration modulus of normally consolidated clay, *Journal of the Soil Mechanics and Foundation Division* **94(2)**, 353-369.

Hjelmstad, K. D., and Popov, E. P., 1983. Cyclic Behavior and Design of Link Beams, *Journal of Structural Engineering* **109(10)**, 2387-2403.

Kasai, K., and Popov, E. P., 1986a. Cyclic Web Buckling Control for Shear Link Beams, *Journal of Structural Engineering, ASCE* **112(3)**, 505-523.

Kasai, K., and Popov, E. P., 1986b. General Behavior of WF Steel Shear Links in Eccentrically Braced Frames, *Journal of Structural Engineering, ASCE* **112(2)**, 362-382.

Kausel, E., Whitman, A., Murray J., and Elsabee, F., 1978. The spring method for embedded foundations, *Nuclear Engineering and Design* **48**, 377-392.

Kim, S., and Stewart, J. P., 2003. Kinematic soil-structure interaction from strong motion recordings, *Journal Geotechnical and Geoenvironmental Engineering* **129(4)**, 323-335.

Knappett, J. A., Haigh, S. K., and Madabhushi, S. P. G., 2004. Mechanisms of failure for shallow foundations under earthquake loading, Volume 2, 713-725. *Proceedings, 11th International of Soil Dynamics and Earthquake Engineering*, University of California, Berkley.

Kramer, S. L., 1996. *Geotechnical Earthquake Engineering,* Prentice-Hall, Upper Saddle River, NJ.

Livermore Software Technology Corporation, 2013. *LS-DYNA Keyword User's Manual – Version R. 7.0*. Livermore, CA.

Malley, J. O., and Popov, E. P., 1983. Shear Links in Eccentrically Braced Frames, *Journal of Structural Engineering, ASCE* **110(9)**, 2275-2295.

Maugeri, M., Musumeci, G., Novita, D., and Taylor, C. A., 2000. Shaking table test of failure of a shallow foundation subjected to an eccentric load, *Soil Dynamics and Earthquake Engineering* **20**, 435-444.

Maravas, A., Mylonakis, G., and Karabalis, D. L., 2007. Dynamic characteristics of simple structures on piles and footings, Paper No. 1672. *Proceedings, 4th International Conference on Earthquake Geotechnical Engineering*, Thessaloniki, Greece.

Marcuson, W. F., and Wahls, H. E., 1972. Time effects on dynamic shear modulus of clays, *Journal of the Soil Mechanics and Foundation Division* **98(2)**, 1359-1373.

Mazzoni, S., McKenna, F., Scott, M.H., and Fenves, G.L. (2007). *OpenSees Command Language Manual*. Open System for Earthquake Engineering Simulation (OpenSees), Pacific Earthquake Engineering Research Center, University of California, Berkeley, CA.

McClelland, B., and Fotch, J. A., 1958. Soil modulus for laterally loaded piles, *Transactions* **123**, 1049-1063.

Menegotto, P., and Pinto, P. E., 1973. Method of analysis of cyclically loaded RC plane frames including changes in geometry and non-elastic behavior of elements under normal force and bending, *Preliminary Report **13***, 15-22, IABSE.

Menq, F.-Y., 2003. Dynamic Properties of Sandy and Gravelly Soils, Ph.D. Dissertation, University of Texas at Austin, TX.

Mosher, R., 1984. Load transfer criteria for numerical analysis of axially loaded piles, *Report No. K-84(I),* US Army Engineers Waterways Experiments Station, Vicksburg, MS.

Mwafy, A., Kwon, O.-S., Elnashai, A., and Hashash, Y., 2000. Wave Passage and Ground Motion Incoherency Effects on Seismic Response of an Extended Bridge, *Journal of Bridge Engineering* **16(3)**, 364-374.

Mylonakys, G., and Gazetas, G., 2000. Seismic Soil-Structure Interaction: Beneficial or Detrimental?, *Journal of Earthquake Engineering* **4(3)**, 277-301.

Mylonakys, G., Nikolaou, S., and Gazetas, G., 2006. Footings under seismic loading: Analysis and design issues with emphasis on bridge foundations, *Soil Dynamics and Earthquake Engineering* **26**, 824-853.

Nakaki, D. K., and Hart, G. C., 1987. Uplifting response of structures subjected to earthquake motions, *Report No. 2.1-3,* U.S.-Japan Coordinated Program for Masonry Building Research.

National Institute of Standards and Technology (NIST), 2012. *Soil-Structure Interaction for Building Structures, GCR 12-917-21,* Gaithersburg, Maryland.

Negro, P., Verzeletti, G., Molina, J., Pedretti. S., Lo Presti, D., and Pedroni, S., 1998. Large-scale geotechnical experiments on soil-foundation interaction: (triseetask 3), *Report No. 1*, European Commission, Joint Research Center, Special Publication.

Nogami, T., Otani, J., Konagai, K., and Chen, H.-L., 1992. Nonlinear soil-pile interaction model for dynamic lateral motion, *Journal of Geotechnical Engineering* **118(1)**, 89-106.

OpenSees, 2015. Open System for Earthquake Engineering Similation: OpenSees, University of California, Berkeley, CA, http://opensees.berkeley.edu

Osaki, T., Engelhardt, M., Nakashima, M., and Suita, K., 2006. Experimental Performance of Link-to-Column Connections in Eccentrically Braced Frames, *Journal of Structural Engineering* **132(8)**, 1201-1211.

Ostadan, F., 2006a. SASSI2000: A System for Analysis of Soil Structure Interaction – User's Manual. University of California, Berkeley, CA.

Pais, A., and Kausel, E., 1988. Approximate formulas for dynamic stiffness of rigid foundations, *Soil Dynamics and Earthquake Engineering* **7**, 213-227.

Paolucci, R., Shirato, M., and Yilmaz, M.T., 2008. Seismic behavior of shallow foundations: Shaking table experiments vs numerical modeling, *Earthquake Engineering and Structural Dynamics*, **37**, 577-595.

Pacific Earthquake Engineering Research Center (PEER) and Applied Technology Council ATC), 2010. Modeling and acceptance criteria for seismic design and analysis of tall buildings, *PEER/ATC 72-1*, Redwood City, CA.

Pacific Earthquake Engineering Research Center (PEER), 2010. Guidelines for Performance-Based Seismic Design of Tall Buildings, *PEER 2010/05*, University of California, Berkeley, CA.

Pacific Earthquake Engineering Research Center (PEER), 2017. PEER Ground Motion Database, available at http://ngawest2.berkeley.edu/ (last accessed 10 June 2012)

Penzien, J., 1970. Soil-pile foundation interaction, *Earthquake Engineering*, R. L. Wiegel (editor), Prentice Hall, NY.

Popov, E. P., Ricles, J. M., and Kasai, K., 1992. Methodology for Optimum EBF Link Design, 3983-3988. *Proceedings of the 10th World Conference on Earthquake Engineering.* Madrid, Spain.

Prinz, G., and Richards, P. W., 2009. Eccentrically brace frame links with reduce web sections, *Journal of Constructional Steel Research* **65**, 1971-1978.

Prinz, G., 2010. Using Buckling-Restrained Braces in Eccentric Configurations, Ph.D. Dissertation, Brigham Young University, Provo, UT.

Psycharis, L., 1983. Dynamics of flexible systems with partial lift-off, *Earthquake Engineering and Structural Dynamics*, **2**, 501-521.

Ramadan, T., and Ghobarah, A., 1995. Analytical model for shear-link behavior, *Journal of Structural Engineering* **121(11)**, 1574-1580.

Raychowdhury, P., 2008. Nonlinear Winkler-Based Shallow Foundation Model for Performance Assessment of Seismically Loaded Structures, Ph.D. Dissertation, University of California, San Diego, CA.

Raychowdhury, P., and Hutchinson, T.C., 2009. Performance evaluation of a nonlinear Winkler-based shallow foundation model using centrifuge test results, *Earthquake Engineering and Structural Dynamics* **38(5)**, 679-698.

Richards, P. W., 2004. Cyclic stability and capacity design of steel eccentrically braced frames, Ph.D. Dissertation, University of California, San Diego, CA.

Richards, P. W., and Uang, C.-M., 2006. Testing Protocol for Short Links in Eccentrically Braced Frames, *Journal of Structural Engineering* **132(8)**, 1183-1191.

Richards, P. W., 2009. Seismic Column Demands in Ductile Braced Frames, *Journal of Structural Engineering* **135(1)**, 33-41.

Ricles, J. M., and Popov, E. P., 1989. Composite Action in Eccentrically Braced Frames, *Journal of Structural Engineering, ASCE* **115(8)**, 2046-2065.

Ricles, J. M., and Popov, E. P., 1994. Inelastic link element for EBF seismic analysis, *Journal of Structural Engineering, ASCE* **120(2)**, 441-463.

Roeder, C. W., and Popov, E. P., 1977. Eccentrically braced steel frames for earthquakes, *Journal of the Structural Division, ASCE* **104(ST3)**, 391-411.

Roësset, J. M., 1996. Seismic response of structures on embedded foundations, *Transactions on the Built Environment* **23**, 0-16.

Roësset, J. M., 1980. Stiffness and damping coefficients of foundations, 1-30. *Proceedings, ASCE Geotechnical Engineering Division National Convention.*

Romero, S. M., and Rix, G. J., 2005. Ground Motion Amplification in the Upper Mississippi Embayment, *Report No. GIT-CEE/GEO-01-1*, School of Civil and Environmental Engineering, Georgia Institute of Technology, Atlanta, GA.

Rosebrook, K. R., and Kutter, B. L., 2001a. Soil-Foundation Structure Interaction: Shallow Foundations, *Data Report No.UCD/CGMDR-01*, Center for Geotechnical Modeling, University of California, Davis, CA.

Rosebrook, K. R., and Kutter, B. L., 2001b. Soil-Foundation Structure Interaction: Shallow Foundations, *Data Report No.UCD/CGMDR-02*, Center for Geotechnical Modeling, University of California, Davis, CA.

Rosebrook, K. R., and Kutter, B. L., 2001c. Soil-Foundation Structure Interaction: Shallow Foundations, *Data Report No.UCD/CGMDR-03*, Center for Geotechnical Modeling, University of California, Davis, CA.

Schellenberg, A., Yang, T., and Kohama, E. *OpenSees Navigator 2.5.6.*, software, University of California, Berkeley, CA.
http://openseesnavigator.berkeley.edu/

Stewart, J. P., Seed, R. B., and Fenves, G. L., 1998. Empirical Evaluation of Inertial Soil-Structure Interaction Effects, *Report No. PEER-98/07*, Pacific Earthquake Engineering Research Center, University of California, Berkley, CA.

Stewart, J. P., Fenves, G. L., and Seed, R. B., 1999a. Seismic soil-structure interaction in buildings. I: Analytical methods, *Journal of Geotechnical and Geoenvironmental Engineering* **125**, 26-37.

Stewart, J. P., Seed, R. B., and Fenves, G. L., 1999b. Seismic soil-structure interaction in b uildings. II: Empirical Findings, *Journal of Geotechnical and Geoenvironmental Engineering* **125**, 38-48.

Stewart, J. P., Kim, S., Bielak, J., Dobry, R., and Power, M., 2003. Revisions to soil structure interaction procedures in NERPH design provisions, *Earthquake Spectra* **19(3)**, 677-696.

Stewart, J. P., and Tileylioglu, S., 2007. Input ground motions for tall buildings with subterranean levels. *Structural Design of Tall and Special Buildings* **16**, 543-557.

Taylor, P. W., Bartlett, P. E., and Weissing, P. R., 1981. Foundation rocking under earthquake loading, Volume 3, 313-322. *Proceedings, 10th International Conference on Soil Mechanics and Foundation Engineering.*

Veletsos, A. S., and Prasad, A. M., 1989. Seismic interaction of structures and soils: Stochastic approach, *Journal of Structural Engineering* **115(4)**, 935-956.

Ugalde, J., 2007. Centrifuge test on bridge columns on shallow square footings, Master's Thesis, University of California Davis.

U.S. Geological Survey (USGS), 2013. U.S. Seismic Design Maps, web-based tool, version 3.1.0, http://earthquake.usgs.gov/hazards/designmaps/ (last accessed 10 June 2017)

USGS (2012). Hazard Curve Application, web-based tool, version 3.2.x, https://earthquake.usgs.gov/hazards/interactive/ (last accessed 10 June 2017)

Veletsos, A. S., and Meek, J. W., 1974. Dynamic behavior of building-foundation systems, *Earthquake Engineering and Structural Dynamics* **3**, 121-138.

Veletsos, A. S., and Nair, V. V., 1975. Seismic interaction of structures on hysteretic foundations, *Journal of Structural Engineering* **101**, 109-129.

Veletsos, A. S., and Prasad, A. M., 1989. Seismic interaction of structures and soils: Stochastic approach, *Journal of Structural Engineering* **115(4)**, 935-956.

Veletsos, A. S., Prasad, A. M., and Wu, W. H., 1997. Transfer functions for rigid rectangular foundations, *Earthquake Engineering and Structural Dynamics* **26(1)**, 5-17.

Vijayvergiya, V., 1977. Load-movement characteristics of piles. *Proceedings, Ports 77 Conference, American Society of Civil Engineers.* March, Long Beach, CA.

Watson, G. N., 1995, *A Treatise on the Theory of Bessel Functions*, Cambridge University Press, United Kingdom.

Wiessing, P. R., 1979. Foundation rocking on sand, *Report No. 203*, School of Civil, University of Auckland, New Zealand.

Wilcock, T., Easton, M., Algaard, W., and Tavolaro, Tabitha, 2015. Grade A Office Space in Mexico City: Tight Sites and Shaky Ground, *Proceedings of the 2015 CTBUH Conference*, New York, October 26-30, Council on Tall Buildings and Urban Habitat.

Whittaker, A. S., Uang, C.-M., and Bertero, V. V., 1989. Seismic Testing of Eccentrically Braced Dual Steel Frames, *Earthquake Espectra* **5(2)**, 429-449.

Wolf, J. P., 1985. *Dynamic Soil-Structure Interaction,* Prentice-Hall, Upper Saddle River, NJ.

Yamada, S., Hyodo, M., Orense, R. P., Dinesh, S.V., and Hyodo, T., 2008. Strain-dependent dynamic properties of remolded sand-clay mixtures, *Journal of Geotechnical and Geoenvironmental Engineering* **134(7)**, 972-981.

Yim, S. C., and Chopra, A., 1985. Simplified earthquake analysis of structures with foundation uplift, *Journal of Structural Engineering* **111(12)**, 2708-2731.